University of Stavanger

KAY THI KYIN
SUPERVISOR: PROF. YIHAN XING

Local Design of the pontoon of Semi-Submersible substructure for a 15-MW floating wind turbine using a Machine Learning approach

Master Thesis (2024)

Master of Science in Structural and Mechanical Engineering

Faculty of Science and Technology

Department of Mechanical and Structural Engineering and Materials Science

Abstract

Active learning has recently been deployed as a reliable tool in engineering projects to expedite discovery of failure points ahead of project phases, thereby saving costs. Such is especially crucial for offshore floating wind turbine projects, where the cost margin is still relatively less competitive than for onshore wind projects. To increase uptake of offshore wind turbines in projects, there lies a need to reduce the existing research gap in active learning of failure points in support structures of floating wind turbines.

The thesis proposes to deal with the local design and structural analysis of the steel semi-submersible platform supporting the International Energy Agency (IEA) 15MW floating wind turbine, specifically the pontoon. This is done by determining the optimum stiffener layout and hull thickness of the support structure using ¨DNV-RP-C201 Buckling Strength of Plated Structures¨, ¨DNV-OS-C101 Design of Offshore Steel Structures¨, ¨DNV-ST-0119 Floating Wind Turbine Structures¨ and AISC Manual of Steel Construction, 9th Edition. Then, the wind turbine simulation tool OPENFAST incorporated TurbSim simulations for wind speeds ranging from the cut-in to the cut-out wind speeds of the wind turbine, to extract the tower base loads. Following which, the finite element program ANSYS was used to build a horizontal pontoon comprising the stiffeners and the hull, and to highlight the failure points under the tower base loads from OPENFAST. As the pontoon FEM (Finite Element Method) model was complex, several learning points were highlighted in the thesis in validating the FEM model.

Thereafter, a machine learning approach is employed to efficiently predict the optimal pontoon layout with fewer design points and at less computational cost. This output is subsequently compared with the ANSYS FEA output, with supporting discussions. The chosen machine learning approach shows promising results in predicting the target outputs, such as von Mises stress and buckling load of the girders in the pontoon, under environmental loads at a mean wind speed of 11m/s. There was an error tolerance of about 17% for the von Mises stress predictions, while a remarkable 0% for predictions of buckling loads. It is concluded that more studies need to be explored in this arena in order to fully embrace use of machine learning for optimum design of the semi-submersible structure.

Acknowledgements

This thesis represents the culmination of my master's degree in Structural Engineering at the University of Stavanger. The successful completion of this work required significant advice and assistance from numerous individuals, for which I am immensely grateful to.

First and foremost, I extend my sincere appreciation to my supervisor, Professor Yihan Xing, for granting me the opportunity to work under his expert guidance on this compelling topic. I am deeply thankful for his unwavering support, encouragement, and invaluable guidance that were instrumental in the completion of this thesis. I also acknowledge the contributions of Post Doc. Chao Ren, whose collaboration, insights, discussions, and feedback greatly enriched this work. Furthermore, I extend my thanks to the Department of Marine and Offshore Technology at the University of Stavanger for providing the necessary resources throughout this endeavour.

I am fortunate to have received continuous encouragement, support, and instruction from the teaching staff of the Mechanical and Structural Engineering department.

Finally, I am grateful for the support of my loved ones, whose encouragement and belief in me were instrumental throughout my master's degree.

Stavanger, 15th June 2024,

Kay Thi Kyin

Contents

List of abbreviations

AI	Artificial Intelligence
AISC	American Institute of Steel Construction
ALS	Accidental Limit State
ASD	Allowable Stress Design
DNV	Det norske Veritas
FEA	Finite Element Analysis
FEED	Front End Engineering Design
FEM	Finite Element Method
FPSO	Floating Production Storage and Offloading
GPR	Gaussian Process Regression
Hs	Significant wave height
IEA	International Energy Agency
IRENA	The International Renewable Energy Agency
LCoE	Levelized Cost of Energy
LRFD	Load and Resistance Factor Design
ML	Machine Learning
PULS	Panel Ultimate Limit State
SLS	Serviceability Limit State
Tp	Peak wave period
ULS	Ultimate Limit State

List of figures

List of tables

List of equations

1. Introduction

1.1 Background and Motivation

The transition towards renewable energy sources, particularly offshore wind turbines, is gaining momentum globally due to the imperative to address climate change. Offshore wind farms are increasingly being placed in deep coastal waters for optimal power generation, driven by factors such as relatively uniform wind velocities, space constraints, and noise concerns. Floating support platforms have emerged as a viable solution, with semi-submersible platforms standing out due to their versatility across various water depths and simplified installation processes (Hu et al., 2016; QFWE, n.d.).

The VolturnUS-S, a steel floating semi-submersible structure developed to support the IEA (International Energy Agency) 15 MW offshore reference turbine (Allen et. al, 2020), represents a significant advancement in the floating offshore wind sector. Projections suggest its Levelized Cost of Electricity (LCoE) could be below $60/MWh, positioning it as a highly cost-effective solution (Matha et al., 2016; Musial et al., 2020). However, achieving broader market competitiveness requires meticulous balance between cost-effectiveness and reliability in platform design, particularly in addressing the gap in load transfer analysis for structural integrity and reliability (Wang et al., 2023).

Structural analysis for floating wind turbines remains a crucial area of research, especially regarding internal forces and moments. Current methods often lack efficiency and fail to adequately predict failure points (Wang et al., 2023). Researchers are exploring machine learning models to address these challenges, such as the AK-MDAmax method, which aims to reduce computational costs while maintaining accuracy (Ren and Xing, 2023). The AK-MDAmax method estimates the maximum cumulative damage of various local spots at the tower base of the wind turbine through an active learning process. When applied to the IEA 15MW wind turbine with monopile support structure, promising results have been demonstrated, substantially improving computational efficiency while maintaining a marginal error of approximately 1% (Ren and Xing, 2023). Extending such an approach to semi-submersible support structures could significantly improve the understanding and optimization of floating wind turbine platforms, bridging critical gaps in structural design and performance evaluation (Ren and Xing, 2023; Wang et al., 2023).

1.2 Objectives

This thesis is two-fold, to examine an optimal stiffener layout for the horizontal pontoon, and to adopt a machine learning model that can expedite the optimal design of the pontoon, with result comparison to an FEM model of the pontoon. Specifically, the objectives of this thesis are as follows:

1. To determine the optimal detailed design of semi-submersible, specifically the horizontal pontoon
2. To establish a sound FEM model of the pontoon
3. To adopt a machine learning model to aid in determining the optimal detailed design of the pontoon

In which, literature review will supplement the execution of these objectives.

1.2.1 Objective 1: Optimal detailed design of semi-submersible (horizontal pontoon)

Since the detailed design of the semi-submersible structure are not provided by IEA or the University of Maine, there is interest to determine the detailed design. The detailed design comprises of the girders, stiffeners and the hull of the horizontal pontoon. The global dimensions of the substructure are provided by University of Maine. With these in mind, along with literature review and validation with relevant design codes from DNV and AISC, an optimal detailed design is obtained.

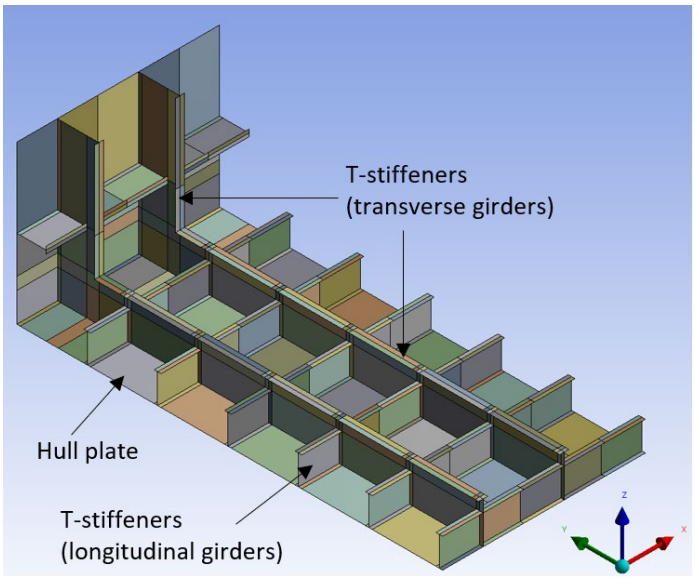

Figure 1.1 Isometric view of section of horizontal pontoon, showing detailed design

1.2.2 Objective 2: Establish sound FEM model of pontoon

It is of interest to determine a good FEM model of the pontoon, along with its failure points under environmental conditions. An FEM model of the pontoon, including its detailed design, was created in ANSYS.

Based on the dimensions and operating conditions of the IEA 15MW wind turbine, a wind turbine simulation tool, OPENFAST, was used to determine the loads at the base of the wind turbine tower. Following which, these loads were applied to the FEM model of the pontoon to extract the failure points under loads.

A thorough study was done via trial and error to determine a sound FEM model of the pontoon in ANSYS.

1.2.3 Objective 3: Adopt a Machine Learning model to determine the optimal design of pontoon

To incorporate Artificial Intelligence (AI) to the offshore wind turbine structural analysis, there is a motivation to adopt and train a Machine Learning (ML) model to predict the failure points of the structure, based on design variables of the pontoon. This is to expedite in the design process of determining the optimal design. Examples of design variables include girder width, girder depth, girder flange thickness, girder web thickness and girder spacing. Since these variables are interdependent and it is time-consuming to determine the optimal design variables based on trial and error, there is great interest to adopt a ML model that can expedite the design process.

In real life FPSO (Floating Production Storage and Offloading) projects, there are three critical engineering phases: FEED (Front-End Engineering Design), Basic Engineering and Detailed Engineering. These are illustrated in the figure below.

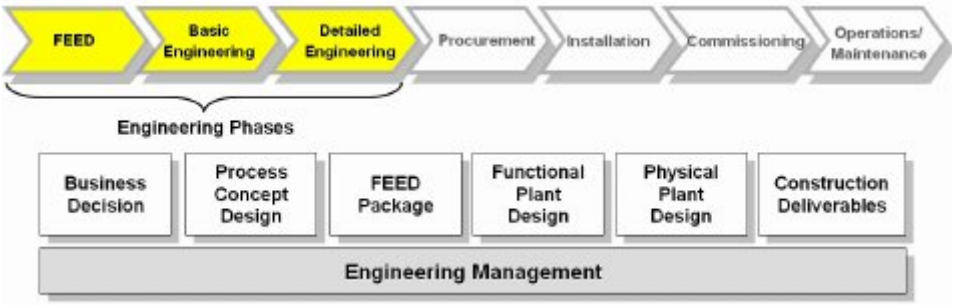

Figure 1.2 Phases of an offshore project (Hwang et al., 2008)

In the FEED phase, preliminary design principles will be verified against more detailed calculations and design procedures. This is to obtain a clearer cost estimate of the project for the client, along with technical feasibility and safety of the structure (Deltamarin Ltd, 2021).

In the basic engineering phase, design must be verified with approval from the relevant classification society, such as DNV. Basic design is usually executed at the shipyard even before the shipbuilding contract is signed (Deltamarin Ltd, 2021).

Often, the phases for basic engineering and detailed engineering tend to overlap, leading to increasing time and monetary losses if revisions have to be made in the designs. For this reason, there is interest to utilise Machine Learning in the FEED phase to highlight the failure points in the structure, so that engineers can amend it before basic and detailed engineering phases commence.

Using the AK-DA approach, Ren and Xing (2023) have investigated the IEA 15 MW wind turbine with monopile support structure under various wind-wave conditions. The approach showed promising results, with computational efficiency increasing by more than 55 times with only a marginal error of approximately 1% (Ren and Xing, 2023). Hence, this thesis will investigate the feasibility of using a simplified ML model to evaluate the design variables of the pontoon structural components.

1.3 Outline

This thesis has been organised into five chapters.

Chapter 1 presents the Introduction detailing the background, motivation, objectives and the scope of the thesis.

Chapter 2 dives into the literature review of semi-submersible design, design and analysis of stiffened plates and machine learning models.

Chapter 3 details the methodology used to develop the detailed design of the pontoon, including preliminary hand calculations as per design codes, FEM modelling and adopting a simplified Machine Learning model to determine suitability of selected design variables of the pontoon.

Chapter 4 concludes with the overall conclusion and recommendations for future work.

Finally, Chapter 5 lists the references, while Appendix is appended in the last section of the thesis.

1.4 Scope

This thesis studies the global and local design of the semi-submersible support structure of the wind turbine. Since the detailed design of the support structure is not known, an iterative multi-phase

approach is taken to propose the design (Figure 1.3). Design phases 1 and 2 have already been completed by IEA and U of Maine. The thesis thus focuses on design phases 3 and 4.

1.4.1 Design phase 3: Stiffener layout in pontoon

The stiffener layout is proposed based on existing literature and validated with relevant design codes from DNV and AISC. Then, an FEM model of the pontoon is created in ANSYS, including the stiffener layout inside the pontoon. Loads from OPENFAST simulations were input into the FEM model.

1.4.2 Design phase 4: Machine learning model

The machine learning (ML) model is developed to optimize pontoon design, significantly enhancing the overall design process of semi-submersible structures. By leveraging advanced algorithms and data-driven insights, the model aims to improve structural performance, increase material efficiency, and reduce costs, thereby streamlining the development of robust and sustainable pontoon designs. A multi-input, single output ML model is considered in this thesis.

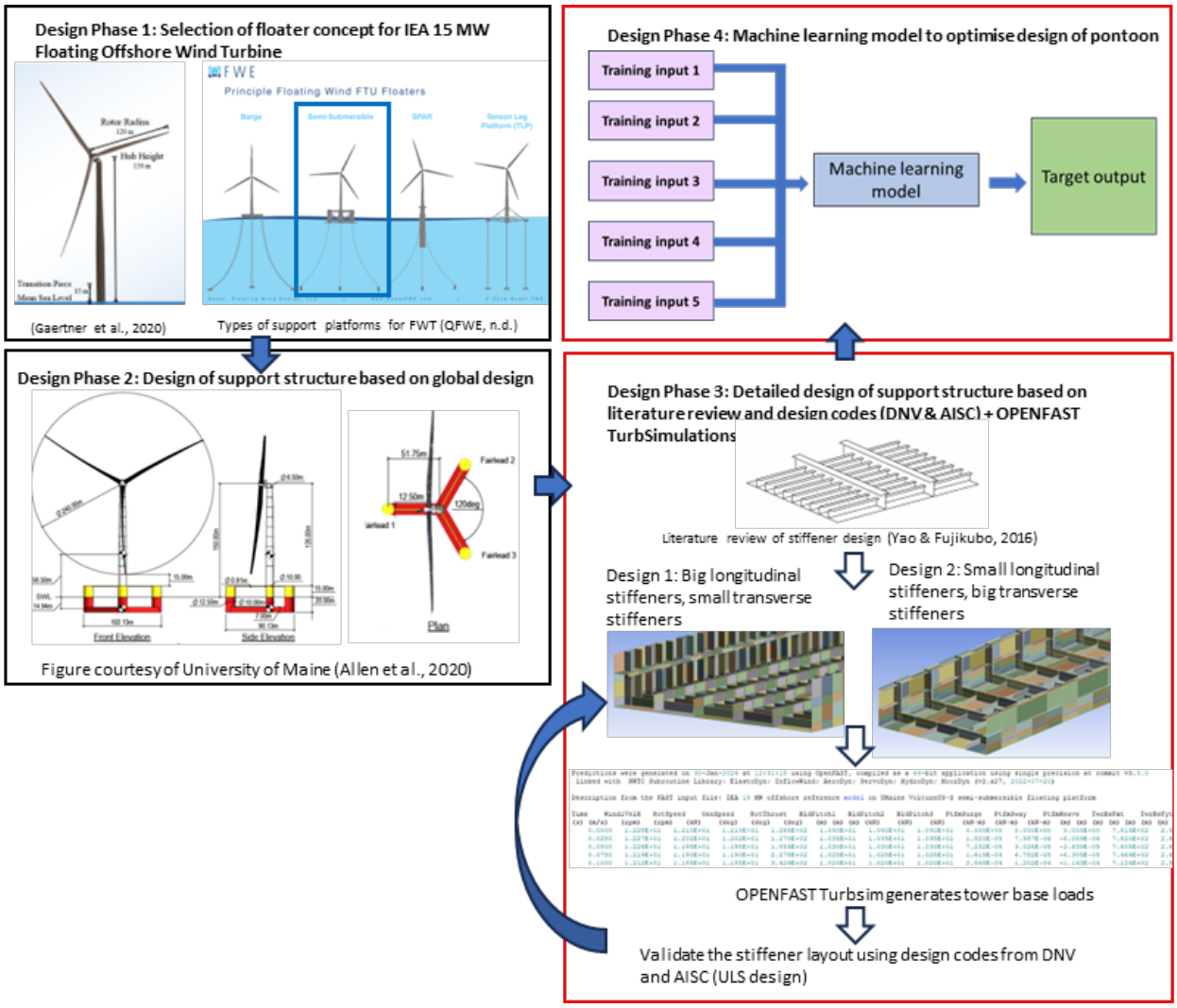

Figure 1.3 Design phases for overall design of pontoon (inspired by Wang et al., 2023)

1.5 Limitations

The results of this thesis are limited by the approaches utilised for the following: (a) material properties and stiffener design, (b) strength assessment of stiffener layout, (c) FEM model, (d) load cases considered and (e) Machine Learning model.

(a) The material properties and detailed design of the horizontal pontoon were not provided by IEA or U of Maine. Suggested designs have to be made in this thesis, with assumptions on the material properties and literature reviews to reference the stiffener layout and hull plate thickness.

(b) For the optimal stiffener design in the horizontal pontoon, the buckling and Ultimate Limit State (ULS) checks of the hull plate thickness, stiffener sizes and stiffener layouts were only verified with formulas and design codes. Design assumptions had to be made in using these formulas

and to simplify the calculations. To capture the non-linear yielding behaviour of the stiffened panel of the pontoon, a more comprehensive approach would be to utilise appropriate buckling check software such as PULS (Panel Ultimate Limit State) or general buckling code check software (i.e. SESAM GeniE) to further validate the strength assessment of the stiffened thin plate pontoon.

(c) The FEM model only comprises the detailed design of one horizontal pontoon idealised as a cantilever with its free end subjected to tower base loads transferred from OPENFAST simulations. A more holistic approach would be to model the entire the semi-submersible structure with the environmental loads incorporated.

(d) The FEM analysis is constrained by the limited number of load cases considered for the environmental conditions. Specifically, the analysis incorporated load cases at a mean wind speed of 11 m/s, chosen due to its magnitude proximity to the turbine's rated wind speed of 10.59 m/s. This selection criterion ensures that the conditions evaluated are representative of typical severe loading and operational scenarios, yet it may not fully encompass the range of environmental loads that the structure might encounter.

(e) The Machine Learning model utilized in this study is trained on a limited set of input data, constrained by the thesis's scope. To enhance the model's accuracy and robustness, a more extensive dataset should be employed for training. This expansion would provide a more comprehensive representation of the variables involved, thereby improving the model's predictive performance and generalizability.

2. Literature review

This chapter provides a literature review of the objectives aforementioned. It begins with a review of trends and challenges in the floating offshore wind market, followed by design principles of the semi-substructure, highlighting parameters critical to their performance. Specifically, structural design principles of the pontoon structure are also reviewed, along with discussing various optimization methods currently used in structural design of pontoon.

The chapter then continues with a detailed survey of Machine Learning models, exploring its application in structural optimization, citing relevant case studies and existing models.

2.1 Trends and challenges in floating offshore wind market

There is urgent imperative to deal with climate change and reduce greenhouse gases. Presently, the power sector produces the largest amount of carbon dioxide emissions than any other sector in the global economy, along with the increasing electrification of the energy sector (IEA, 2024). This is further exacerbated by the fact that, due to growing populations and increasing industrialisation, a whopping average growth of 3.4% is expected in electricity demand from 2024 to 2026 (IEA, 2024). Therein lies the benefit of utilising offshore wind power, an energy source that is infinite and always renewable, without any production of harmful greenhouse gas emissions (National Grid, 2022). The energy sector recognises this, with a marked increase in uptake of offshore wind power as seen by the rising state subsidies and investments (GWEC, 2020). This leads to a significant drop in production costs, with, as of 2020, a projected 55% reduction in Levelized Cost of Energy (LCoE), increasing the market competitiveness of offshore wind against fossil fuels (IRENA, 2020). Figure 2.1 supports this by showing the estimated reduction in LCoE for floating offshore wind in the long term.

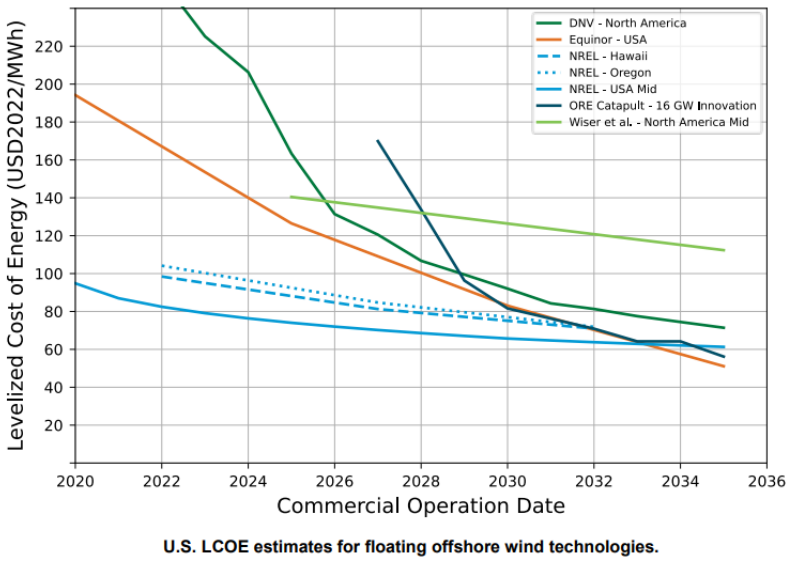

Figure 2.1 Projected decline in LCoE for offshore wind (Musial et al., 2023)

Besides environmental benefits, there are other stellar advantages of floating offshore wind turbines (Equinor, 2024):

- With greater distance away from the shore and to the sea, there is less surface roughness, leading to stronger and more consistent winds. About 80% of global offshore wind resources are in waters deeper than 60 metres, which only floating offshore wind turbines can access, unlike bottom-fixed offshore and onshore wind turbines.
- Floating offshore wind can directly meet power demands through delivery to global markets, which include 2.4 billion people residing within a shoreline distance of 100 km.

Offshore wind is projected to rise from a global growth of 8% of the total wind production in 2020, to 34% in 2050 (DNV, 2023). As the total installed capacity of offshore wind is expected to reach 300GW, with floating offshore wind contributing 6% (DNV, 2023), suitable locations in shallow waters are increasingly scarce, pushing offshore wind technology into deeper waters (Li et al., 2013). This further highlights the benefits of floating offshore wind turbines.

Henceforth, the floating offshore wind market, projected to have an installed capacity of estimated 50 GW in 2035 (Menon, 2022), shows promising potential. However, this potential is dogged by the following factors (National Grid, 2022):

- Offshore wind farms are more costly to construct as they require more intricate support systems.
- Since floating offshore wind turbines are in deep waters where there are higher wind speeds and strong seas, the challenging environmental conditions impose difficulties in accessibility for maintenance and repair.

In the pursuit of broader market competitiveness for floating offshore wind turbines, it becomes imperative to strike a meticulous balance between cost-effectiveness and reliability in platform design (Wang et al., 2023).

One way to improve the platform design is to expedite the design process in structural analysis. The current analysis of wind turbine simulation codes, encompassing aerodynamics, hydrodynamics control systems, and rigid/flexible structures in the time domain, is robust. However, there is a recognized shortfall in transferring loads for structural analysis, where most traditional methods focus on global load transfer, but insufficient coverage on analysis of internal forces of the structures (Wang et al., 2023). Addressing this gap in load transfer analysis is crucial for the continued evolution and optimization of these turbines, ensuring they not only meet economic benchmarks but also uphold structural integrity and reliability in challenging offshore environments.

2.2 Semi-submersible support structure

Presently, various support platform ideas exist for floating wind turbines, with the four primary concepts being barge, spar, semi-submersible, and tension leg platforms (QFWE, n.d.). Among these, the semi-submersible stands out as a prominent choice, occupying roughly 75% of the global floating substructure market share in 2020 (Musial et al., 2021). There are three reasons for this: 1) its suitability for commercialization due to its applicability for a wide range of water depths (Maximiano et al., 2021), generally from 30m shallow water to deep water (Li et al., 2024); 2) simple transportation and installation allowing ease of turbine integration at port; 3) simple mooring design via catenary lines which are more cost-effective than the tension-leg system in TLP.

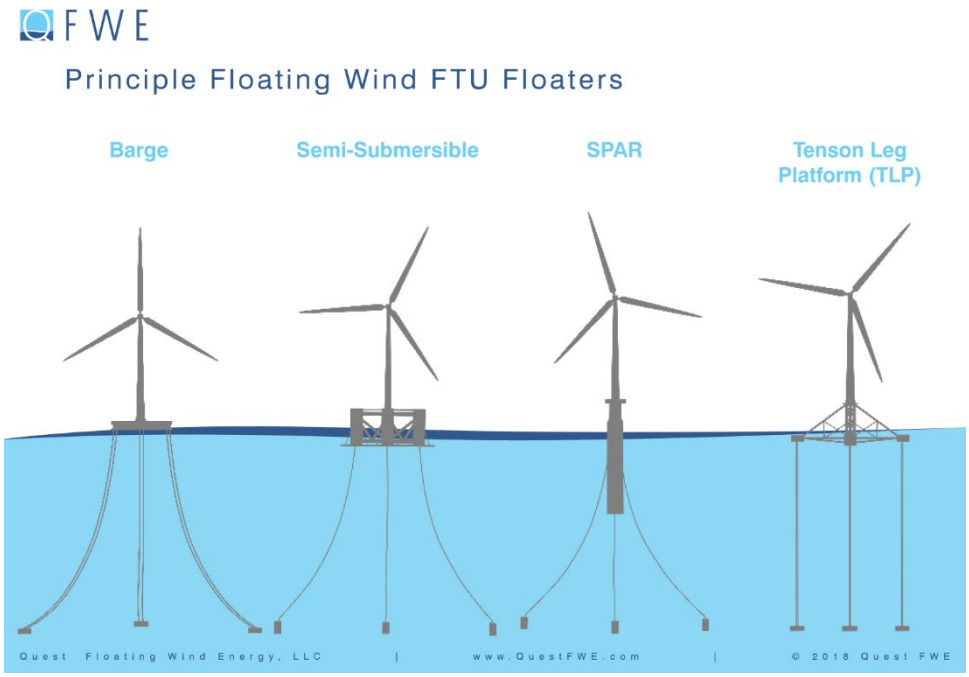

Figure 2.2 Types of support platforms for FWT (QFWE, n.d.)

There exist several semi-submersible hull concepts to support the horizontal axis wind turbines. Typically, there are two main types of concepts: 1) floater with three columns with the turbine supported on one side column; 2) floater with four columns, with the turbine supported on the central column (Li et al., 2024). The columns are connected by pontoons, beams or braces (Vittori, 2015). These concepts are based on the stability and cost considerations involving three to four columns (Yang et al., 2022).

In general, there are three stabilising mechanisms for floating support structures (Leimeister et al., 2018):

- Buoyancy (or waterplane) stabilised

When the floater experiences rotational displacement, it needs to have a restoring moment to counter-tilt it back to a stable position. The waterplane area is the largest contributor to this restoring moment. The larger the second moment of area with respect to the rotational axis of the platform, the larger the waterplane area.

In general, the semi-submersible performs the best among support types due to its significantly bigger water plane areas in the floaters (Alvaro, 2018).

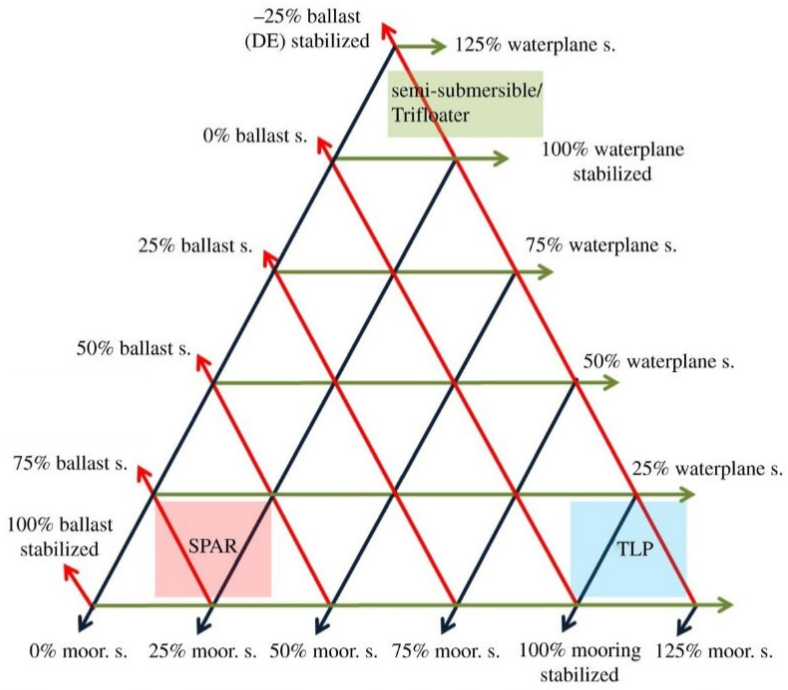

Figure 1. Stability triangle for floating structures, adapted from [7].

Figure 2.3 Semi-submersible with largest waterplane area (Leimeister et al., 2018)

- Mooring stabilised

Mooring lines that have been high tensioned provide the necessary restoring moment when the structure is tilted.

- Ballast stabilised

At the base of the floating structure, large ballast is needed to shift the centre of gravity of the entire system below the centre of buoyancy. As a result, there is stabilising righting moment to counter the rotational displacement when the structure is tilted.

The semi-submersible considered in this thesis is a combination of buoyancy and ballast stabilised. It has pontoons and buoyant columns which provide the required waterplane area. Furthermore, its pontoons are submerged and are ballast-filled at the base (Allen et al., 2020). The pontoons also provide a significant heave natural period outside of the spectrum of the sea wave (Vittori, 2015), due to its relatively wide width of 12.5m.

Figure 2.4 UMaine VolturnUS-S Semisubmersible platform considered in this thesis (Allen et al., 2020)

2.3 Principles for design and analysis of semi-submersible platform design

First principles should be the foundation of a reliable and cost-effective platform design. First principles are based on the fundamental concepts of structural design, which design codes are dependent on.

The design codes/guides considered in this thesis are:

- AISC Specification for Structural Steel Buildings—Allowable Stress Design (ASD) and Plastic Design, 9th Edition (AISC, 1989)
- Recommended Practice for Buckling strength of plated structures, DNV-RP-C201 (DNV, 2002) and Recommended Practice for Structural Design of Offshore Ships, DNV-RP-C102 (DNV, 2002)
- Roark's Formulas for Stress & Strain (Young & Budynas, 2002)

The design procedures considered for the pontoon are based on a mixture of allowable stress design (ASD) as per AISC, and load and resistance factor design (LRFD) as per DNV. ASD considers the allowable stress as the yield stress after dividing by a safety factor, and it must be greater than the required stress (Fisher, 2005). On the other hand, LRFD looks at whether the design strength is greater than the required strength (Fisher, 2005).

Both design methods ensure safety is achieved by applying safety factors to characteristic values of the relevant variables (Ege, 2019). The safety factors considered are material, resistance and load

factors, and they are chosen to induce unfavourable responses such that the desired safety level is obtained (Ege, 2019). The material factor γ_M of 1.15 was considered, as per DNV-RP-C201 (DNV, 2002).

The pontoon is designed for the Ultimate Limit State (ULS). In a study on the steel semi-submersible for a 10 MW floating wind turbine, Wang et al. (2023) highlights the focus on criteria including ¨intact stability and natural periods of rigid body motions¨, which are associated with global performance of the platform. Hence, to determine the optimal detailed design specifications of the pontoon, ULS is considered to analyse the local stress. DNV defines a limit state as ¨a condition beyond which a structure or structural component will no longer satisfy the design requirements¨ (DNV, 2010). The ULS corresponds to the maximum load carrying resistance (DNV, 2011), and requires the capacity check of the structure in both yielding and buckling (Ege, 2019).

Roark's theory of stress and strain was considered to determine the hull plate thickness under global loads. It is based on calculating the ultimate strength of the plate by determining the maximum bending stress based on assumed boundary conditions of the plate.

The thesis chooses to focus on the horizontal pontoon design, and an iterative design process is considered. The iteration begins with proposing a preliminary design and then proceeds till an optimal design solution is reached. The stages of the iteration overlap as new information is found during the design process.

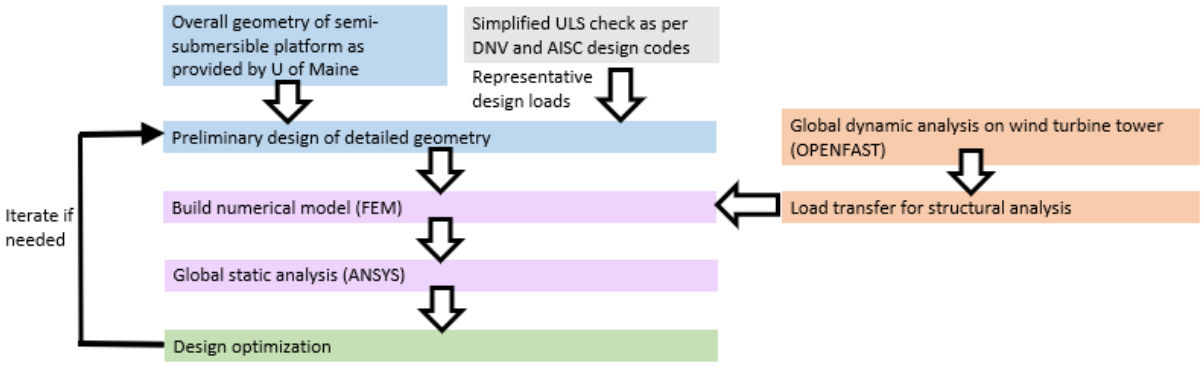

Figure 2.5 Iterative design process of semi-submersible platform, as inspired by (Wang et al., 2023)

2.3.1 Loading conditions considered for semi-submersible design

There are two primary load cases to account for when checking for the ¨intact stability and bulking strength¨ of the semi-submersible support structure (Wang et al., 2023):

- Load case 1: normal operating condition, at rated wind speed (produces largest rotor thrust)

- Load case 2: extreme operating condition, severe storm with 50-year return period in the Northen North Sea

Load case 1 is necessary for ULS design, while load case 2 is needed for fatigue design. The thesis focuses on load case 1.

2.3.2 Environmental conditions considered for semi-submersible design

The environmental conditions need to be accounted when determining the representative design loads transferred to the semi-submersible support structure. A representative location of the sea conditions must be selected. Typically, in the context of Norway, a location in the North Sea is chosen.

Following which, simultaneous hourly wind and wave hindcast data for a period of 10 years are used as a database. For the representative location, the long-term joint distributions of the mean wind speed, significant wave height Hs and spectral peak period Tp are obtained (Wang et al., 2023), via fitting statistical distributions (i.e. Rayleigh, Gumbel) to the hindcast data (Li et al., 2013). The most probable values of Hs and Tp are then selected for each mean wind speed considered.

For instance, the probability distribution of the Hs is fitted with a Rayleigh distribution, and then the value with the highest probability is the Hs. This is illustrated in Figure 2.6 below.

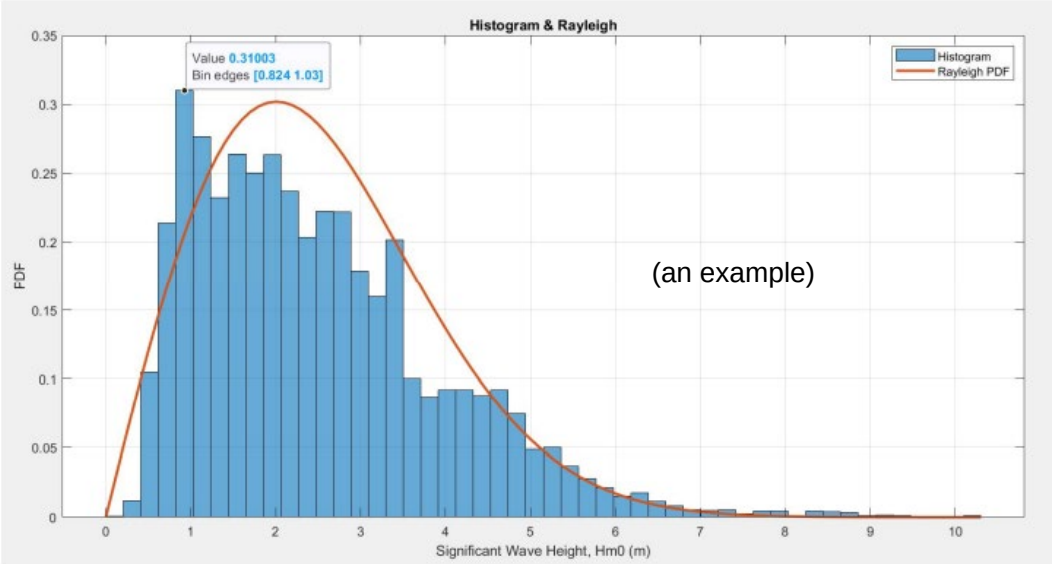

Figure 2.6 Histogram and Rayleigh distribution of significant wave height Hs

Similarly, from the histogram distribution of Tp (Figure 2.7), Tp is the average of the bin edges 9.6 seconds and 10.1 seconds, which is 9.85 seconds. This is the most common Tp value as it has the highest probability.

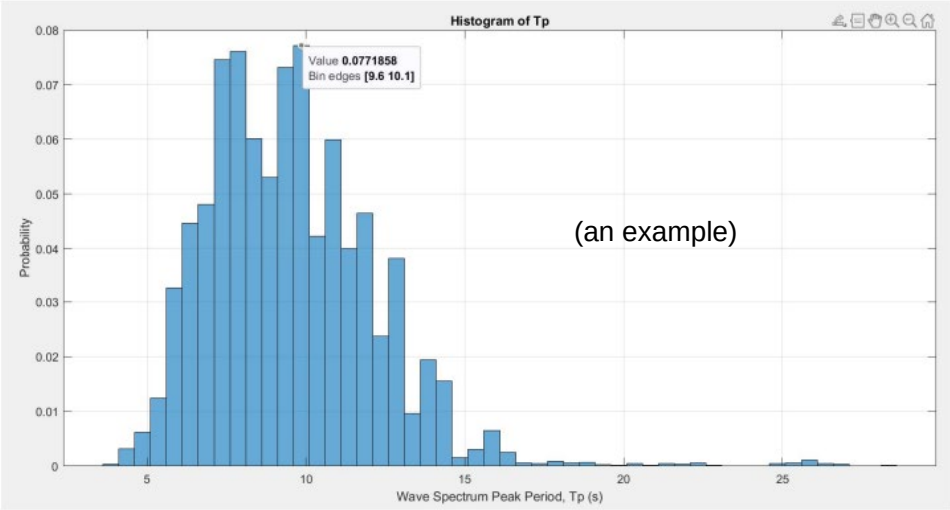

Figure 2.7 Histogram of Tp to obtain the most probable value of Tp

2.4 Stiffened plate

In marine structures such as the semi-submersible, the horizontal pontoon is constructed of thin plates. Stiffeners are provided to effectively maintain the strength and stiffness of thin plates (Yao & Fujikubo, 2016). Common profiles used for stiffeners include T-sections, rectangular flat bars and angle channels (Laftah, 2007). The plates, along with the stiffeners, are termed stiffened plates, which serve as basic strength members of offshore structures (Wang et al., 2016). They are advantageous due to their stable post-buckling behaviour under shear load, enabling them to resist ultimate loads beyond the critical buckling loads (Kim et al., 2007).

Stiffened plates are commonly employed as load-bearing elements in marine structures. Examples of their usage include the hull girder in ships, the pontoons of semisubmersibles, and the decks of offshore platforms. In hull girders, the primary framing system typically involves closely spaced longitudinal stiffeners, complemented by heavier girders placed at wider intervals in the transverse direction (Bai & Jin, 2016).

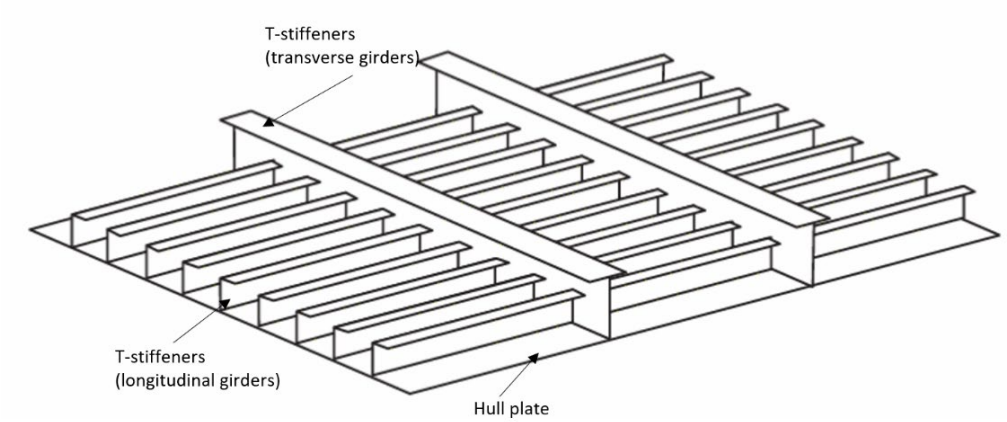

Figure 2.8 Cross section of stiffened plates in the base of a marine structure (Yao & Fujikubo, 2016)

The design of stiffened plate adheres to the following principles (Nguyen, 2011):

1. Elastic local buckling of the stiffened plate is accepted, however elastic buckling deflection is not acceptable
2. Permanent buckling of the stiffened plate is not acceptable
3. Global overall buckling of the stiffened plate is not acceptable

The effects of shear lag and warping are not considered in the design to simplify the scope, as they are deemed insignificant for the purposes of this study. Hence, the stresses due to moment and shear can be determined by conventional beam theory (Ostapenko & Moore, 1982). This means that the normal stresses vary linearly across the flange widths and web depths of the girders/ T-bar stiffeners (Ostapenko & Moore, 1982). Meanwhile, the shear stresses are constant in the web, while they vary linearly in the flanges (Ostapenko & Moore, 1982).

2.4.1 Buckling failure of stiffened plate

The smallest structural unit of the stiffened plate structure is a rectangular plate bounded by longitudinal and transverse stiffeners. This rectangular plate is idealised as simply supported along its four sides (Yao & Fujikubo, 2016). This is because when this plate buckles under loading and develops lateral deflection, the stiffeners along its perimeter weakly restrain against rotation of the plate (Nguyen, 2011).

The stiffened plates are mainly affected by (Bai & Jin, 2016):

1. Stiffener slenderness and spacing
2. Plate geometry
3. Material yield stress

4. Others: residual stresses, initial deformations, boundary conditions, types of loadings imposed on the plates

The stiffened plates are subjected to combined loads from the tower base, longitudinal and transverse bending of the bottom pontoon, torsional buckling of the pontoon and the hydrostatic pressure from wave loads. In general, the possible failure modes of the stiffened plate under such loads are (Bai & Jin, 2016):

1. Buckling of plates due to lateral deflection.
2. Yielding/collapse of plates when the ultimate strength reached/exceeded.
3. Collapse of stiffeners with plates via beam-column mode buckling, due to combined axial stress and bending stress from lateral load.
4. Tripping of stiffeners due to buckling and loss of rotational restraint provided by plating. This occurs when there is a large web height-to-thickness ratio and/or the flange has insufficient stiffness to resist the loads and inevitably twists sideways under tripping failure.
5. Grillage buckling where there is bending of transverse girders and longitudinal stiffeners.

In general, there are essentially two ways the stiffened plates can fail: overall buckling and local buckling (Jang, 2007). In overall buckling, both the stiffeners and the plate buckle. In local buckling, either the stiffeners buckle before the plate or the plate buckles between the stiffeners (Jang, 2007).

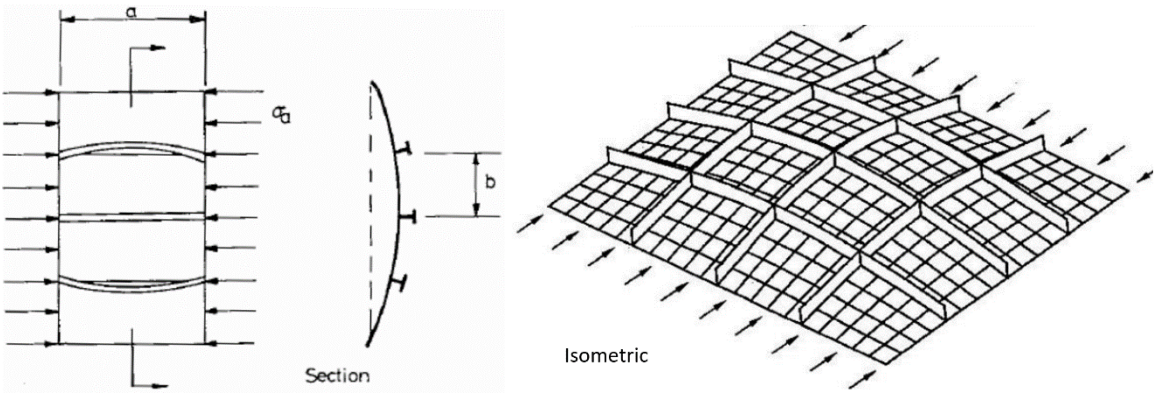

Figure 2.9 Overall buckling of stiffened panel (Jang, 2007)

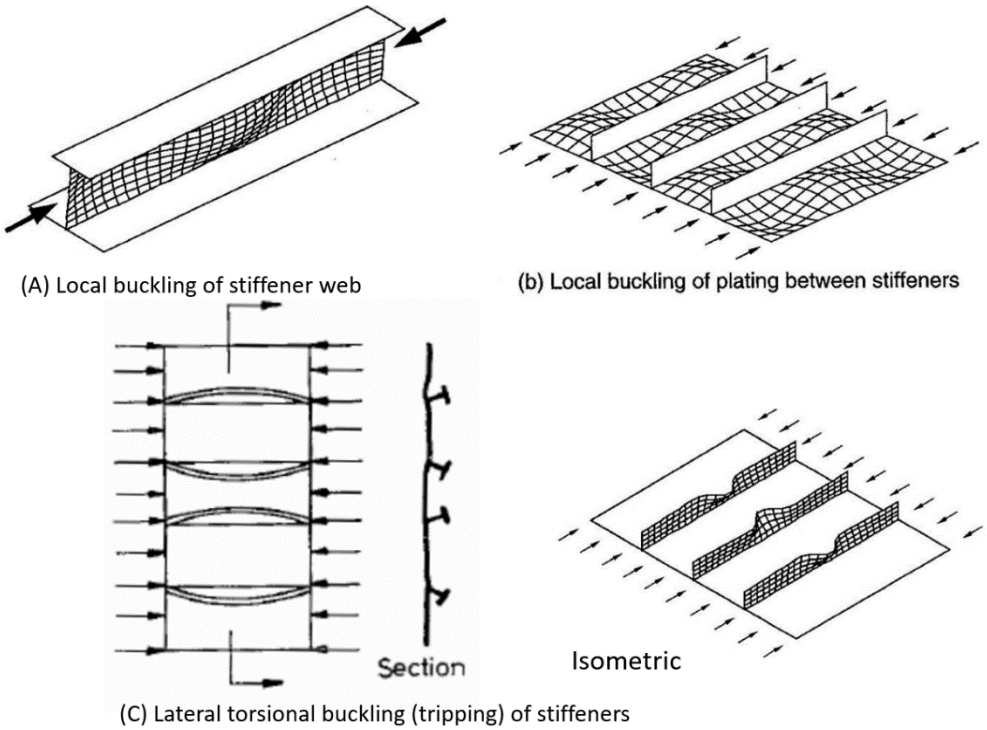

Figure 2.10 Local buckling of stiffened panel (Jang, 2007)

The Recommended Practice for Structural Design of Offshore Ships, DNV-RP-C102, highlights two possible failure modes of the stiffened plates (DNV, 2002):

1. Plate buckling
2. Panel buckling
    a. Plate-induced failure
    b. Stiffener-induced failure

Stiffened panels which are not symmetric in geometry about the plane of the plate, should be checked for both stiffener-induced failure and plate-induced failure (DNV, 2002).

2.4.1.1 Plate buckling

Plate buckling is defined as the ¨local buckling of plate panels between stiffeners¨ (DNV, 2002). The plate undergoes buckling when the in-plane load acting on the plate exceeds its allowable value. The plate could experience either in-plane loading, distributed lateral loads or a combination of both (DNV, 2002). Plate buckling causes ultimate collapse of the stiffened plate before significant yielding of the stiffeners (Nguyen, 2011). In general, there are 4 buckling modes of a simply supported rectangular plate (Yao & Fujikubo, 2016):

1. Longitudinal thrust
2. Transverse thrust

3. Bending moment
4. Shear force

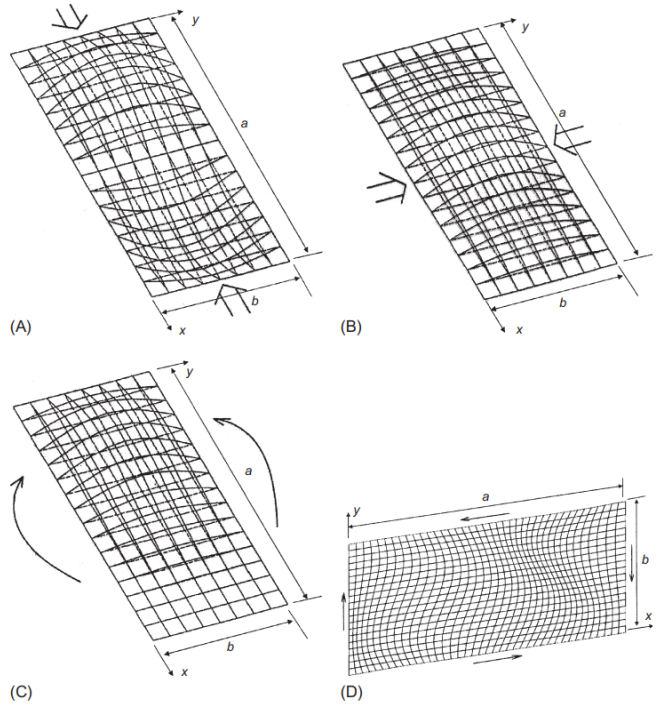

Figure 2.11 Four buckling modes of idealised stiffened panel (Yao & Fujikubo, 2016)

2.4.1.2 Panel buckling

While stiffened plates refer to the plates between stiffeners, stiffened panel refers to the plate between girders (longitudinal stiffeners).

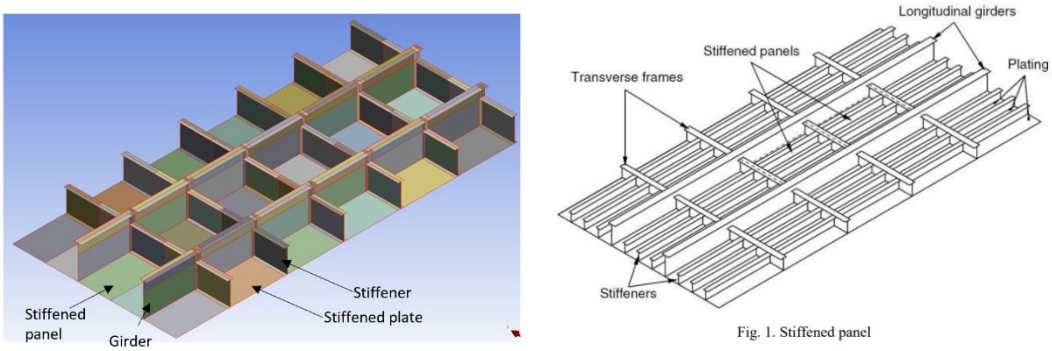

Figure 2.12 Isometric view of stiffened panel and stiffened plate; Stiffened panel (Yu et al., 2018)

Panel buckling is defined as the buckling of stiffened panels between the girders. There are two possible failures under this buckling mode, plate-induced failure and stiffener-induced failure.

Plate-induced failure occurs due to yielding in compression at the connection between the plate and the stiffener, causing deflection to occur away from the plate (DNV, 2002). The characteristic material resistance of the plate has to be used in the check for plate-induced failure (DNV, 2002).

Stiffener-induced failure causes deflection towards the plate. It occurs due to torsional buckling of the stiffener or yielding in compression in the top of the stiffener (DNV, 2002).

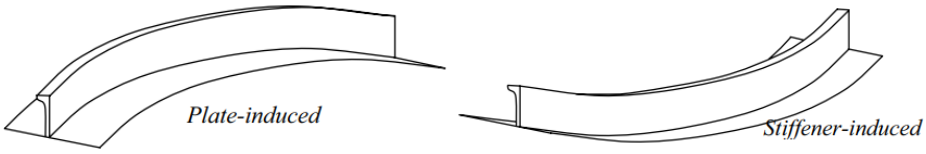

Figure 2.13 Plate-induced failure and stiffener-induced failure (DNV, 2002)

2.4.2 Analytical method of solving buckling problem

In general, there are two analytical methods to solve buckling problems. The stiffened panel is treated as either a discrete beam or an orthotropic plate. The method of treating the stiffened panel as a discrete beam is more accurate as it considers both the plate and stiffener as a combined problem resisting the loads (Jang, 2007). This would capture the load transfer at the connection between the stiffener and the plate. On the other hand, treating the stiffened panel as separate entities comprising the orthotropic plate and the stiffener, is less accurate, but easier to execute. This method is valid when the stiffeners are very closed spaced (Jang, 2007).

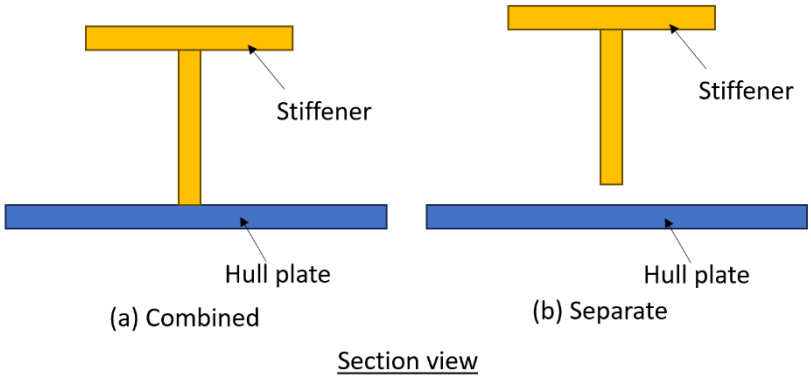

Figure 2.14 Analytical methods to solve buckling problems of stiffened panel

The addition of stiffeners to a plate increases the in-plane load the plate can withstand without buckling. However, this poses more challenges in the stress analysis of the overall stiffened plate, as the number of variables and buckling modes increase (Laftah, 2007). As a result, much of engineering applications relies on simplified equations when designing these plates (Bleich & Ramsey, 1951).

The complexity in determining the ultimate strength of stiffened panels is further exacerbated by the lack of experimental research on the ultimate strength of stiffened panels, partly due to the challenges in experimental study of their buckling behaviour (Laftah, 2007). Furthermore, inelastic buckling governs the structural design criteria required to prevent the ultimate limit state yielding of the stiffened panels (Laftah, 2007).

2.4.3 Beam-column idealisation of stiffened plate

Under the environmental loads, the ship hull girders are subjected to bending, shear and torsion. There are several literature discussing efficient methods to determine the ultimate strength of ship hull girders. The most common approach, by theory, has been to consider the individual components of the hull girders. However, Ostapenko (1981) highlights that each of the components attain ultimate strength at different levels of deformation. For instance, at a certain applied load on the structure, some segments have just reached their ultimate strength, while other segments are already in the post-ultimate stress range of reduced capacity (Ostapenko, 1981). There is a real danger of overestimating of the ultimate strength of the structure. Hence, the behaviour of individual components is not sufficient to accurately estimate the ultimate strength of the ship hull girder (Ostapenko, 1981).

To overcome this, Ostapenko (1981) proposed a method that provided reasonable accuracy when compared to laboratory testing results of a structure under moment and shear loads. While the pontoon of focus in this thesis is subjected to moment, shear and torsion loads, torsion is deemed as relatively insignificant to the failure of the pontoon. Furthermore, the floating wind turbine can generate the moment on its support several times higher than when compared to the same turbine on land (Jonkman, 2007). As such, moment and shear loads are more critical to the failure of the pontoon, and Ostapenko's method is of interest for further study in this thesis. The analytical method, sought to determine the ultimate strength of longitudinally and transversely stiffened box girders under the combined action of bending, shear and torsion.

Ostapenko (1981) treats the ship cross section as a box section (Figure 2.15). The overall non-linear behaviour of the box section is accounted for by analysing the compatibility of deformations between the individual components.

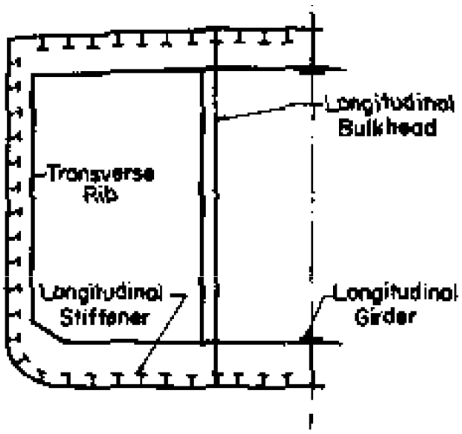

Figure 2.15 Box cross section of ship (Ostapenko, 1981)

The compression flange of the girders is idealised as a beam-column consisting of the T-bar profile and a plate strip of the stiffened plate. The width of the hull plate is taken as the centre-to-centre spacing of the adjacent girders. The beam-column experiences a combination of axial compressive force P and bending moment M, with lateral load applied as a line load q.

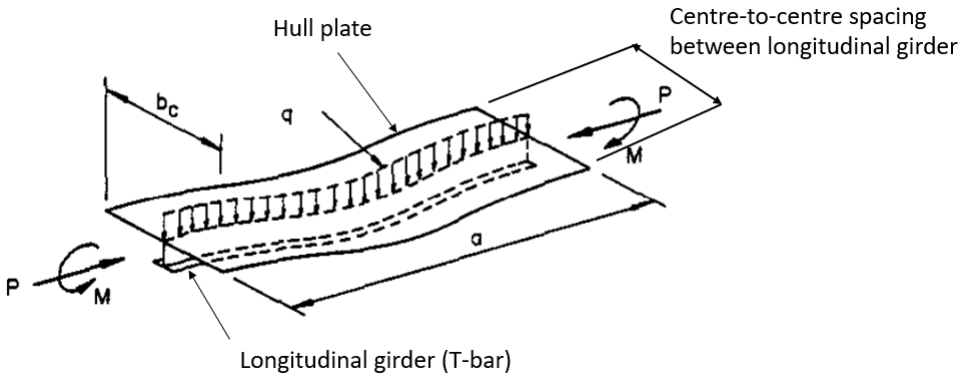

Figure 2.16 Beam-column idealisation (Ostapenko, 1981)

Furthermore, the hull plate is studied via the redistribution of shear and axial forces in the plate between girders. Lateral loading on the plate was not considered as it was deemed to have negligible effect on the buckling and post-buckling behaviour (Rutledge & Ostapenko, 1968).

The hull plate is assumed to be very flexible as compared to the longitudinal girders, which are relatively larger (Ostapenko, 1981). As such, there is negligible interaction between the longitudinal girders through the plate (Ostapenko, 1981). Thus, there is valid assumption in idealising the beam-column to comprise of the girder and a portion of the hull plate.

The plate buckling stress can be determined as follows:

Table 1 Reference Buckling Stresses

Pure Stress	Aspect Ratio $\alpha=a/d_i$	Buckling Coefficient k	Relative Plate Slenderness	For λ	Buckling Stress / Yield Stress
Shear 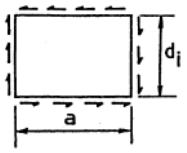		$k_v = 5 + \frac{5}{\alpha^2}$	$\lambda_v = 0.8 \frac{d_i}{t_w}\sqrt{\frac{F_y}{E\,k_v}}$	$\leqslant 0.58$	$\frac{F_{vcr}}{F_y} = 0.58$
				$\geqslant 0.58$ $\leqslant 1.41$	$\frac{F_{vcr}}{F_y} = 0.58 - 0.357(\lambda_v - 0.58)^{1.18}$
				> 1.41	$\frac{F_{vcr}}{F_y} = 0.58(1/\lambda_v^2)$
Bending 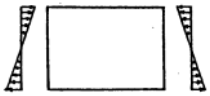	$> \frac{2}{3}$	$k_b = 24$	$\lambda_b = \frac{d_i/t_w}{0.95}\sqrt{\frac{F_y}{E\,k_b}}$	$\geqslant 0.65$ $\leqslant 1.5$	$\frac{F_{bcr}}{F_y} = 0.072(\lambda_b - 5.62)^2 - 0.78$
	$< \frac{2}{3}$	$k_b = 24 + 73(\frac{2}{3} - \alpha)^2$		$\geqslant 1.5$	$\frac{F_{bcr}}{F_y} = 1/\lambda_b^2$
Axial 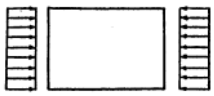	> 1	$k_c = 4$	$\lambda_c = \frac{d_i/t_w}{0.95}\sqrt{\frac{F_y}{E\,k_c}}$	$\geqslant 0.65$ $\leqslant 1.5$	$\frac{F_{ccr}}{F_y} = 0.072(\lambda_c - 5.62)^2 - 0.78$
	< 1	$k_c = (\alpha + \frac{1}{\alpha})^2$		$\geqslant 1.5$	$\frac{F_{ccr}}{F_y} = 1/\lambda_c^2$

Figure 2.17 Reference buckling stresses for plate under pure buckling (Ostapenko & Moore, 1982)

In summary, Ostapenko's method involves decomposing the hull cross section into a compression flange comprising of the idealised beam-column, while the tension flange encompasses the hull plate between the beam-columns. Furthermore, the transverse girders are treated as web stiffeners, stiffening the web of the longitudinal girders. The tension flange and web stiffeners are assumed to deform in a bi-linear and elastic-plastic behaviour (Ostapenko & Moore, 1982).

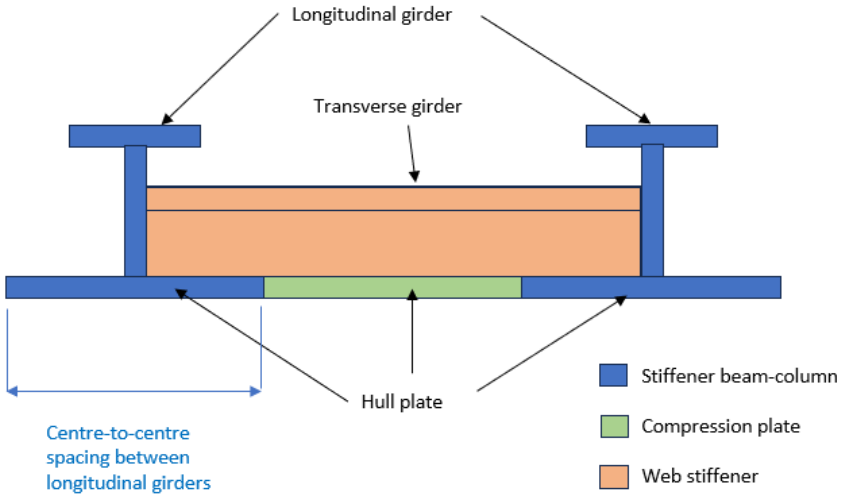

Figure 2.18 Ostapenko's decomposition of the hull cross section under compression

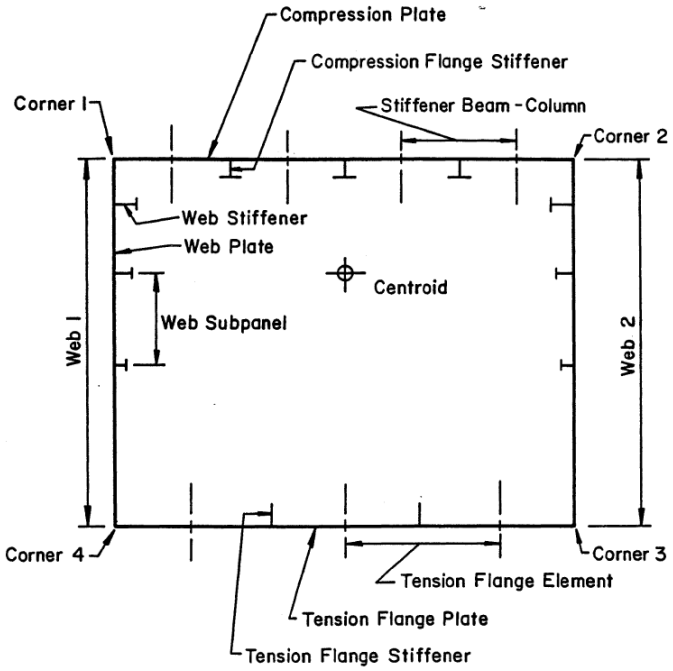

Figure 2.19 Ostapenko's decomposition of the hull cross section under compression and tension (Ostapenko & Moore, 1982)

2.4.4 Empirical formula for buckling mode of stiffened plate

As discussed previously, plate buckling can be a possible mode of failure of the stiffened plate. There are two general methods used in the buckling analysis of the structure: the energy method and the equilibrium method. The energy method, which is more commonly used, will be discussed.

The energy method entails assuming a shape function for the buckling deformation, which includes some unknown coefficients (Wang et al., 2016). By applying the principle of minimum potential energy, these unknown coefficients in the shape function can be identified, allowing for the determination of the critical Euler buckling stress. Consequently, the accuracy of the assumed shape function directly impacts the precision of the buckling analysis (Wang et al., 2016).

A shape function for the buckling mode of the plate between stiffeners has been derived by Fujikubo and Yao (1999), using the energy method to determine the critical Euler stress (Wang et al., 2016):

$$w(x,y) = W_1 sin\frac{m\pi x}{a} sin\frac{\pi y}{b} + \frac{W_2}{2} sin\frac{m\pi x}{a}\left(1 - cos\frac{2\pi y}{b}\right)$$

Equation 2-1

Where:

- a = length of the stiffened plate
- b = width of the stiffened plate
- m = half wave number in the longitudinal direction during buckling deformation

- W_1 and W_2 are unknown coefficients to be determined via the boundary and loading conditions of the plate
- $w(x, y)$ refers to the deflection of the plate in the x (lateral) and y (vertical) axis directions

The first term of Equation 2-1 refers to the buckling mode of a plate simply supported on all edges, while the second term corresponds to the deflection when the plate edges along its length are clamped (Wang et al., 2016).

2.4.4.1 Plate aspect ratio

The plate aspect ratio is defined as a/b, where a is length of the stiffened plate and b is the width of the stiffened plate. Wang et al. (2016) points out that the plate aspect ratio is a dominant factor in static buckling analysis, influencing the buckling load and the precision of various approaches to determine the critical buckling stress (Euler stress). Wang et al. (2016) summarised, from existing studies on the relationship between Euler stress and plate aspect ratio, that the Euler stress decreases with the increase in the plate aspect ratio. This is an important point of consideration when determining the optimal detailed design for the pontoon.

2.5 Structural modelling concept of pontoon

Accounting for the various characteristics of floaters, designing a floating structure for a wind turbine is complex due to the numerous variables involved, such as aerodynamics, hydrostatics, hydrodynamics, mooring lines, control systems, and structural response (Vittori, 2015).

There is no single design methodology, as it varies depending on the design stage and specific requirements. Typically, the methodology involves multiple steps and iterations to refine the initial model for functionality, where these factors should be modelled simultaneously. One such methodology is illustrated in a flowchart developed by Wayman et al. (2006), in a study investigating the impact of integrating a wind turbine with a floating structure on the system's dynamics to identify the most cost-effective floating structures that ensure optimal operational performance of the wind turbine. The flowchart begins with a static design process develops two cost-effective structures that ensure stability and acceptable steady-state operation. These structures then undergo static and dynamic analyses to evaluate their performance under different wind speeds and sea states, assessing response amplitude operators, natural frequencies, and motion standard deviations (Wayman et al., 2006).

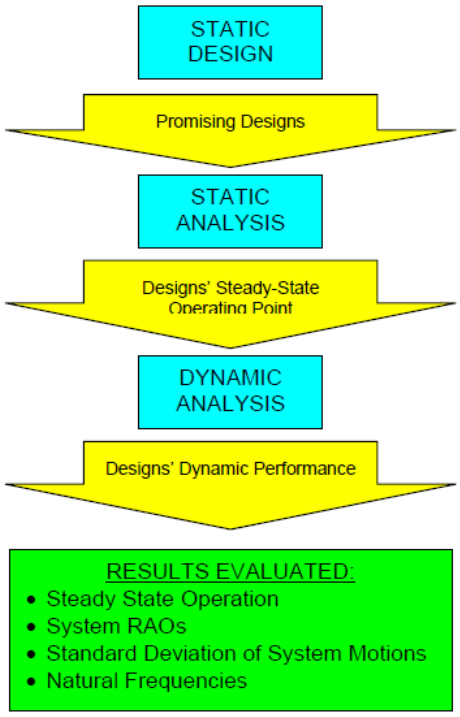

Figure 2.20 Flowchart developed by Wayman et al. (2006)

However, this approach requires time-consuming time domain simulations, which are impractical for an iterative design process (Vittori, 2015). Therefore, an initial simplified analysis is recommended. This involves a static analysis considering only static wind loads to assess the floating stability and static inclination, enabling adjustments to dimensions, mass distribution, and water ballast (Vittori, 2015). In the static analysis stage, the steady-state operating point of the turbine shall be evaluated at various representative wind speeds. Furthermore, the initial criteria governing the design of floating platforms is the performance of the floating wind turbine under static performance (Wayman et al., 2006). Hence, this thesis will focus on the static analysis of the pontoon structure.

Different elements and assumptions are considered in the structural modelling of the offshore wind turbine (OWT) (Alvaro, 2018). In this thesis, the hull will not be considered as rigid body. Instead, it will be modelled as FEM elements. This is to analyse the internal stresses in the hull structure.

2.5.1 Column-pontoon connection

The floating wind turbine experiences a combination of wind and wave loads. This thesis concentrates on the horizontal pontoon that links the central column and the side column of the floating wind turbine, emphasizing the importance of considering fatigue loads primarily from wind and wave impacts. Specifically, the central column, which supports the wind turbine, endures aerodynamic and

wave loads directly. It is thus imperative to sufficiently strengthen the connection between the cylindrical column and the rectangular pontoon, while ensuring a smooth structural transition between the two to prevent sharp corners, and minimise stress concentrations (Tvare, 2014).

For instance, in the FE model of central column and pontoon studied by Tvare (2014), the free end of the pontoon had to be improved by adding an end transverse stiffener. This is to reduce the hot spot stress concentration.

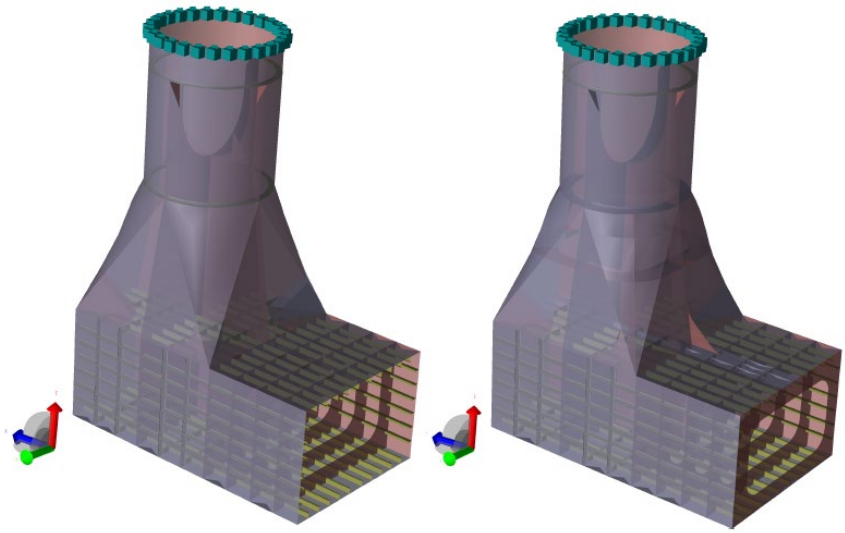

(a) Original FE-model (b) Improved FE-model

Figure 3.1: Finite element model before and after improvements

Figure 2.21 Addition of end transverse stiffener to free end of model (Tvare, 2014)

2.6 Machine learning

The advancement of machine learning (ML) and artificial intelligence has significantly impacted various science and engineering fields, including offshore renewable energy (Masoumi, 2023). These technologies have transformed discovery, ideation, implementation, and result presentation processes (Masoumi, 2023). As global efforts to increase renewable energy generation intensify (Kirby & Briol, 2023), the need to expand capacity and create efficient, eco-friendly infrastructures has become critical (Masoumi, 2023). A typical offshore wind facility requires over £1 billion in capital investment (WindEurope, 2022), with costs rising recently (FT, 2023) due to supply chain inflation and increasing interest rates (Kirby & Briol, 2023). Consequently, policymakers, energy companies, and investors must ensure that future wind farms are designed to maximize energy production while minimizing construction costs (Kirby & Briol, 2023). This urgency underscores the importance of machine learning (ML), which provides tools to make the design, optimization, development, implementation, and maintenance processes more cost-effective and efficient (Masoumi, 2023).

Machine learning is a subset of artificial intelligence (AI) (IBM, n.d.) that enables computers to learn from experience (Brown, 2021), using computational methods that enable machine learning algorithms to derive information directly from data without depending on a pre-established model equation (MATLAB & Simulink, n.d.). Machine learning deploys the method of enabling computers to "learn to program themselves through experience", starting with data that is gathered and used as training data (Brown, 2021). Training data is essentially information that the ML model will be trained on, and the accuracy of the ML model improves with the size of the training data set (Brown, 2021).

Traditional programming involves providing explicit, detailed instructions for a computer to follow. (Brown, 2021). However, this method can be impractical or impossible to execute manually for certain tasks, like training a computer to recognize several design variables involved in the design of a pontoon. Given the numerous components that constitute an offshore wind turbine and its support structure, machine learning significantly aids in this area with its capacity to learn from accumulated experience.

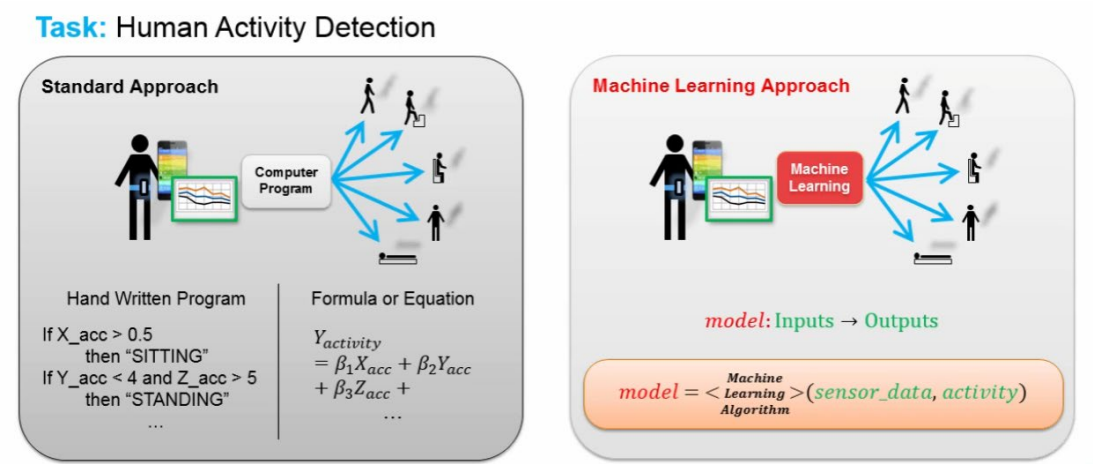

Figure 2.22 Difference between standard computing approach and ML approach (Prasanna, 2015)

There are three branches of machine learning:

1. Supervised ML
2. Unsupervised ML
3. Reinforcement learning

The following sections will detail each of these three branches.

2.6.1 Supervised ML

Supervised ML models are trained using labelled datasets, enabling them to improve accuracy over time (Brown, 2021). For instance, an algorithm would be trained with a set of design parameters of the pontoon, which are all manually named by humans. The ML model would then independently learn to identify the different variables. The algorithm essentially captures a known set of input and output

and trains the model to predict, with reasonable accuracy, the target output in response to new data input. Supervised ML are best when there is known input data for the unknown output to be estimated (MATLAB & Simulink, n.d.). To date, supervised ML models are by far the most commonly used (Brown, 2021).

2.6.2 Unsupervised ML

Unsupervised ML is best for data composing of unlabelled input data, as it identifies patterns and makes inferences from the data (MATLAB & Simulink, n.d.). A common technique used is clustering. For example, to find the optimal hull plate thickness of the pontoon, the ML model can predict the number of clusters of failure points on the hull plate which are directly impacted by the plate thickness. The hull plate thickness is a single variable that can only accommodate a single thickness value per trial simulation, so the ML model employs clustering algorithms to attain the best optimal hull plate thickness that has less failure points.

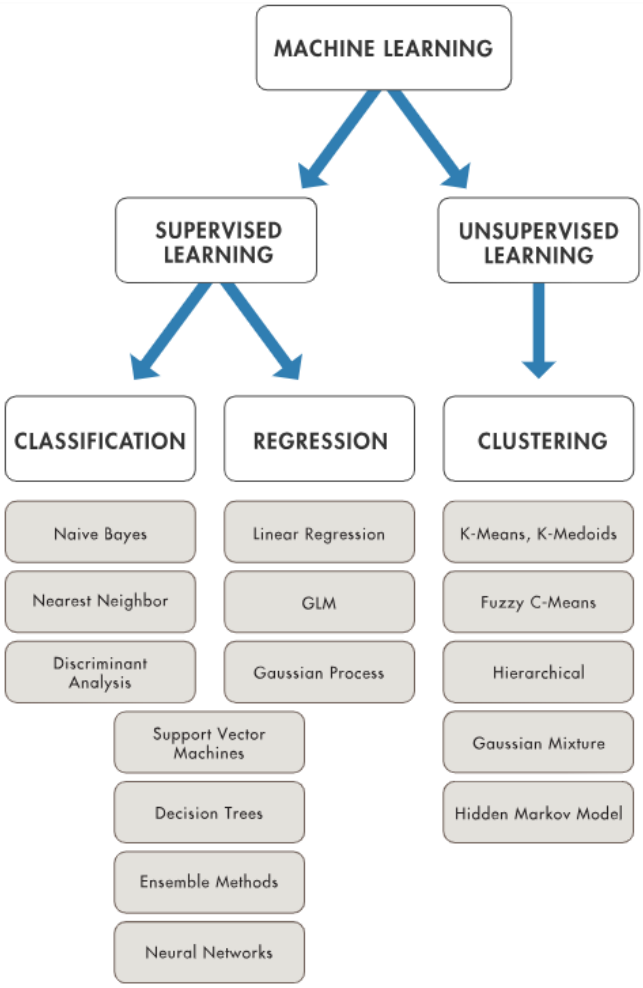

Figure 2.23 Types of ML models under supervised and unsupervised learning (MATLAB & Simulink, n.d.)

2.6.3 Reinforcement ML

Reinforcement ML adopts a trial-and-error approach that rewards the model for taking the best course of action, allowing the model to gather learned experience in deciding which actions to take (Brown, 2021).

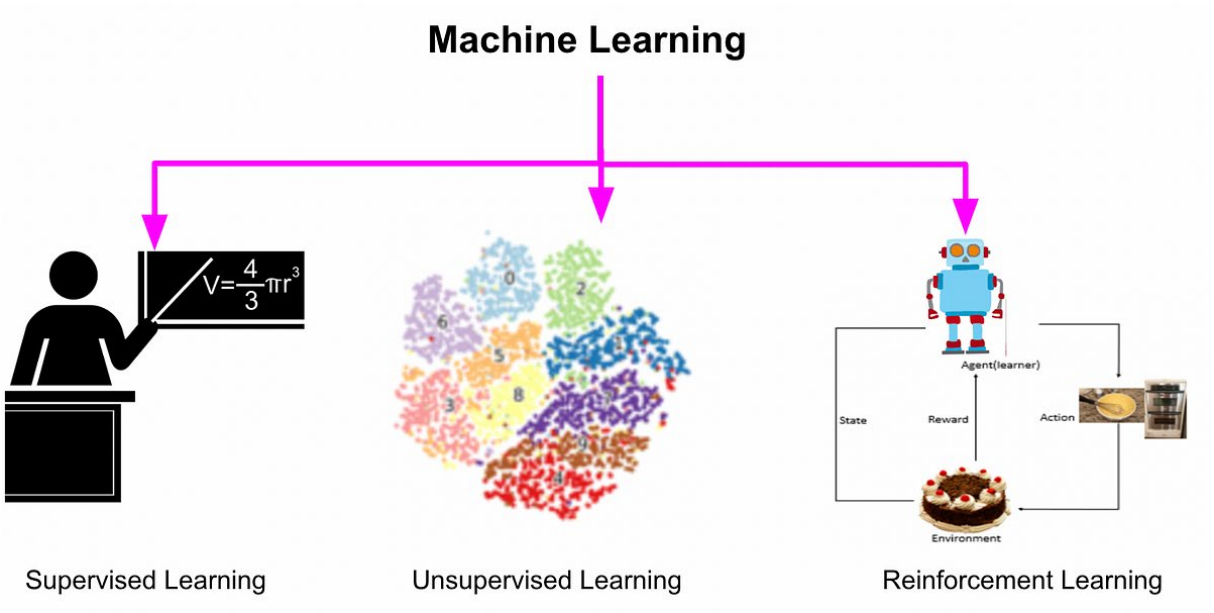

Figure 2.24 Branches of machine learning (Khandelwal, 2022)

2.6.4 Choice of ML model

There is no perfect ML model or one that is appropriate for all design problems. A large part of selecting the right ML model requires trial-and-error, and factors such as the size and data type also govern the selection process (MATLAB & Simulink, n.d.). The following Figure 2.25 below shows a useful decision tree to choose the branch of ML system appropriate for the problem.

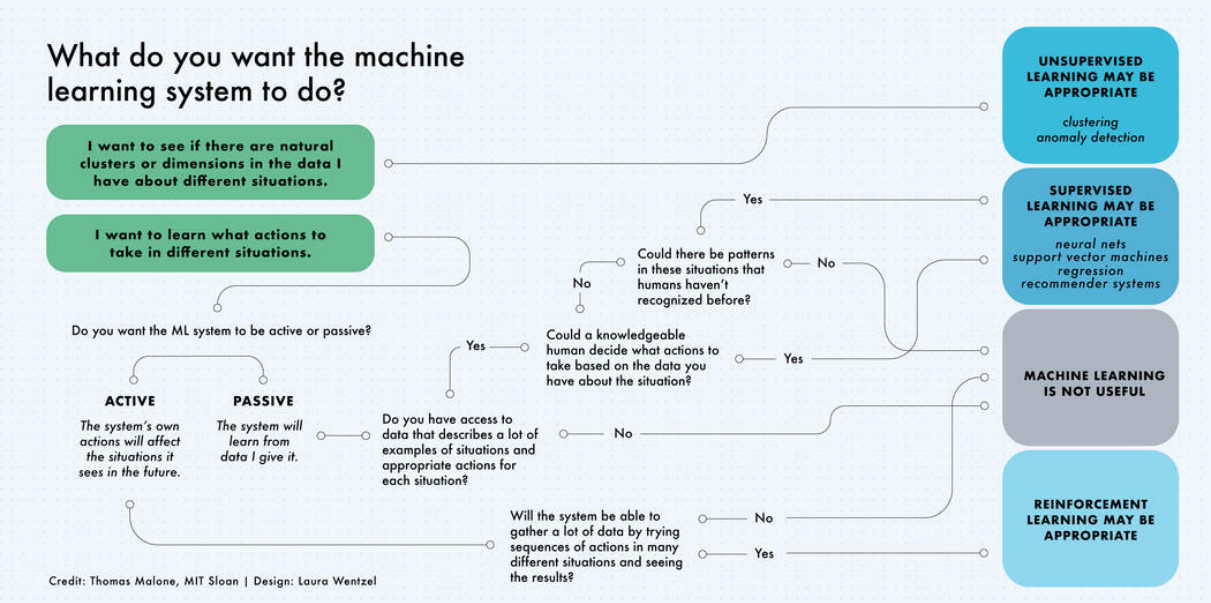

Figure 2.25 Decision tree to select appropriate ML model for the problem (Malone, 2021)

The main problem this thesis aims to tackle is determining the optimal pontoon design amid the complex loading scenarios the wind turbine experiences. To determine the optimal pontoon design, there is an aim to determine which design parameters to adjust for different loading scenarios. The ML system should also be passive, as it will receive training input data from the FEM simulations, for instance. The input data would encompass a representative set of loading scenarios at different mean wind speeds, with their respective outputs. Since the design variables involved in designing a pontoon are interdependent in a complex manner, it is practically impossible for a human to decide based on the training input data, which makes supervised ML the best option.

Among the models of supervised ML, Gaussian Process Regression (GPR), also known as Kriging, is selected as the best option for this design problem. GPR models are non-parametric in nature, which means that the data does not have to fit a normal distribution (Grant, 2021). GPR models utilise kernel-based learning methods to process uncertainty in measurements to give predictions of reasonable accuracy (Yadav et al., 2023). In this case, the design parameters of the pontoon, such as girder depth and girder web thickness, are modelled in a random Gaussian process, with covariances used in each of the input variables (MATLAB & Simulink, n.d.). The uncertainty of the predicted output is also modelled.

2.6.4.1 Kriging surrogate model

Kriging surrogate model has been a widely used technique. Kriging model consists of a linear regression model and a random function.

Ren & Xing (2023) studied the use of the active learning Kriging approach to assess wind turbine structures' cumulative fatigue damage. The active learning approach involves training machine learning (ML) models with a small initial dataset and then iteratively updating the models with “new enrichment samples” (Ren & Xing, 2023). The Kriging model is initially used to estimate fatigue damage at different wind-wave conditions, and the active learning approach is employed to update the model and reduce prediction errors.

Presently, there exists the AK-DA approach, which focuses on one location of the wind turbine structure at a time. To address this limitation, the AK-DA approach is extended to consider multiple locations, resulting in the AK-MDAmax approach (Ren & Xing, 2023). The extended approach aims to estimate the maximum cumulative fatigue damage, considering different locations in wind turbine structures. The efficiency and accuracy of the AK-MDAmax approach are demonstrated using a 15 MW floating wind turbine from the International Energy Agency (IEA) project, delivering promising accuracy with an absolute error less than 1% (Ren & Xing, 2023). As such, there is great interest to apply Kriging model to optimise the pontoon design.

2.6.4.2 Framework of ML model

For every machine learning model, it is crucial to establish a robust framework. The proposed framework is outlined as follows:

- Data Collection: Describe the data required for the model, including design parameters, environmental conditions, material properties, and performance metrics. Outline the sources of this data (e.g., existing design databases, experimental results, simulation outputs).
- Model Selection: Justify the choice of machine learning algorithms (e.g., regression models, neural networks, genetic algorithms) suitable for optimizing pontoon design.
- Model Training and Validation: Explain the training process, including data splitting, cross-validation techniques, and performance metrics for model evaluation (e.g. accuracy, error and precision)
- Optimization Framework: Develop the framework for optimization, integrating the machine learning model with design constraints and objectives (e.g., minimizing girder flange width while maximizing girder spacing so that overall, less girders are used).

2.7 Concluding remarks on literature review

The literature review has provided a comprehensive overview of the current trends and challenges in the floating offshore wind market, highlighting the critical role of semi-submersible support structures in advancing this technology. The principles for the design and analysis of semi-submersible platforms were explored, emphasizing the importance of robust structural integrity and stability. The review also delved into the specifics of stiffened plate design and the structural modelling concepts of pontoons, underscoring their significance in enhancing the durability and performance of floating platforms. Furthermore, the integration of machine learning techniques was examined, illustrating their potential to significantly increase the efficiency of the design process and optimize pontoon designs. Collectively, these insights underscore the multifaceted approach required to address the complexities of floating offshore wind technology and pave the way for more innovative and efficient solutions in the field.

The literature review also highlights several gaps in this arena:

1. There is a lack of a comprehensive framework in structural analysis to design for the pontoon based on both global and local forces. This includes a framework to establish a sound FEM model of the pontoon, complete with internal details such as stiffeners and girders.
2. Much of literature propose empirical or estimated equations to describe the behaviour of stiffened plates, particularly for estimates of ultimate strength and buckling strength. Such are insufficient to fully describe the true behaviour of the stiffened plates.
3. There is limited literature studying the potential of incorporating ML models in the design of semi-submersible structures.
4. There is limited literature related to the buckling of stiffened plates using Gaussian Process Regression (GPR) Machine Learning (ML) models.

In lieu of this literature review, the significance of this thesis becomes evident, and the subsequent chapters will now proceed to address these identified gaps and explore innovative solutions to enhance the design and efficiency of semi-submersible structures in the floating offshore wind market.

3. Methodology

This chapter details the methods used to conduct the thesis in achieving the main aim of determining the optimum design of the pontoon in an efficient way while incorporating Artificial Intelligence (AI). First, the reference wind turbine system properties are described, along with the loading conditions used for the OPENFAST simulations of the wind turbine. The load cases used in the analysis are explained. Following which, the semi-submersible platform design is discussed, with particular focus on the pontoon. This is supported by hand calculations with design codes and FEM modelling. The FEM model is studied in detail to achieve the optimum model for design. Finally, machine learning models are explored, and the best one is selected for this design problem.

3.1 IEA 15 MW reference wind turbine

In 2020, the International Energy Agency (IEA) Task 37 developed the IEA 15 MW reference offshore wind turbine. To date, it is the largest reference wind turbine available publicly in the wind energy sector (Allen et al., 2020). Such reference wind turbines are highly useful as benchmarks in exploration and pursuit of new technologies and innovations (Allen et al., 2020), especially in the context of this thesis.

The IEA 15MW reference wind turbine is studied with a floating semi-submersible support. It is mounted on the Volturn US-S steel semi-submersible platform developed by the University of Maine (Papi & Bianchini, 2022).

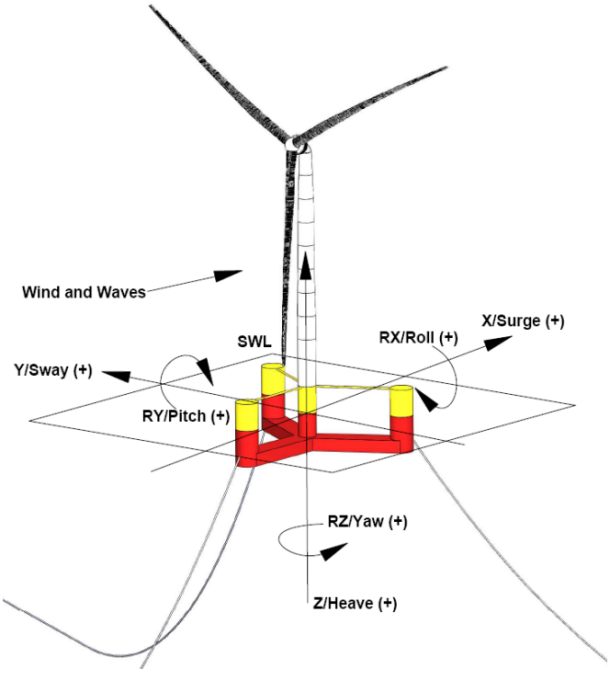

Figure 2. Floating offshore wind turbine reference coordinate system. *Figure courtesy of the University of Maine*

Figure 3.1 IEA 15 MW Wind turbine on semi-submersible (Allen et al., 2020)

The IEA 15MW OWT uses a tri-column floater that is of semi-submersible type (Papi & Bianchini, 2022). The 3 main columns are connected to the main column via 3 radial pontoons of rectangular cross section. The centre column is connected to the wind turbine tower through a transition piece.

3.1.1 System properties

As referenced from IEA, the wind turbine has the following system characteristics:

Parameter	**Value**
Turbine rating	15 MW
Hub height	150 m
Platform type	Semisubmersible
Cut-in wind speed	3 m/s
Rated wind speed	10.59 m/s
Cut-out wind speed	25 m/s

Table 3.1 System characteristics of the IEA 15MW wind turbine (Gaertner et al., 2020)

There are three representative wind speeds that capture the turbine performance throughout its operational spectrum: (a) the cut-in wind speed at 3m/s, (b) the rated wind speed at 10.59m/s, where the turbine first achieves its rated power and (c) the cut-out wind speed at 25m/s which is the highest sustained wind speed during the turbine's operation. When wind speeds exceed the rated wind speed,

the wind turbine adjusts its blade angles (feathers its blades) to maintain a constant rated power output (Wayman et al., 2006).

Of critical concern is the loads at the base of the wind turbine tower, at the rated wind speed of 10.59 m/s. This is because at the rated wind speed, the power output and thrust of the wind turbine are maximum, resulting in significant tower base loads which may lead to significant structural yielding in the semi-submersible.

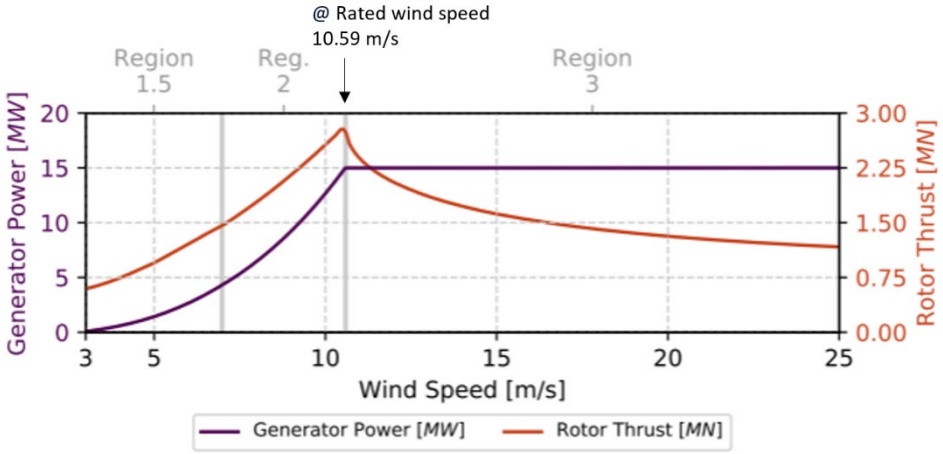

Figure 3.2 Power and thrust curve of IEA 15MW wind turbine (Gaertner et al., 2020)

3.1.2 Layout and specifications of the 15 MW steel semi-submersible platform

The layout of the semi-submersible is such that three 12.5 m diameter columns are radially spaced equidistant from the centre column, at a distance of 51.75m from the vertical axis of the centre column.

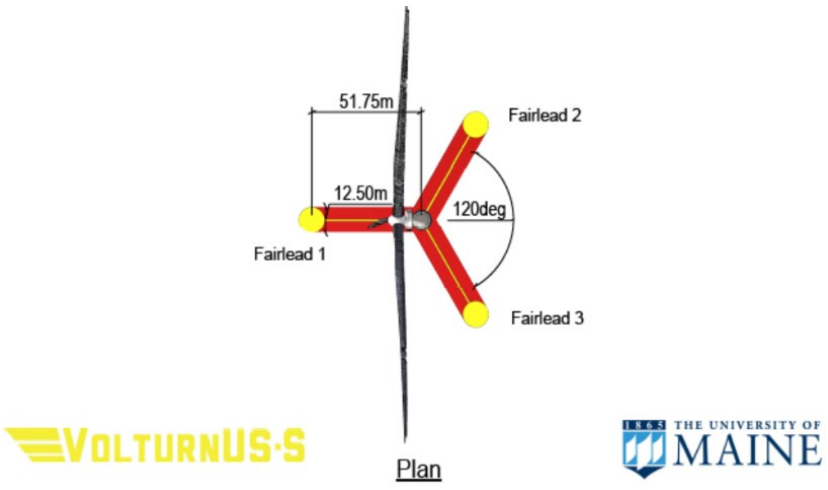

Figure 3.3 Plan view of IEA 15MW wind turbine (Allen et al., 2020)

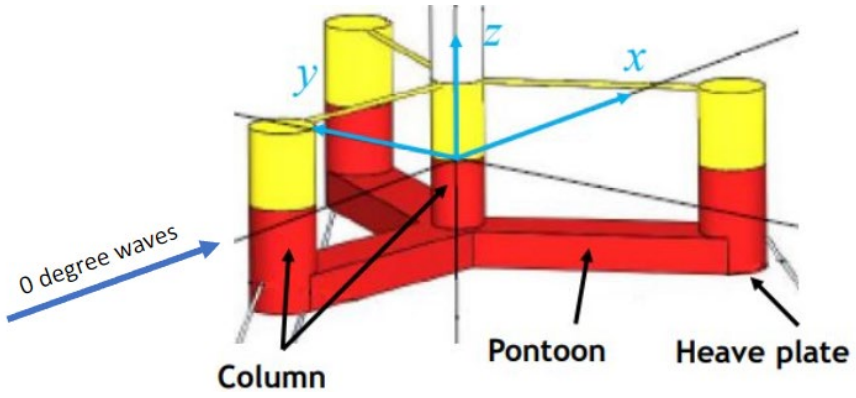

Figure 3.4 15MW steel semi-submersible platform (Sandua-Fernández et al., 2022; Allen et al., 2020)

The global dimensions of the 15 MW steel semi-submersible are as shown:

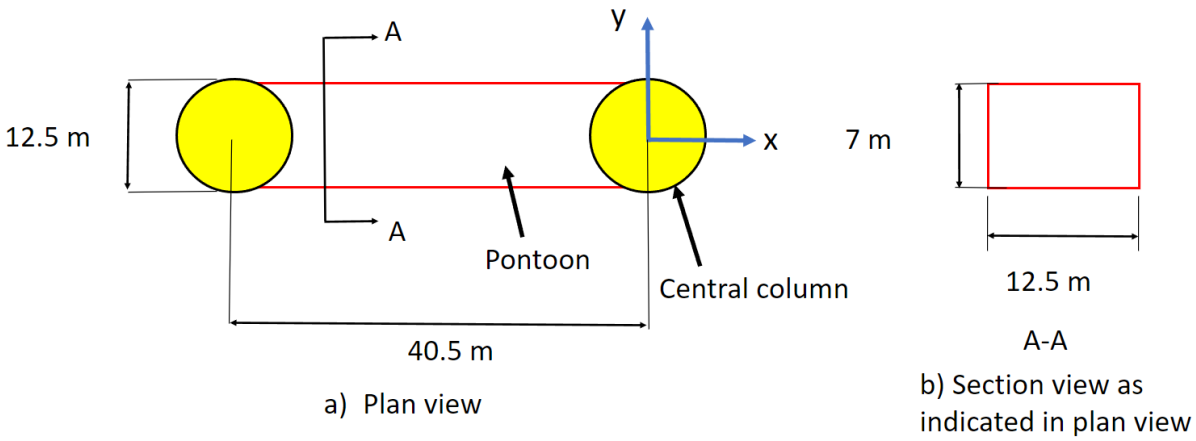

Figure 3.5 Global dimensions of semi-submersible platform

3.2 Loading conditions in OPENFAST

OPENFAST was used to generate the global response analysis results for representative wind and wave conditions. In OPENFAST, turbulent wind conditions from mean horizontal wind speeds of 3m/s to 25m/s, with increments of 1m/s, were run with binary TurbSim. 3m/s and 25m/s are the cut-in and cut-off wind speeds of the wind turbine respectively.

3.2.1 Wave conditions

The wave conditions are as follows:

Wave condition	Value	Definition
Wave model	JONSWAP/Pierson-Moskowitz spectrum (irregular)	This wave model assumes a deep sea and a fully developed sea state (Bai and Jin, 2016)

Wave condition	Value	Definition
Wave Stretching Model	No stretching	Model for stretching incident wave kinematics to instantaneous free surface
WaveTMax	4000 seconds	Analysis time for incident wave calculations. First 600 seconds are “removed” as this is noise in data, and to remove the transient effect caused by the start-up of the wind turbine.
WaveDT	0.25 seconds	Time step for incident wave calculations
WaveHs	2 metres	Significant wave height of incident waves
WaveTp	10 seconds	Peak spectral period of incident waves

Table 3.2 Wave conditions in OPENFAST simulations

3.2.2 Initial conditions of wind turbine

The initial conditions must be input so that negative damping of the wind turbine will not occur. Negative damping will cause the control system of the turbine to stall, resulting in errors in OPENFAST analysis.

The initial conditions were referenced from the technical report for the NREL offshore 5MW wind turbine. A linearization analysis was conducted, based on the blade-pitch sensitivity for the wind turbine producing 5MW of power at each wind speed, at a constant rotor speed of 12.1 rpm (Jonkman et al., 2009). A series of FAST simulations were executed at given steady and uniform wind speeds with pitch and torque control enabled (Jonkman, 2014). Each simulation was conducted long enough to ensure all transient behaviour had died out, then the steady-state values were recorded.

The initial conditions of the wind turbine are as follows:

Mean horizontal wind speed (m/s)	Blade pitch angle (deg) Same for all 3 blades	Rotor speed (rpm)
3 (cut-in wind speed) to 11[1]	1	7.55[2]
12		
13		
14	8.70	12.1
15	10.45	
16	12.06	
17	13.54	
18	14.92	
19	16.23	
20	17.47	
21	18.70	
22	19.94	
23	21.18	
24	22.35	
25 (cut-off wind speed)	23.47	

Table 3.3 Initial conditions of the wind turbine

3.2.3 Parked load case

Offshore wind turbines are elaborate structures whose dynamics can change greatly due to variations in operating conditions such as rotor speed and pitch angle, as well as changes in environmental conditions like wind speed, wave height, and wave period (Shirzadeh et al., 2014). In particular, during parked conditions, the turbine is subjected to significant forces, making it a critical area of study to ensure the safe operation of the turbine (Sakib & Griffith, 2022).

A parked wind turbine has its blades feathered and put parallel to the wind direction to keep the aerodynamic loads to a minimum (Jiang et al., 2013). During parked conditions when aerodynamic damping forces are reduced, the response to wave actions with frequencies near the structural resonance frequencies can be significantly amplified. (Shirzadeh et al., 2014).

Furthermore, wind turbines are designed to withstand environmental events with a return period of 50 years (Jiang et al., 2013). Hence, the wind turbine is considered parked in the simulations, so as to correspond to the maximum significant wave height Hs and peak wave period Tp with a probability of occurrence being 50 years at the site where the turbine is to be located.

[1] 10.59 m/s is the rated wind speed. 11m/s was chosen to represent the rated wind speed as it was an integer.
[2] 7.56 rpm is the maximum rotor speed of IEA 15MW wind turbine.

3.3 Semi-submersible platform design

With reference from the design methodology of Wang et al. (2023) for steel semi-submersible platform design, a flowchart showing the design process of determining the detailed design of the semi-submersible is developed.

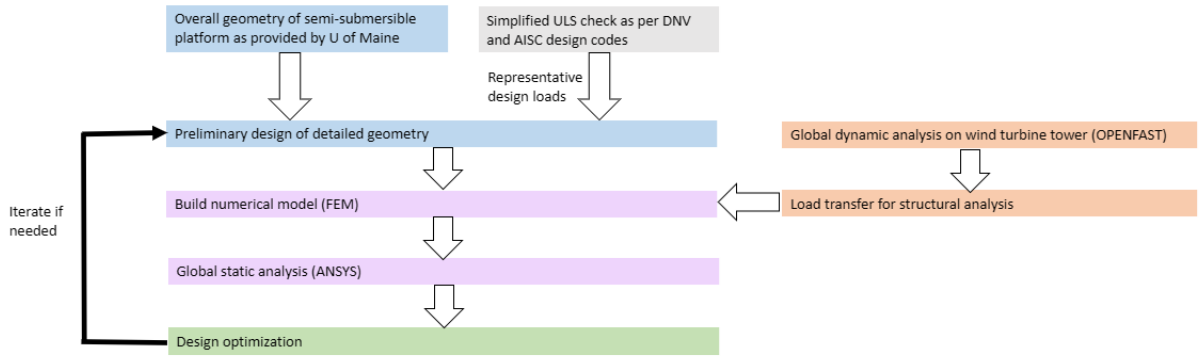

Figure 3.6 Flowchart of semi-submersible platform design

3.3.1 Material properties of semi-submersible

The material properties of the semi-submersible are not explicitly mentioned in the documents under IEA or U of Maine. It is only mentioned that the semi-submersible is made of steel. A numerical study and analysis (Wang et al., 2023) of the Technical University of Denmark (DTU) 10 MW reference wind turbine shows the following material properties of the steel semi-submersible platform. As a reference, this set of material properties will be used for this thesis. From DNV-OS-C101, Section 4, Table D1, S235 steel is classified as Normal strength steel (DNV, 2011).

Parameter	Value
Density	7850 kg/m^3
Yield strength	235 MPa
Young's modulus	2.11× 10^5 MPa
Poisson's ratio	0.3

Table 3.4 Material properties of semi-submersible platform

3.3.2 Load transfer in the pontoon

It is essential to identify the load path in the pontoon. The loads are first transferred to the blades of the turbine, then to the turbine tower, through the transition piece to the central column and then transferred to the horizontal pontoons. Finally, the loads are transferred from the horizontal pontoons to the side columns.

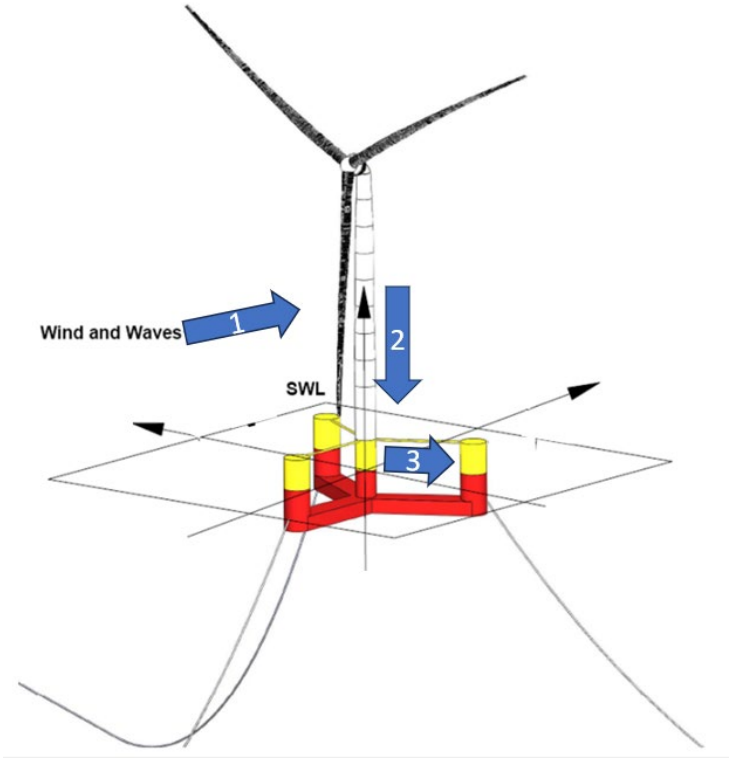

Figure 3.7 Load path direction, image modified from (Allen et al., 2020)

In terms of the detailed design in the pontoon, it comprises of a framework of girders and stiffeners. The loads are transferred from the hull plate to the webs of the longitudinal girders, and through beam action transfer the loads to the transverse girders (Bai & Jin, 2016).

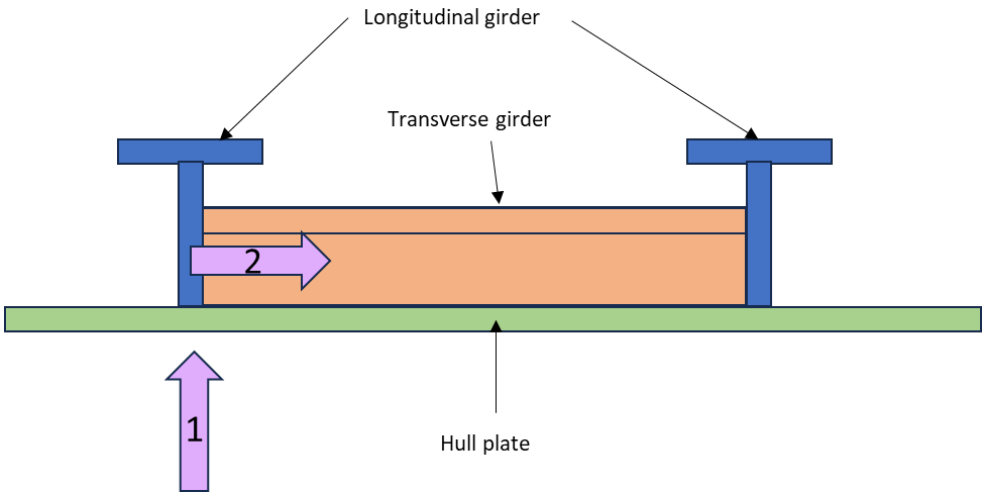

Figure 3.8 Load path in bottom part of pontoon cross section

3.3.3 Load effects on stiffener design

Since the detailed internal design of the semi-submersible support structure is unavailable, a design is proposed. The load effects on the pontoon first need to be considered. The loads acting on the cross section of the hull are affected by the motions and accelerations in heave and pitch (Li et al., 2023). When heave and pitch motion resonance occur, the structural loads effects increase. In addition, critical wave periods induce major splitting or prying force on the hull columns. Hence, the girder and stiffener layout in the pontoon should account for these two factors (Li et al., 2023):

1. Heave and pitch motion resonance cause an increase in structural load effect on the cross section of the hull.
2. Critical wave periods result in major splitting or prying effects on the hull columns.

3.3.4 Naming of girders and stiffeners in pontoon

The typical cross section of a ship hull (Ostapenko, 1981) comprises of a longitudinal girder, longitudinal stiffener, transverse rib and longitudinal bulkhead.

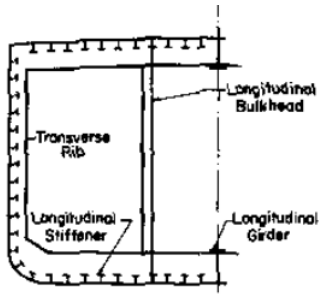

Figure 3.9 Typical cross section of ship hull (Ostapenko, 1981)

However, such terms can be confusing, especially for a structural engineer when looking at the longitudinal stiffener and longitudinal girder. To ease the confusion and to align with structural engineering terms, the following naming convention is proposed for the pontoon.

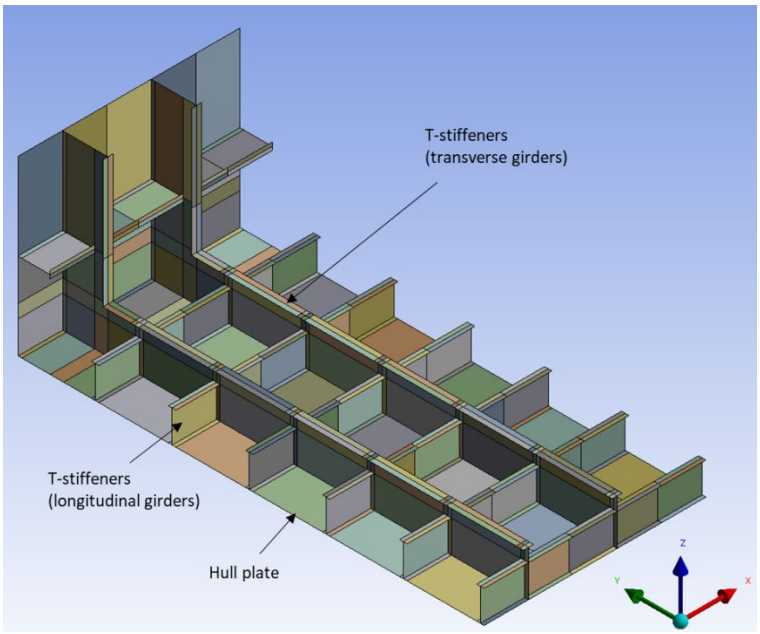

Figure 3.10 Naming of girders and stiffeners in pontoon

3.3.5 Preliminary design of pontoon – hull thickness

In the early stage of the preliminary design of the pontoon, a uniform hull plate thickness of 30 mm was considered. This was referenced from similar studies done by Ivanov et al. (2023) where a simplified model of the column and pontoon were developed with no reinforcement, bar the bulkheads. In another study on semi-submersible hulls of floating wind turbines by Li et al. (2024), a plate thickness of 50mm was assumed for the hull structure.

Eventually, a hull thickness of 50 mm was used after verifying with hand calculations for bending stress, since it is assumed that the main bending resistance is provided by the hull. The tower base forces and moments from OPENFAST Turbsim simulations at 11m/s mean wind speed were resolved and applied at the hull cross section. Such was chosen because 11m/s is close to the turbine's rated wind speed of 10.59m/s. The hull thickness was determined via verifying the hull cross section as a box cross section subjected to bending as per DNV-OS-C101, DNV-ST-0119 and AISC 9th Edition. An additional shear stress check was performed to further validate the chosen hull thickness.

Detailed calculations be found in the Appendix B – Detailed calculation for hull plate thickness.

3.3.6 Preliminary design of pontoon – girder and stiffener layout in pontoon

As there is no publicly available information on the girder and stiffener layout in the pontoon from IEA or other relevant sources, it must be proposed in this thesis. The stiffeners in the pontoon do not provide bending stiffness but help to prevent buckling of the hull structure.

3.3.6.1 Girder section profile and layout

The girder layout in the horizontal pontoons were based on literature from Park and Choung (2023). They studied the structural design of a substructure supporting a 10MW offshore wind turbine. It can be observed that in the pontoon cross section, there is use of T-profile girders for both the longitudinal and the transverse girders.

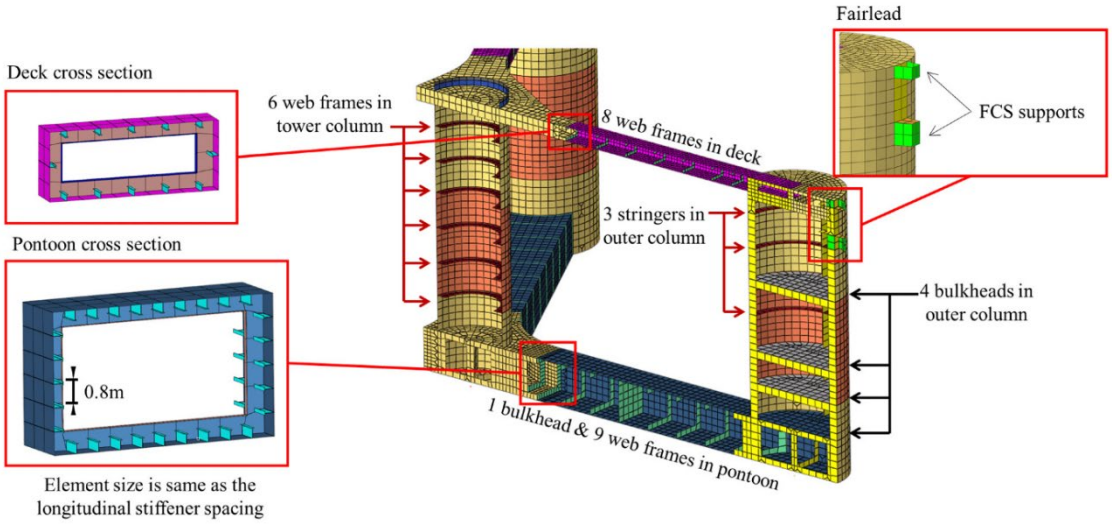

Figure 3.11 Stiffener design in Park and Choung's study (2023)

A T-beam has a cross section with a T shape. The top flange of the T-beam serves as a compression member resisting compressive forces, while the web withstands shear stress (Wikipedia, 2023). One drawback of the T-beam in comparison to the I-beam is the absence of a bottom flange to resist tensile forces (Benmusa, 2020). Yet, in ship hull design, T-beams are favoured as they can be welded to the hull plate, giving the role of tension flange to the hull plate.

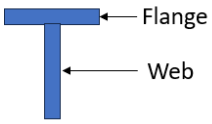

Figure 3.12 Cross section of T-beam

It is also noted from Park and Choung's study (2023) that longitudinal girders tend to be smaller in size than the transverse girders. Furthermore, Bai and Jin (2016) highlighted that the main frame system in hull girders typically comprise of "relatively closely spaced" longitudinal girders along with "more widely spaced" heavier transverse girders. However, there also exist literature that study hull frameworks where the longitudinal girders are larger in size as compared to the transverse girders. In a study of a pontoon under boat attack, the cross section of the pontoon had larger longitudinal girders

termed “stiffeners”, along with smaller transverse girders (Li et al., 2022). Hence, this thesis will cover both configurations before concluding which is optimal in the context of the thesis.

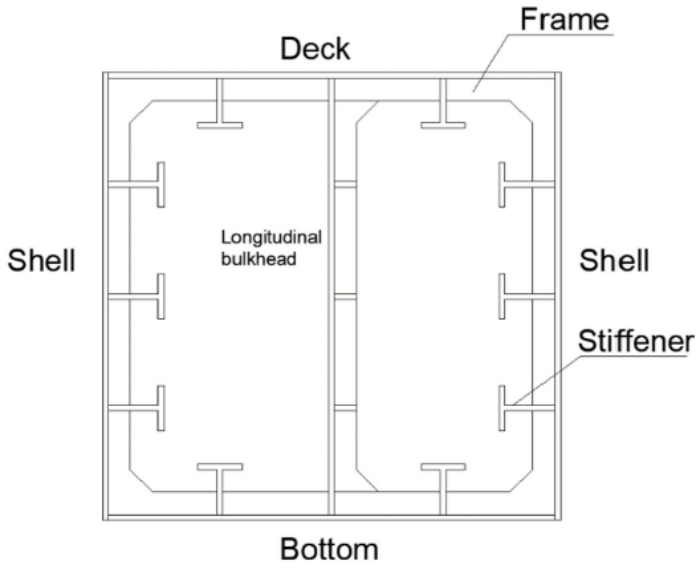

Figure 3.13 Cross section of pontoon (Li et al., 2022)

3.3.6.2 Type of stiffener

As per DNV-RP-C201, Section 7.1 (2010), there are 2 types of stiffeners classified based on their structural purpose: continuous stiffener and simple supported stiffener (sniped stiffener).

The continuous stiffener, connected to the hull frame and the girders, contributes its full moment capacity to the global strength of the hull structure (Hacihamud, 2022) (DNV, 2010).

Figure 3.14 Continuous stiffener (DNVGL-PS, n.d.)

Sniped stiffeners are sniped at the intersection with the hull frame and the girders. This makes the intersection point a simple support. Sniped stiffeners do not contribute to the global strength of the hull structure, as they only prevent buckling of the plate between the girder spans (Hacihamud, 2022). In this thesis, the stiffener is treated as continuous.

Figure 3.15 Sniped stiffener (DNVGL-PS, n.d.)

3.3.7 Proposed designs for pontoon

This section will cover three proposed designs for the pontoon. Design 1 considers a larger longitudinal girder, and relatively smaller transverse girder. Design 2 swaps the girder profile sizes in Design 1 for the longitudinal and transverse girders, while considering relatively widely spaced transverse girders. Meanwhile, Design 3 upsizes the longitudinal girder in Design 2, while keeping the transverse girders closely spaced as in Design 1 and spacing the longitudinal girders even closer than in Design 1.

Design	Longitudinal girder size	Longitudinal girder centre-centre spacing on top/bottom face of hull	Longitudinal girder centre-centre spacing on side face of hull	Transverse girder size	Transverse girder centre-centre spacing
1	Tbar885x200x14x35	2.5 m	1.75 m	Tbar425x120x12x25	0.9 m
2	Tbar425x120x12x25	2.5 m	1.75 m	Tbar885x200x14x35	2.25m
3	Tbar625x150x12x25	1.5625 m	1.75 m	Tbar885x200x14x35	0.9 m

Table 3.5 Summary of proposed layouts for pontoon

Design	Longitudinal girder size	Longitudinal girder centre-centre spacing on top/bottom face of hull	Longitudinal girder centre-centre spacing on side face of hull	Transverse girder size	Transverse girder centre-centre spacing
1	Bigger	Wider	x[3]	Smaller	x
2	Smaller	x	x	Bigger	Wider
3	Smaller	Narrower	x	Bigger	x

Table 3.6 Summary of comments for proposed layouts for pontoon

3.3.7.1 Section profile of girders

The section profiles of the girders were referenced from SESAM's semi-pontoon workshop (DNV GL, 2015). The section properties were obtained from SESAM GeniE's section profile database, and appended in Appendix C – Section profile properties of girders.

3.3.7.2 Design 1

For Design 1, the transverse stiffeners were spaced at 0.9m centre-to-centre spacing, as referenced from Gaspar et al. (2014)'s study on stiffened plates. The longitudinal stiffeners were spaced at 2.5m centre-to-centre spacing for the bottom face of the pontoon, and 1.75m centre-to-centre spacing for the side face of the pontoon. These dimensions were considered based on the 40.5m length of the pontoon, its 12.5m width and 7m height.

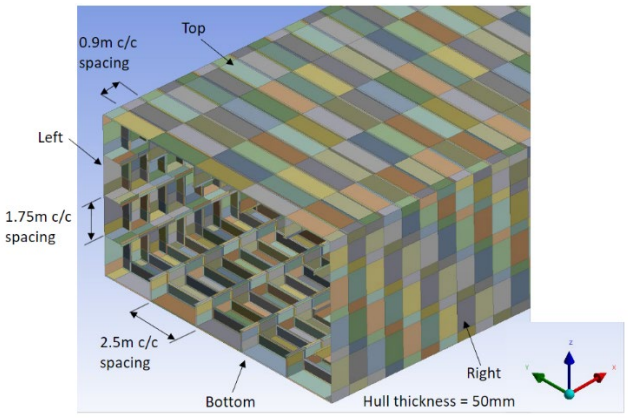

Figure 3.16 Stiffener and plate dimensions, and location with respect to hull (Design 1)

[3] "x" indicates no comment.

3.3.7.3 Design 2

In the Recommended Practice for Structural Design of Offshore Ships, DNV-RP-C102, section 6.2 highlights that stiffeners are usually oriented longitudinally (i.e. along the pontoon length), because under compressive forces, the longitudinal direction is the most dominant direction (DNV, 2002). Larger girders, placed in the transverse direction and spaced at wider intervals, would then support the stiffeners (DNV, 2002). This concept forms the basis of Design 2.

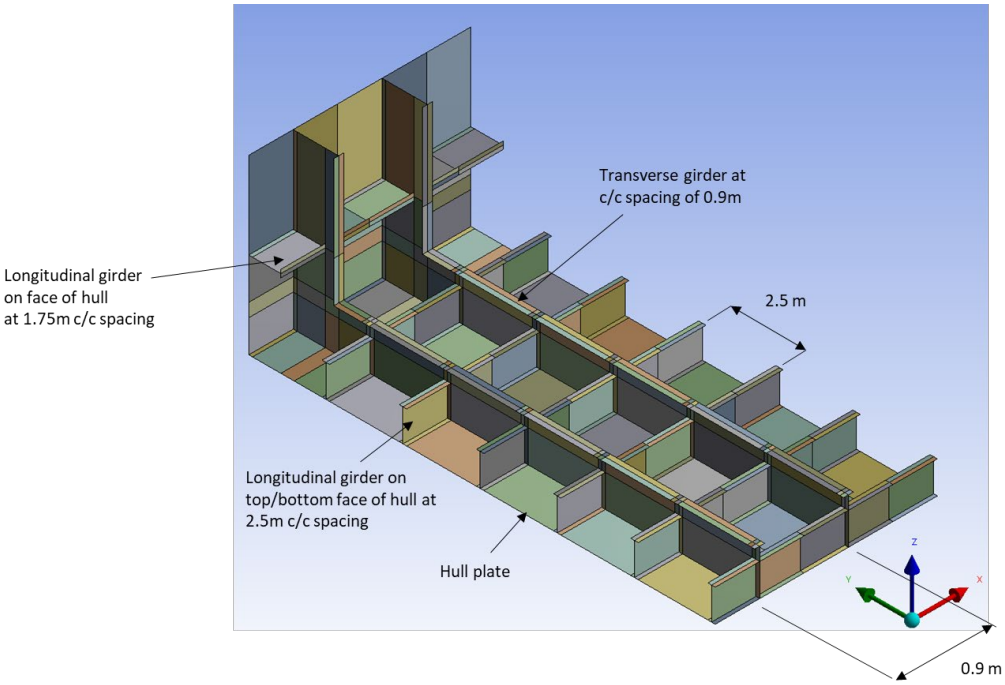

Figure 3.17 Design 2 layout

3.3.7.4 Design 3

Design 3 is a variation of both Designs 1 and 2. Design 3 is proposed to study the relationship of transverse girder size, its spacing and longitudinal girder size and its corresponding spacing.

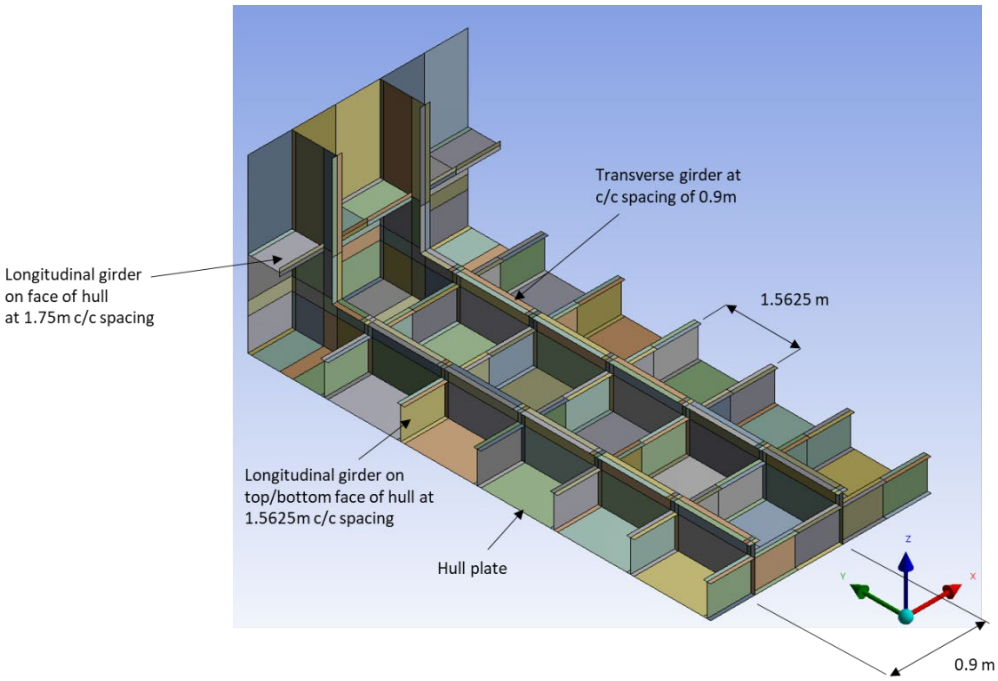

Figure 3.18 Design 3 layout

3.3.8 Verify stiffener layout as per DNV-RP-C201

The next step would be to verify the stiffener layout proposed. Beginning with Design 1, the procedure to verify the stiffener layout, with the basis of DNV-RP-C201 as follows:

1) Analyse one portion of the stiffened panel as idealised, as per DNV-RP-C201
2) By tributary area, distribute the applied loads at rated wind speed (use 11m/s)
3) Check hull plate thickness: Use Roark's theory of stress and strain to check if the hull thickness of 50mm OK?
4) Check stiffened plate 50mm thickness OK for shear stress as per DNV-RP-C201, section 7.6
5) Check stiffener axial capacity as per DNV-RP-C201, Section 7.2
6) Check general buckling of stiffeners as per DNV-RP-C201, Clause 7.5.1
7) Shear check for stiffener, as per DNV-RP-C201, Section 7.8
8) Check stiffener spacing as per DNV-RP-C201, equation 7.13

Detailed calculations can be found in Appendix D – Detailed calculation for stiffener layout.

3.3.8.1 Idealised stiffened panel under consideration

The figure below shows the idealised stiffened panel under consideration, as referenced from DNV.

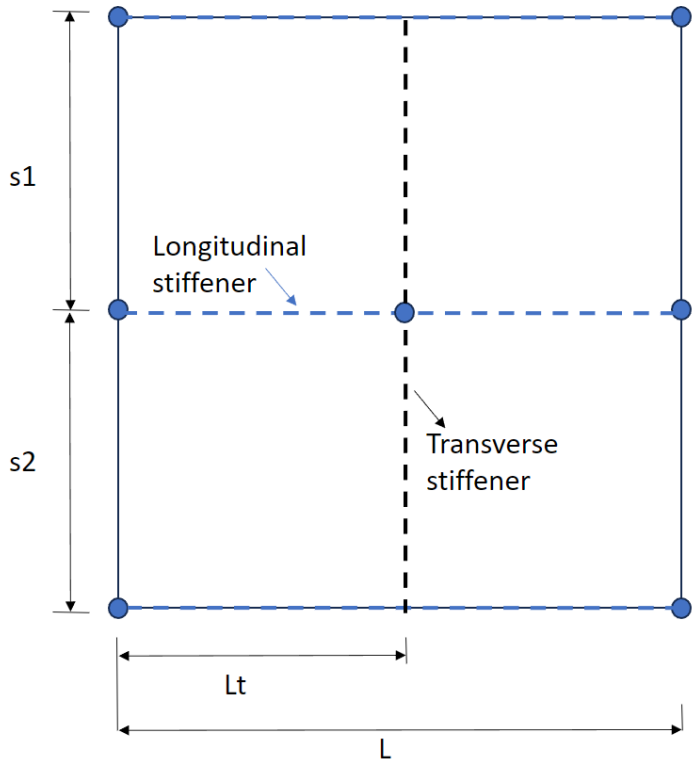

Figure 3.19 Idealised stiffened panel (DNVGL-PS, n.d.)

Where:

- S1 and s2 refer to the centre-centre spacing between longitudinal stiffeners
- Lt is centre-centre spacing between transverse stiffeners

3.3.8.2 Assumptions of boundary conditions of stiffened plates

The boundary conditions of the loaded edges of the stiffened plates are assumed as follows (Bai & Jin, 2016):

- Boundary edges maintained straight due to the presence of supporting structures.
- Due to yielding, the boundary conditions of the plates are assumed as simply supported.

These assumptions are made to simplify the problem and lead to conservative but sufficient results. Furthermore, the boundary conditions do not have significantly impact the ultimate strength (Bai & Jin, 2016).

The actual restraints on the stiffened plates are complex. To simplify the problem and create a calculation model that is close to the actual boundary conditions, the plate is assumed to be simply supported on all sides. This avoids any out-of-plane displacement of the plate (Wang et al., 2016).

3.3.8.3 Distribute load by tributary area

At mean wind speed of 11m/s (close to rated wind speed of 10.59m/s), the forces transferred from the tower base to the pontoon are:

Force / moment type *axis orientation as per ANSYS model	Value
Fx (kN)	5.64×10^3
Fy (kN)	-7.77×10^2
Fz (kN)	-2.43×10^4
Mx (kNm)	1.16×10^5
My (kNm)	6.72×10^5
Mz (kNm)	2.49×10^4

Table 3.7 Force and moment at mean wind speed of 11m/s

These loads are distributed to the idealised stiffened panel by area, as a simple estimate. The area ratio between the actual full stiffened panel of the pontoon to the idealised stiffened panel is used as the load factor. This load factor is applied to all the aforementioned loads transferred from tower base to pontoon.

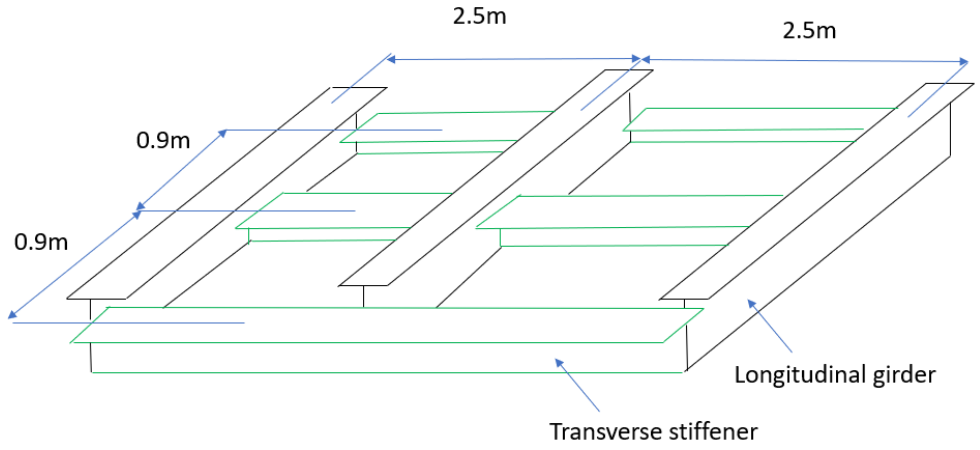

Figure 3.20 Idealised stiffened panel

Area of entire top or bottom face of hull (m^2)	Area of idealised stiffened panel (m^2)	Scale factor
40.5 x 12.5 = 506.25	9	506.25÷9 = 56.25

Table 3.8 Scale factor of loads based on area ratio

Loads on idealised stiffened panel	
Force / moment type *axis orientation as per ANSYS model	Value
Fx (kN)	100.27
Fy (kN)	-13.81
Fz (kN)	-432
Mx (kNm)	2062.22
My (kNm)	11946.67
Mz (kNm)	442.67

Table 3.9 Load distribution to idealised stiffened panel

3.3.8.4 Check hull plate thickness with Roark's theory of stress

Assume the idealised stiffened panel as simply supported all sides, the Roark's theory of stress was incorporated to validate the stress check at centre of the plate. The downward force Fz was applied as a pressure load onto this plate. Detailed calculations can be found in the Appendix D – Detailed calculation for stiffener layout.

3.4 FEM modelling

This section deals with the FEM modelling of the pontoon, and the methodology involved.

3.4.1 FEM Software: Ansys

The FEM software used in this thesis is Ansys Mechanical, known for its FEA solvers designed to tackle structural engineering challenges. In Ansys Mechanical, static analysis focuses on examining how a structure or component responds to static loads, reaching equilibrium without accounting for time-dependent effects (ELEATION, 2023). The suite's FEA solvers allow for the customization and automation of solutions to structural mechanics problems, enabling the parameterization of multiple design scenarios for comprehensive analysis (Ansys, 2024).

3.4.2 Constitution of the FEM model

The ANSYS software was used to develop the finite element model of the pontoon. The wind turbine was not included in this model. Nevertheless, the weight of the wind turbine (i.e. the tower, blades

and nacelle) and the environmental loads that acted on the wind turbine were equivalently applied as tower base loads to the pontoon.

3.4.3 Material properties of steel in ANSYS

The figure below shows the material properties of S235 steel used in the Ansys model.

Properties of Outline Row 3: Structural Steel

	A	B	C	D	E
1	Property	Value	Unit		
2	Material Field Variables	Table			
3	Density	7850	kg m^-3		
4	Isotropic Secant Coefficient of Thermal Expansion				
5	Coefficient of Thermal Expansion	1.2E-05	C^-1		
6	Isotropic Elasticity				
7	Derive from	Young's M...			
8	Young's Modulus	2.11E+11	Pa		
9	Poisson's Ratio	0.3			
10	Bulk Modulus	1.7583E+11	Pa		
11	Shear Modulus	8.1154E+10	Pa		
12	Strain-Life Parameters				
20	S-N Curve	Tabular			
24	Tensile Yield Strength	2.35E+08	Pa		
25	Compressive Yield Strength	2.35E+08	Pa		
26	Tensile Ultimate Strength	4.6E+08	Pa		
27	Compressive Ultimate Strength	2.35E+08	Pa		

Figure 3.21 Material properties in Ansys model

3.4.4 Choice of element type in FEM

The shell element is chosen to simplify the FEM of the 3D structure of the pontoon. Shell elements are 2D approximations of the 3D geometry, storing the thickness of a body as a physical property (Ferris, 2020). In the Ansys FEM, the thickness of each element was defined as a physical section property, as shown in the figure below.

The aim is to reduce the computational cost when performing FEA in Ansys, while ensuring all elements are as well shaped as possible to enhance convergence and accuracy (Vedvik, 2021). Hence, the shell element is chosen. The nodes of the shell element have both displacement and rotational degrees of freedom (Vedvik, 2021). Another benefit of the shell element is that they avoid issues of shear locking (Roehm, 2017). Shear locking occurs in first-order 3D elements that experience bending. Due to the numerical formulation of these elements, parasitic shear may result, leading to shear strains that do

not actually exist, and as such, these elements would showcase overly stiff behaviour in bending modes (Vedvik, 2021).

Shell elements are applicable to the geometry of the bottom pontoon, since the hull and stiffeners are thin-walled with a length far greater than its thickness, rendering the shear deformation as negligible (Ferris, 2020). Furthermore, since the shell element has to sustain transverse and plane loading, the stress state must allow for transverse shear stress and plane stress. Hence, it is sufficient to enforce the classical stress assumption that $\sigma_{33} = 0$, where the "3" direction is normal to the mid-surface of the shell element (SesamX, 2020).

Modelling the beam-column as shell element and beam element give more or less same result, as verified by the study done by (Li et al., 2017) on steel beam-columns under axial compression. Hence, it is a sound assumption to model the pontoon as a shell element.

3.4.5 Mesh size and mesh order

Mesh size refers to the characteristic length of the edge of the element, while mesh order details the shape function used to compute the element displacements (Ferris, 2020).

The hexahedral element (aka brick element) was chosen for the mesh size because they generally lead to more accurate results at lower element counts than tetrahedral elements (Ferris, 2020). Furthermore, the geometry of the stiffeners and the hull faces are regular in rectangle shape, so the hexahedral element is more appropriate to model the element displacements. Hence, during the meshing process, tetrahedral elements were avoided as much as possible.

For the mesh order, first-order and second-order elements are commonly used. First-order elements only have corner nodes and linear displacement between the nodes. On the other hand, second-order elements have additional mid-side nodes between the corners, and displacements are calculated quadratically. For the preliminary FEM, it is sufficient to consider first-order elements.

In general, a smaller mesh size leads to a higher number of elements in the FEM, leading to longer run times and more accurate results (Ferris, 2020). The figure below shows the difference between first-order and second-order tetra and hex elements.

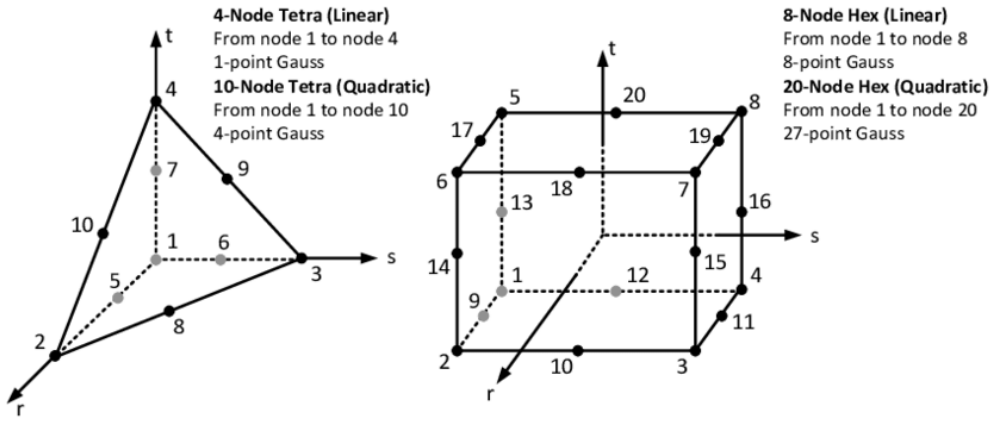

Figure 3.22 1st and 2nd order tetra and hex elements (Albino et al., 2019)

3.4.5.1 Quadrilaterial face mesh

In the Ansys model, an all-quadrilateral face mesh was opted, as much as possible, with some inevitable triangle meshing created.

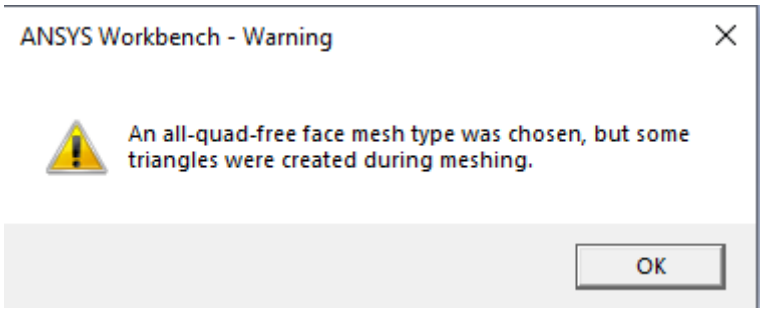

Figure 3.23 Quadrilateral face mesh

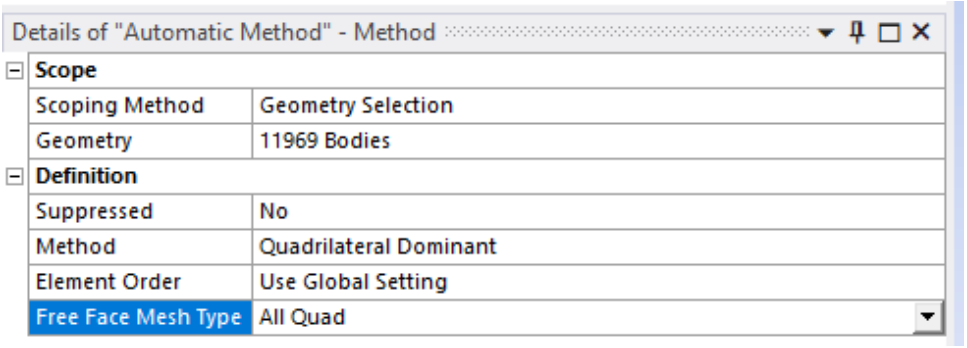

Figure 3.24 Quadrilateral mesh element size imposed on all elements

3.4.5.2 Supressed contact analysis

It is important to ensure that all the mesh elements have proper and continuous meshing across all faces of the pontoon. "Contacts" was suppressed in the FEM, as contact analysis is not utilised in the FEM.

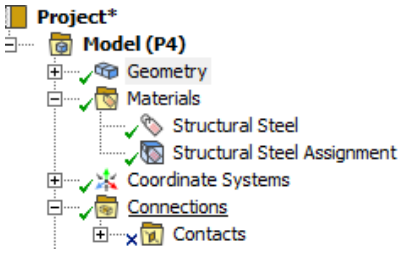

Figure 3.25 Contacts suppressed in ANSYS FEM

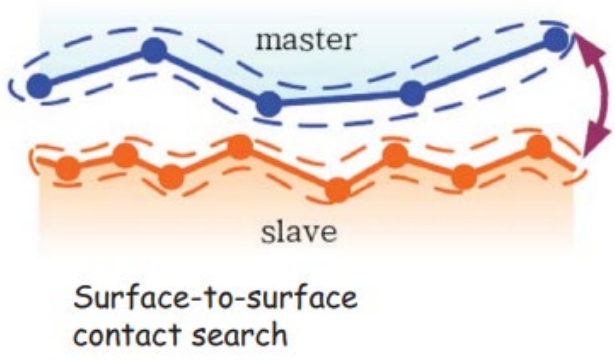

Figure 3.26 Contact analysis between two adjacent connecting surface (Kim, n.d.)

The penalty method is used in contact analysis, where an opposing contact force is applied proportional to the penetration, when penetration between two surfaces in contact reaches the "penalty". The figure below illustrates this.

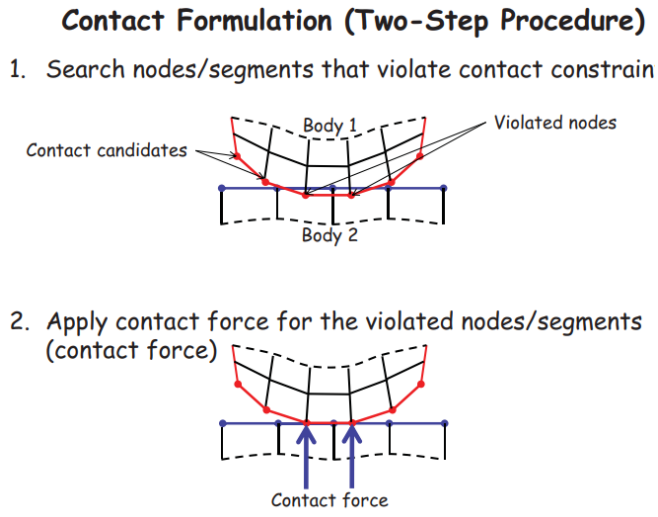

Figure 3.27 Contact analysis (Kim, n.d.)

Moreover, in this FEM, as all the elements are modelled as shell elements, using contact analysis on a 2D line element is not appropriate. Further, as the FEM comprises of several surfaces in contact, the contact analysis would not be time-efficient on the computation as the penalty method would have to be applied on all surfaces in contact. Hence, meshing without contact analysis was executed.

3.4.5.3 Poor meshing, good meshing

Previously, when the structure was modelled in entire length instead of by parts, the meshing that was automatically generated in ANSYS was irregular. Figure 3.28 below shows poor meshing between the transverse stiffener (small one) and the longitudinal stiffener, because the web of the longitudinal stiffener was not divided at the flange edge of the transverse stiffener. When the mesh is distorted and/or curved, the quadrilateral element is not planar, so the mesh is bad. Poor meshing prevents stress from distributing accurately across elements.

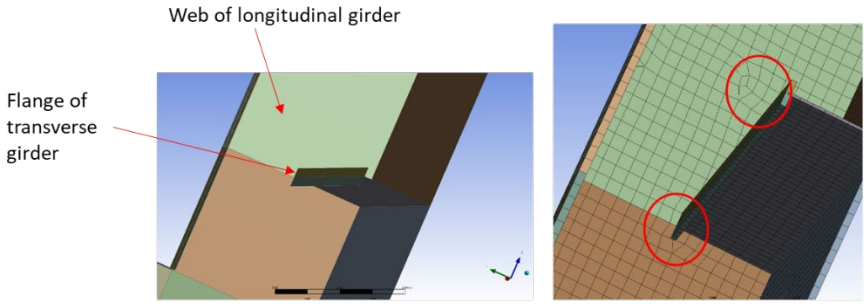

Figure 3.28 Poor mesh

On the contrary, when the longitudinal stiffener is divided at flange edge of transverse stiffener, there is good and continuous mesh, as shown in Figure 3.29.

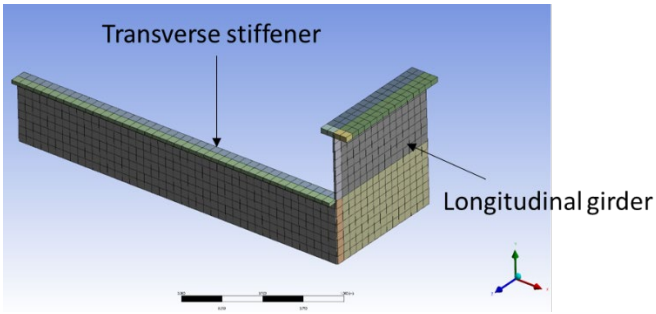

Figure 3.29 Good mesh

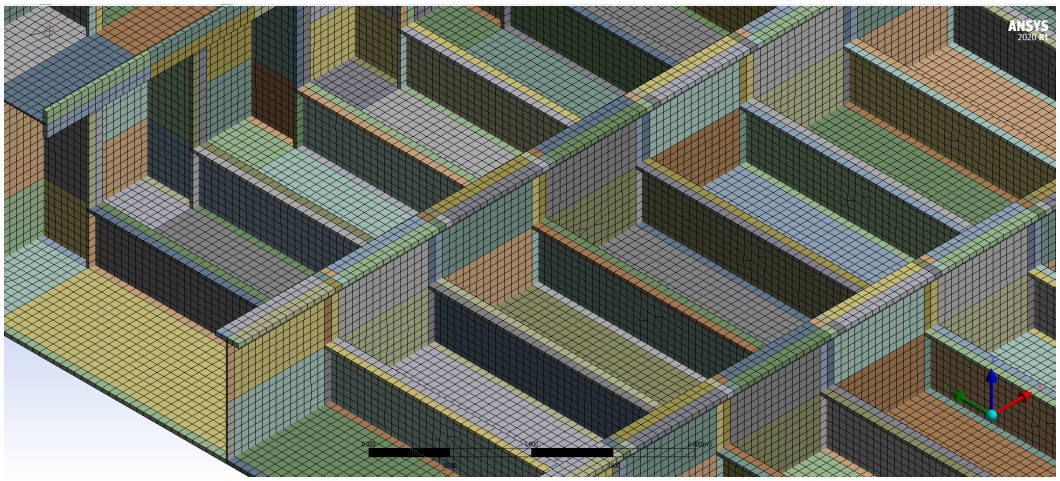

Figure 3.30 Isometric view of bottom face of pontoon, showing good contact between mesh elements

3.4.5.4 Thickness definition in Ansys

n DesignModeler, the elements are modelled as thin surfaces with zero thickness. The thicknesses of all elements were then specified in Ansys Mechanical. This is to ease the modelling process of such an intricate structure like that of the pontoon.

Sketching | Modeling

Details View

Direction	Normal
Extent Type	Fixed
FD1, Depth (>0)	0.06 m
As Thin/Surface?	Yes
FD2, Inward Thickness (>=0)	0 m
FD3, Outward Thickness (>=0)	0 m
Merge Topology?	Yes
Geometry Selection: 1	
Sketch	Sketch42

Figure 3.31 Thickness not defined in DesignModeler

Details of "HULLFACE"

Graphics Properties	
Definition	
Suppressed	No
Dimension	3D
Model Type	Shell
Stiffness Behavior	Flexible
Stiffness Option	Membrane and Bending
Coordinate System	Default Coordinate System
Reference Temperature	By Environment
Thickness	5.e-002 m
Thickness Mode	Manual
Offset Type	Middle
Treatment	None
Material	
Assignment	Structural Steel
Nonlinear Effects	Yes
Thermal Strain Effects	Yes
Bounding Box	
Properties	

Figure 3.32 Thickness defined in Ansys Mechanical

3.4.6 Boundary conditions of FEM model

The end of the pontoon which is connected to the side column is constrained in all 6 DOF (degrees of freedom). This end of the pontoon is of particular interest, since it will receive the wind turbine tower base loads transferred from the other end of the pontoon, which is connected to the central column. The loaded end of the pontoon has all 6 DOF free.

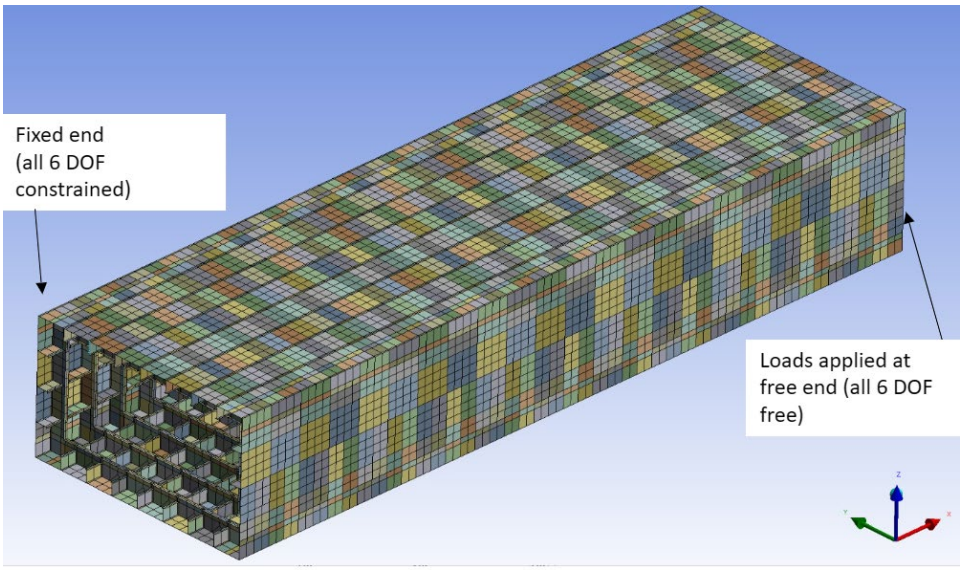

Figure 3.33 Boundary conditions of FEM model

These boundary conditions assumed are conservative. In reality, the fixed end of the pontoon would experience some displacement under the dynamic wind and wave induced loads from the wind turbine. The free end of the pontoon would also be partially rigid, since it is connected to the central column which provides some form of rigid constraint. However, in a similar FE model of a pontoon connected to the central column, Marin (2013) found that stresses in the specified area of interest are almost unaffected by the choice of boundary condition. Hence, the assumed boundary conditions are chosen to simplify the FE model.

3.4.7 Transfer structural loads from OPENFAST simulations to ANSYS FEM model

The tower base moments and forces were transferred from the OPENFAST simulations to the ANSYS FEM. The Table 3.10 lists the definitions of the tower base loads as per NREL, while the Figure 3.34 shows what the tower base moments and forces refer to (Yilmaz, 2014).

Name	Definition
"TwrBsFxt"	Tower base Fore-aft shear (platform)
"TwrBsFyt"	Tower base side-to-side shear force
"TwrBsFzt"	Tower base axial force
"TwrBsMxt"	Tower base roll (or side-to-side) moment (i.e., the moment caused by side-to-side forces) (platform)
"TwrBsMyt"	Tower base pitching (or fore-aft) moment (i.e., the moment caused by fore-aft forces), about Y axis
"TwrBsMzt"	Tower base yaw (or torsional) moment about Z axis

Table 3.10 Load definitions (Jonkman, 2007)

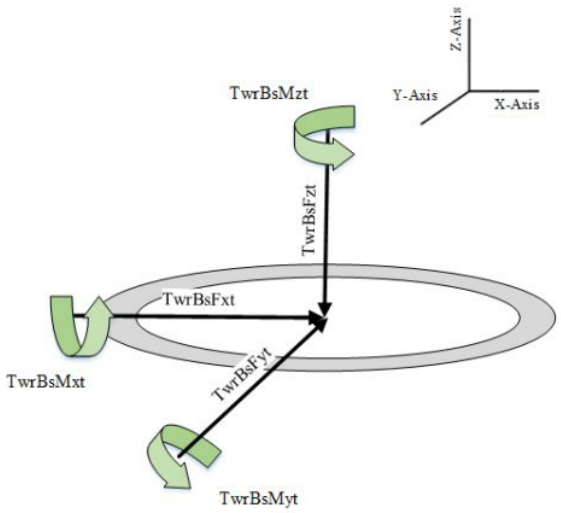

Figure 3.34 Visual definition of forces and moments (Yilmaz, 2014)

The Figure 3.35 below indicates where the tower base is located. There is a lever arm distance of 28m from the tower base to the top face of the horizontal pontoon.

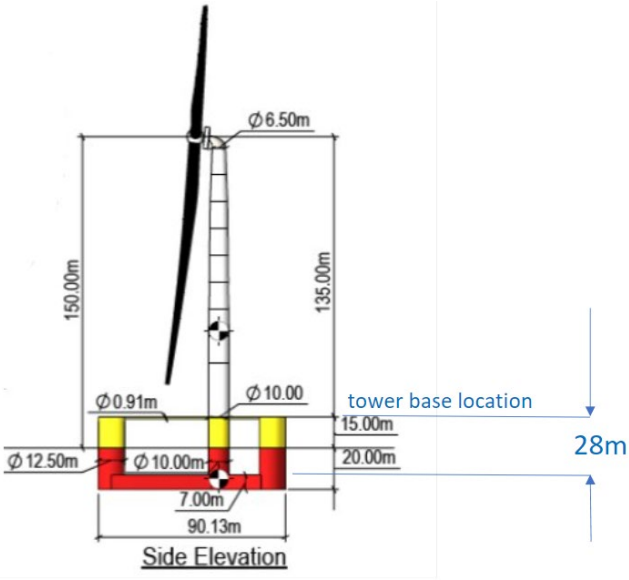

Figure 3.35 Lever arm distance from tower base to pontoon (Allen et al., 2020)

Since there is a lever arm of 28m, the "TwrBsFxt" and "TwrBsFyt" additionally contribute to My and Mx respectively. Similarly, "TwrBsFzt", with a lever arm of 5m (radius of the tower), provides an additional contribution to Mx and My.

3.4.7.1 Loads applied on FEM model of pontoon

First, the FEM model needs to be checked if it is sound. The first load case considered was at the turbulent wind speed of 25m/s. Once the FEM model is OK, the loads corresponding to rated wind speed will be considered since that is the most severe load case from a structural point of view.

The pontoon is idealised as a cantilever beam. Static loads were applied on the FEM model of the pontoon – gravity, tower base loads and 0.1G acceleration in the x and y directions as an approximation to account for wave loads (Ivanov et al., 2023). "G" refers to the gravitational acceleration of 9.81 m/s^2. The loads are applied in the positive direction for y direction and applied in the negative direction (downwards) in the x and z directions, while moment was applied in the positive direction for all directions. These directions are considered to induce the maximum loading effect on the pontoon.

The tower base loads are resolved by the moment arm of the tower and applied at the face of the end plate, which is located at the free end of the pontoon. The 0.1G acceleration was applied on the entire pontoon body.

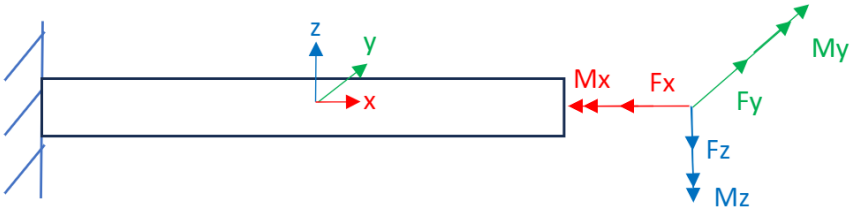

Figure 3.36 Pontoon idealised as cantilever beam

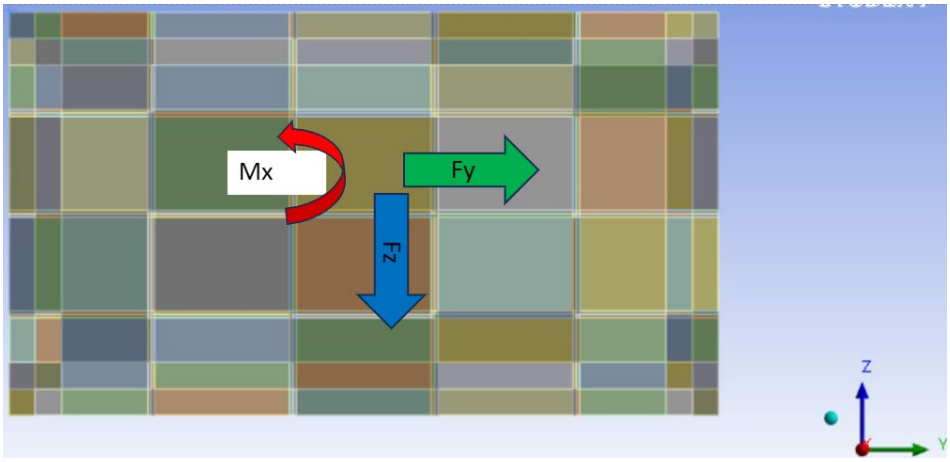

Figure 3.37 Tower base loads applied on face at free end of pontoon

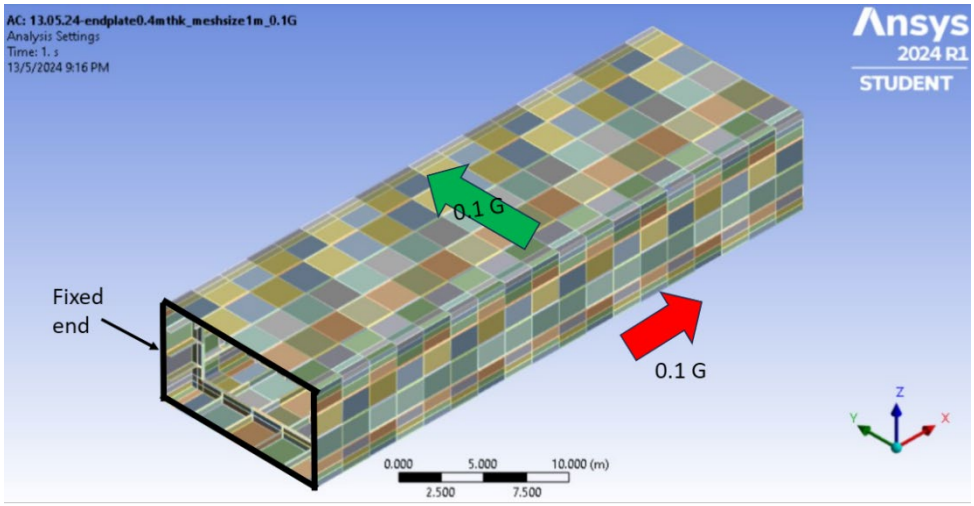

Figure 3.38 0.1 G acceleration applied on entire body

3.4.8 Need for constraint on free end of idealized cantilever to control deformation

The pontoon is idealised as a cantilever beam, with the left end restrained as a fixed support on the outer edges, while the right end of the beam is free. When the actual forces and moments are transferred from the tower base to the free end (under load case of 25m/s turbulent wind from OPENFAST Turbsim simulations), there is a significant local deformation of 2.14 m, using Design 2 as

an example. The local deformation is significant in the hull plate itself, which is nearest to the free edge of the beam.

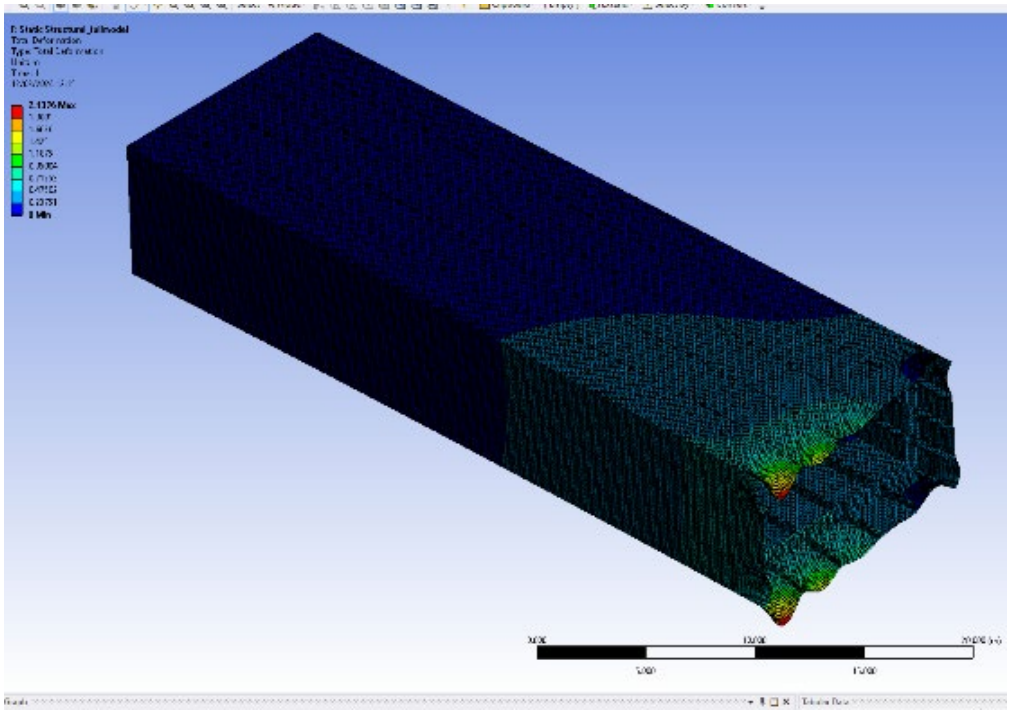

Figure 3.39 Significant local deformation in hull plate (Design 2)

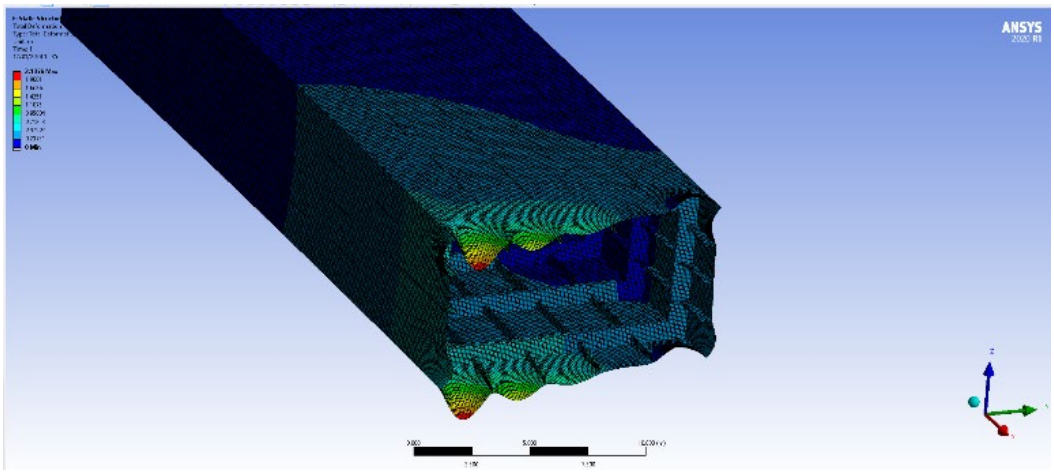

Figure 3.40 Significant local deformation in hull plate (Design 2)

Hence, a transverse stiffener was added at the free end of the model to 'control' the deformation. Figure 3.41 and Figure 3.42 show the transverse stiffener added at the free end. With the same loads applied on the outer edge of the end transverse stiffener, the total deformation was controlled and no longer localized, with a maximum at the end as 0.45 m.

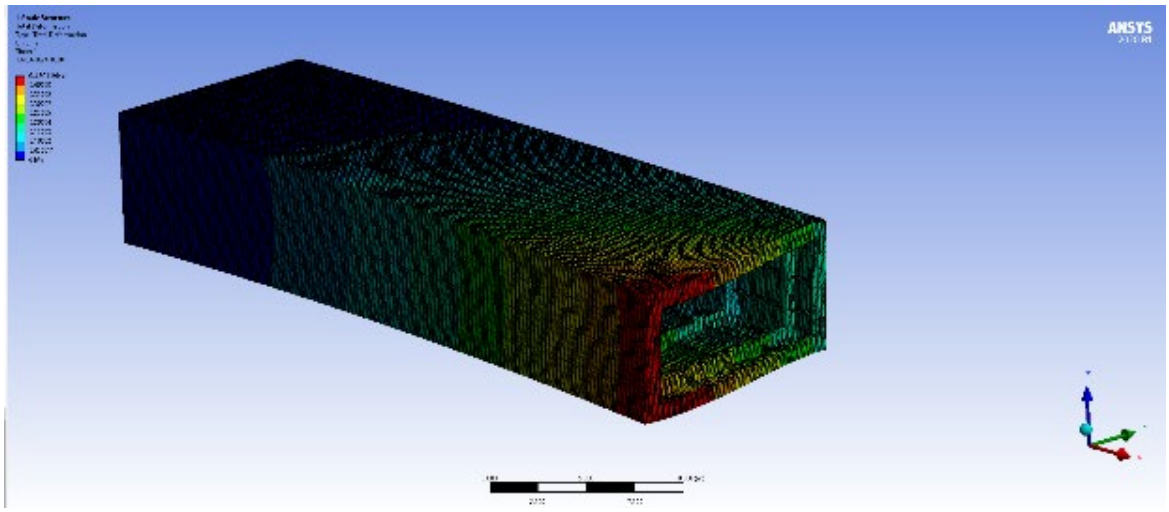

Figure 3.41 Deformation controlled with addition of end transverse stiffener (Design 2)

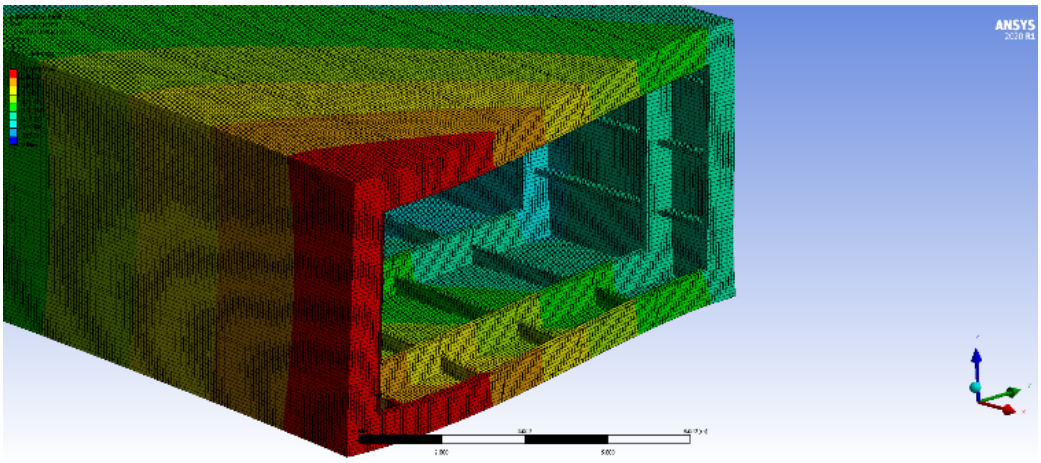

Figure 3.42 Close up of controlled deformation (Design 2)

However, the most critical von Mises stress was at the corner, where the boundary condition was applied. The von Mises yield stress was used to check for yielding in the pontoon as it was assumed that the onset of yielding represents the ultimate strength of the pontoon components. Figure 3.43 shows this, with the maximum as labelled.

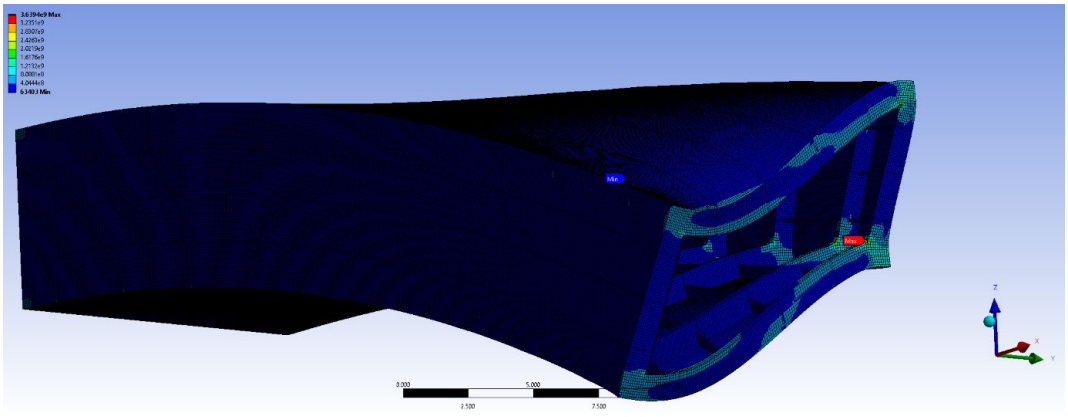

Figure 3.43 Localized maximum von Mises stress at end transverse stiffener (Design 2)

Thus, the other alternative is to model an end plate instead of an end transverse stiffener and apply the forces onto the entire end plate, instead of on the outer edge of the plate. This would follow the actual condition more.

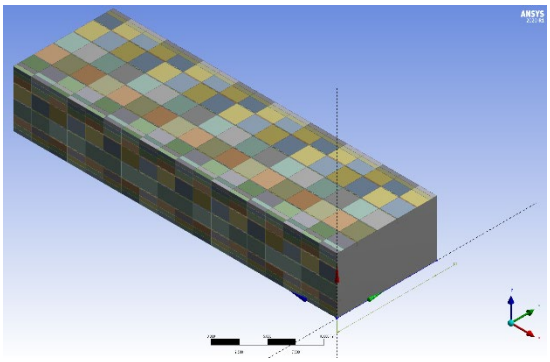

Figure 3.44 End plate modelled at free end of beam (Design 2)

However, when the end plate is modelled as a single piece and not subdivided at the intersections with the adjacent stiffeners and hull plate, and the force is applied at the 4 edges of the end plate, the total deformation and von Mises stress were significant at 0.275 m and 1.0226×10^5 MPa respectively.

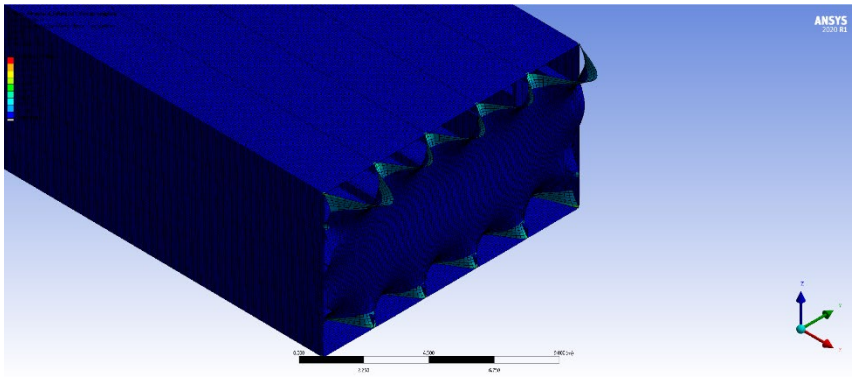

Figure 3.45 Localised high deformation and significant von Mises stress (Design 2)

After the nodes were merged, the deformation was more uniform across the beam. However, the maximum stress was at the free end, not at the fixed support as expected.

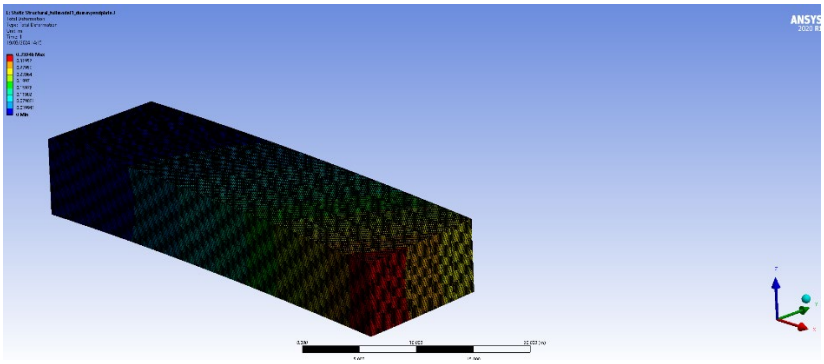

Figure 3.46 Uniform deformation across the beam and location of maximum von Mises stress (Design 2)

After trial and error, an end plate thickness of minimum 0.4m was needed to properly transfer the loads at the free end throughout the beam. In summary, an end plate thickness of minimum 0.4m was needed for Designs 1 and 2, and 0.6m for Design 3, to properly transfer the loads at the free end throughout the beam.

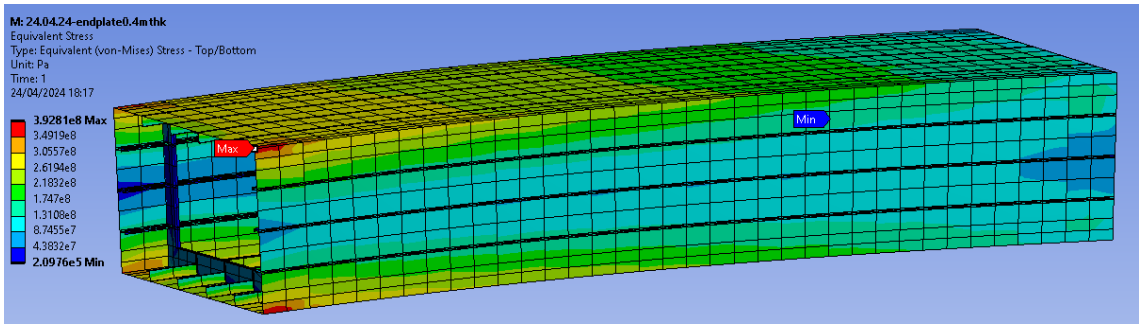

Figure 3.47 0.4m thickness end plate modelled (Design 2 at 11m/s mean wind speed)

It is noted that the change in end plate thickness adjusts the location of the von Mises stress, because thicknesses lower than 0.4m is too thin and will suscept the plate to local buckling. For end plate thicknesses 0.4m and above, the von Mises stress magnitude and location does not change. Figures below illustrate this with end plate thicknesses of 0.2m, 0.3m, 0.4m, 0.5m and 1m.

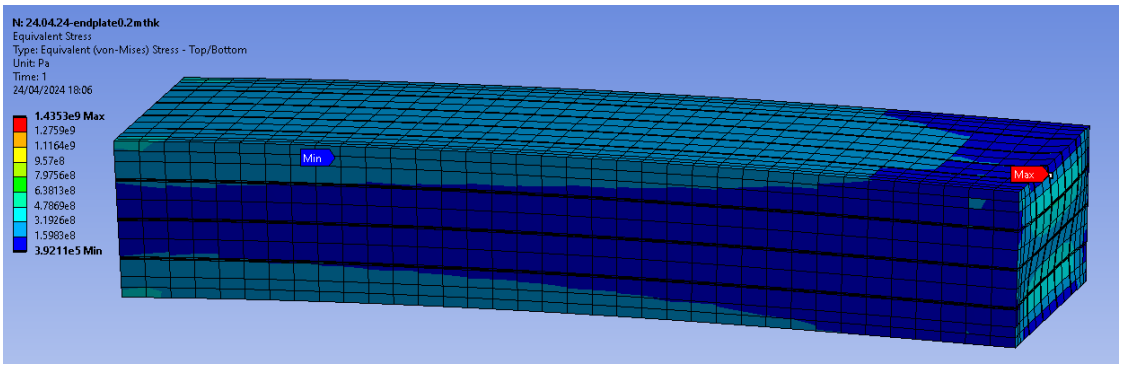

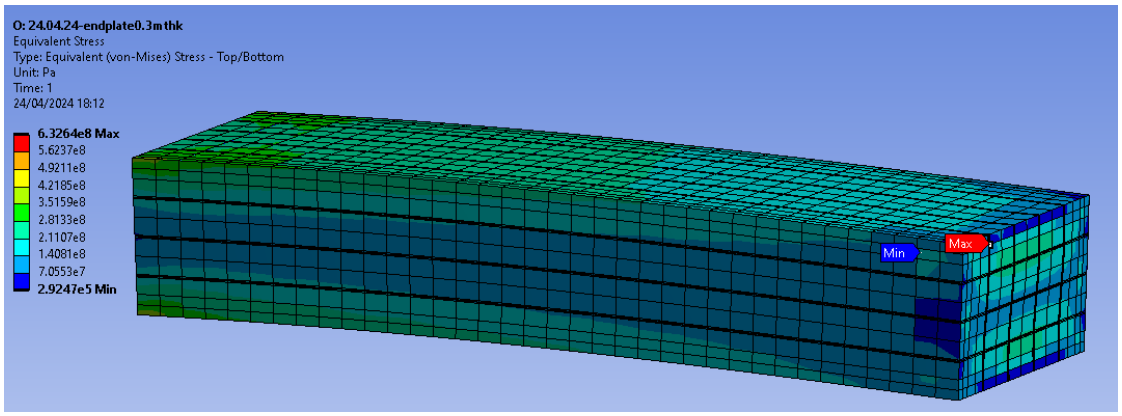

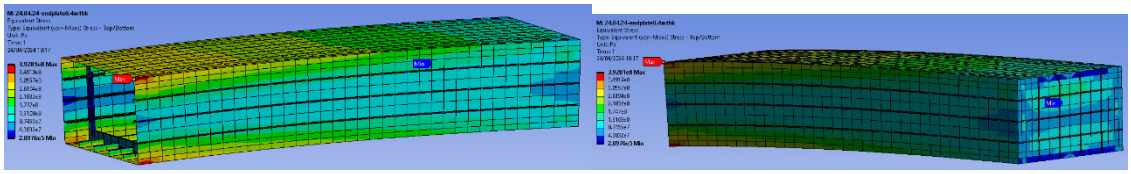

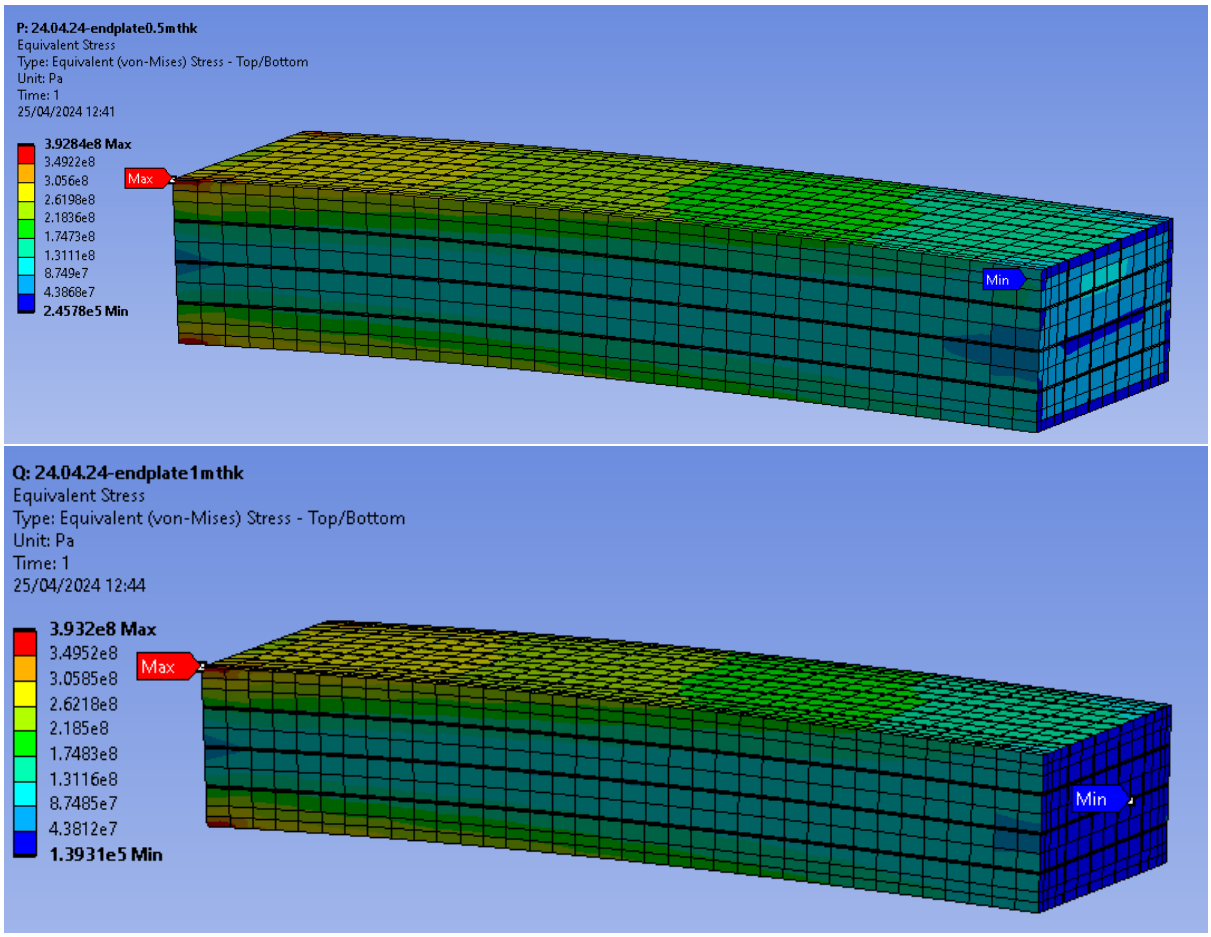

Figure 3.48 Varying end plate thicknesses showing shift in location of maximum von Mises stress (Design 2)

3.4.9 Mesh convergence study

It is necessary to validate the mesh convergence of the FE analysis to ensure reliability of the results. This is performed through mesh refinement, where the element size is halved in each FE analysis until the results converge. For this FE analysis which is non-linear, mesh convergence is achieved with a convergence error of 5% on the total strain (DNVGL-RP-F112 Appendix A1.1, 2018). Four different mesh sizes were studied: coarse, intermediate, fine, and very fine.

3.4.9.1 Stress singularity in mesh convergence study

In the mesh convergence study, it is important to check for stress singularity, which occurs when the stress increases to infinity as the mesh size reduces to zero (Stevens, 2019). Stress singularity is an artificial by-product of the FEM model, and give wrong results to the mesh convergence study. Stress singularities typically show up in sharp corners of the model, at locations of point load applied and at locations that have been idealised (Stevens, 2019). For example, in this FEM, the corners of the

horizontal pontoon are idealised as sharp corners, when in reality, they would be welded at the sharp joints or chamfered.

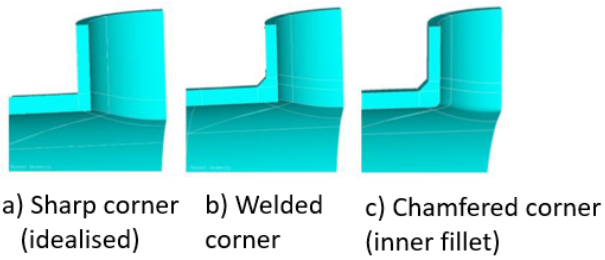

Figure 3.49 Three ways to model the sharp corner in a general FEM model (Bozkurt et al., 2019)

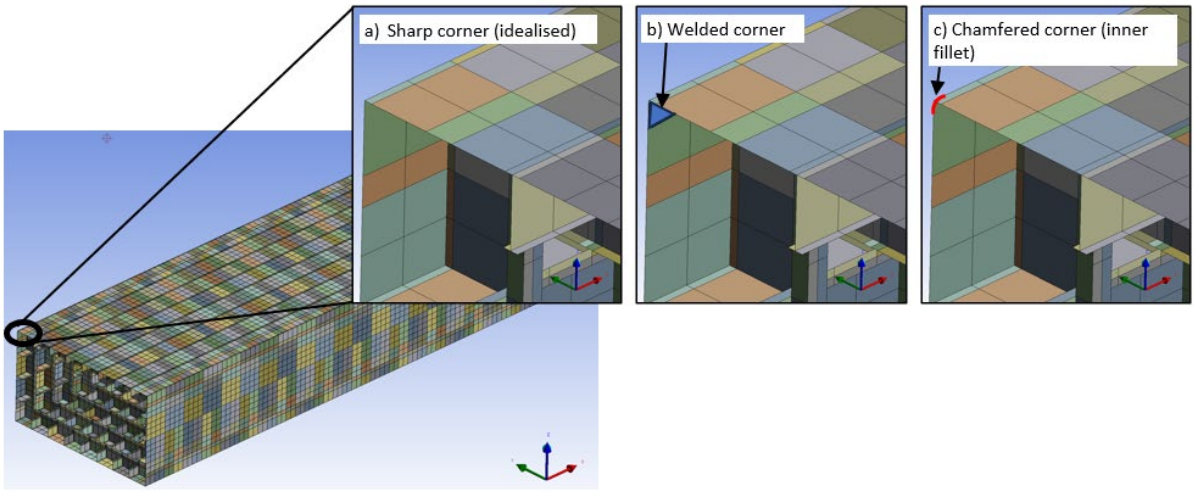

Figure 3.50 Three ways to model the sharp corner in the FEM model of this thesis

Since the FEM modelling is an iterative process as part of design optimization of hull layout, it is imperative to reduce any complexities in the modelling as much as possible. To reduce complication in the modelling of the FEM model, it is opted to idealise the corners as sharp corners. As a result, there is stress singularity observed in the models (all 3 designs). This is deduced from the increase in von Mises stress as the mesh size decreases, leading to a null in mesh convergence. Regardless of the mesh refinement, the stress diverges, as shown in Table 3.11, using Design 3 as an example.

mesh size (m)	mesh quantity (no. of nodes)	mesh quantity (no. of elements)	total deformation (m)	equivalent von Mises stress (MPa)	total convergence error on Von Mises stress (%)
1	12449	16505	0.28017	411.22	-
0.5	78213	28020	0.28728	581.95	29.34
0.25	222821	77832	0.28891	945.3	38.44
0.125	656983	224902	0.28957	1215.5	22.23

Table 3.11 Mesh results diverge with mesh refinement (Design 3)

In the model design 3, with a mesh size of 0.5m, very high von Mises stress is observed at the sharp corners of the pontoon, at the location where fixed support is imposed. The sharp corners induce a numerical singularity.

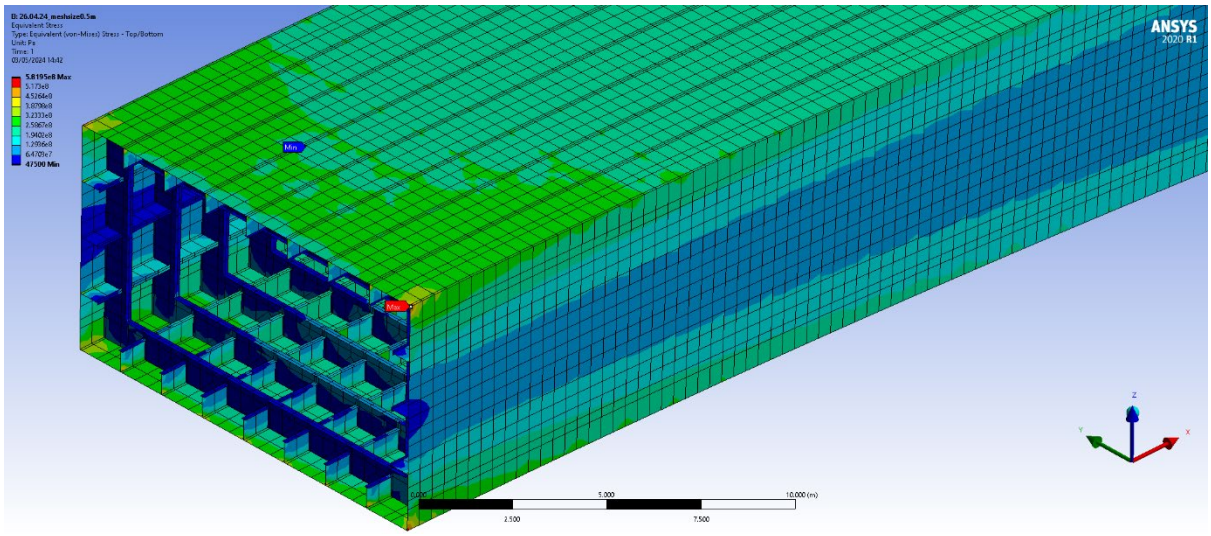

Figure 3.51 Design 3, at mesh size 0.5m, stress singularity observed at sharp corners

3.4.9.2 Resolve stress singularity

To resolve the stress singularity, the membrane and bending stress was obtained at the same location across all mesh sizes considered. The location chosen was a web plate of a girder that was near to the corner of highest stress singularity. Then, the membrane and bending stress was checked for convergence with mesh refinement.

As a start, the Figure 3.52 below shows for Design 3, at a mesh size of 0.5m, the membrane and bending stress (equivalent von Mises stress). The accompanying Figure 3.53 shows the stress path along the marked web plate.

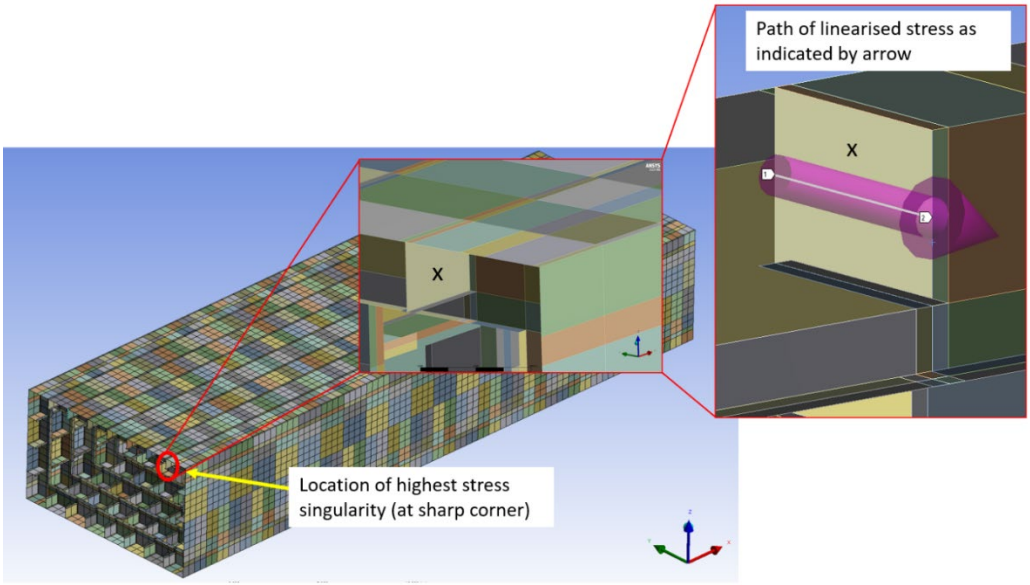

Figure 3.52 Observe linearised stress on the web plate of girder marked ¨x¨, located near the point of highest stress singularity

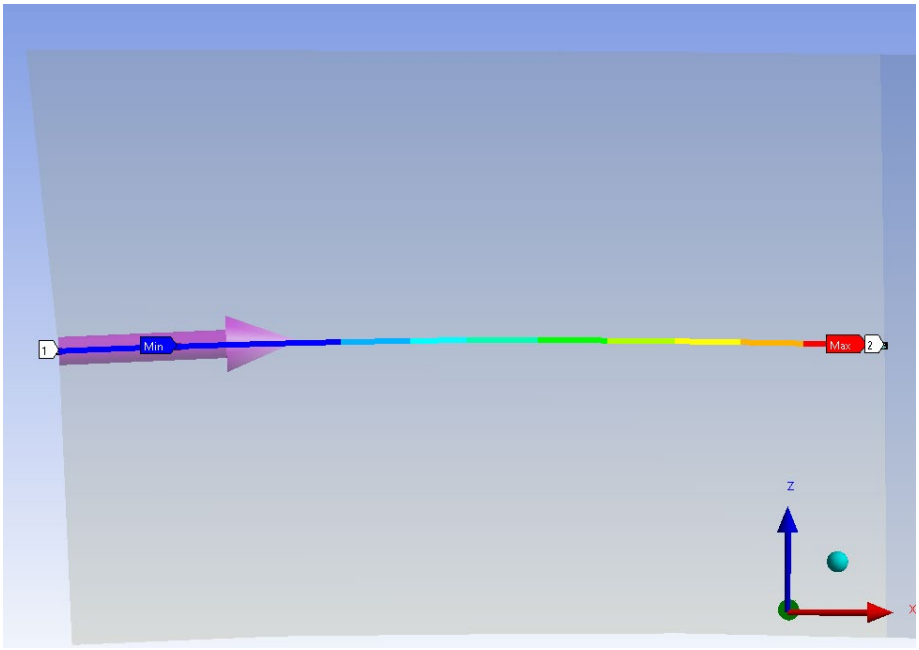

Figure 3.53 Linearised stress path along web plate of longitudinal girder (Design 3)

3.4.9.3 Mesh convergence results

The linearised stress was observed for all three designs. It can be seen that at a mesh size of 0.125m, all three designs achieved mesh convergence, with a convergence error of less than 5%.

Design 1				
mesh size (m)	mesh quantity (no. of nodes)	mesh quantity (no. of elements)	membrane + bending stress (von Mises stress) (MPa)	convergence error on membrane + bending stress (%)
1	79678	29286	242.81	-
0.5	123863	42231	252.18	3.72
0.25	86643	88141	266.82	5.49
0.125	250127	251934	265.25	0.59
Design 2				
mesh size (m)	mesh quantity (no. of nodes)	mesh quantity (no. of elements)	membrane + bending stress (von Mises stress) (MPa)	convergence error on membrane + bending stress (%)
1	6551	9144	237.09	-
0.5	17020	17468	261.27	9.25
0.25	49101	49676	280.65	6.91
0.125	165802	166680	281.32	0.24
Design 3				
mesh size (m)	mesh quantity (no. of nodes)	mesh quantity (no. of elements)	membrane + bending stress (von Mises stress) (MPa)	convergence error on membrane + bending stress (%)
1	12449	16505	213.18	-
0.5	78213	28020	222.69	4.27
0.25	222821	77832	257.15	13.40
0.125	656983	224902	249.42	3.10
0.0625	802129	818416	240.02	3.92

Table 3.12 Mesh convergence results

Figures below show the mesh convergence for all three designs.

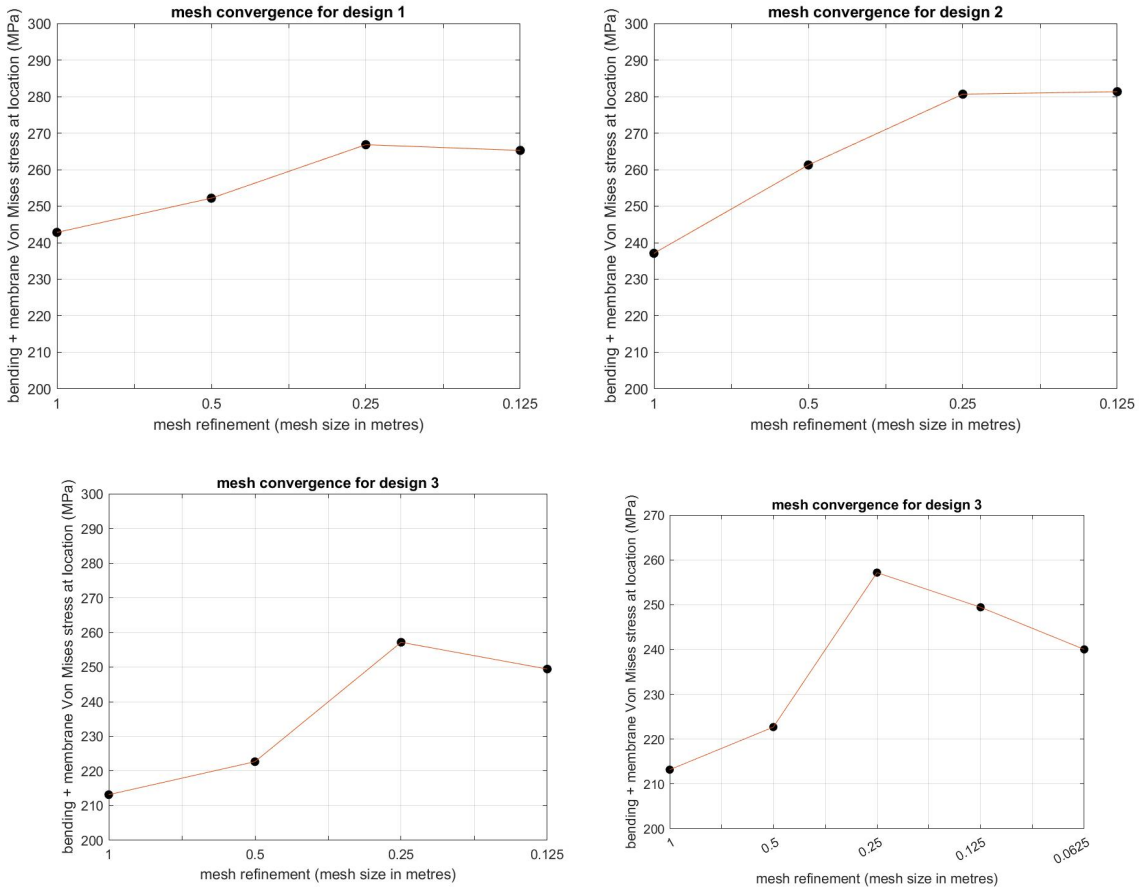

Figure 3.54 Mesh convergence plots for all designs

Hence, it can be concluded that a mesh size of 0.125 m is the optimum for the pontoon FEM model.

3.5 Machine learning models on Matlab

In the attaining the optimum design of the pontoon, there are mutliple variables to consider, such as the stiffener profile, stiffener spacing, girder profile, girder spacing and hull thickness. It is a time-consuming process to verify each component of the pontoon against the design codes and run the FEA simulations. Amidst this, design changes almost always occur even in the mature stages of the project, due to a variety of reasons. This leads to a potential time delay in the relevant project stage. Often, in large scale projects such as offshore wind turbines, there are several phases that are interdependent and incur huge monetary losses should any phase experience a delay. It is thus prudent to adopt machine learning models to optimise the design of the pontoon.

Since there are multiple variables involved, there is great interest to study the use of multi-output regression models. The primary aim of multi-output regression is to estimate multiple real valued output variables. This is done by training the model and optimising it to the specific target, which is the output to be predicted. Typically, a simple approach would be to use a combination of several

single output regression models (Sadoughi, 2017). However, such an approach comes with the following drawbacks (Karkera, 2017):

- Not time-efficient because training multiple single-output models may consume a significant amount of time. This is especially pronounced for large sets of data.
- Each single-output model is trained and optimised for a specific single target. Since the model focuses on a single target, the single-output model is incapable of capturing the interdependencies and correlations among multiple targets.

In lieu of these drawbacks, it is imperative to consider multi-output regression models that can account for both the relationships between input parameters and its respective targets, and the interdependencies between output targets (Sadoughi, 2017). Presently, several regression methods abound for this purpose, such as multi-target Support Vector Machine (SVM) and Random Forest (Sadoughi, 2017). This thesis seeks to simplify the design process as much as possible in order to achieve its overall aim of being cost and time-efficient. Hence, a multi-output regression method incorporating the Gaussian Process Regression (GPR) model is considered.

In the approach adopted from Mohammadkazem Sadoughi (2017), the Matlab code implements Gaussian Process Regression (GPR) using the Gaussian Processes for Machine Learning (GPML) toolbox. The multivariate GP model is trained with the MSRM function developed by Sadoughi (2017). Further details on the Matlab code and its functionality are provided in Appendix G – Supporting Matlab codes for ML models.

In this thesis henceforth, Sadoughi's approach will be called the MSRM function.

3.5.1 MSRM function to predict the stress in web of transverse girder

First, the MSRM function was used to train a simple multi-input, single output model. The aim is to train the model to predict the Von Mises stress in the web of the transverse girder, based on existing input from various design parameters of the transverse girder. There are three learning data sets to train the model, each set representing each of the three designs. The input data comes from the FEA simulations performed at a mesh size of 0.125m, which was the common mesh convergent size among all three designs. All simulations were run in an environment of 11 m/s mean wind speed, which was close to the rated wind speed of 10.59m/s.

The transverse girder of focus is the one at the idealised fixed end of the pontoon, with a linearised stress path constructed in the mid-depth of the girder. Its maximum membrane and bending linearised stress are studied.

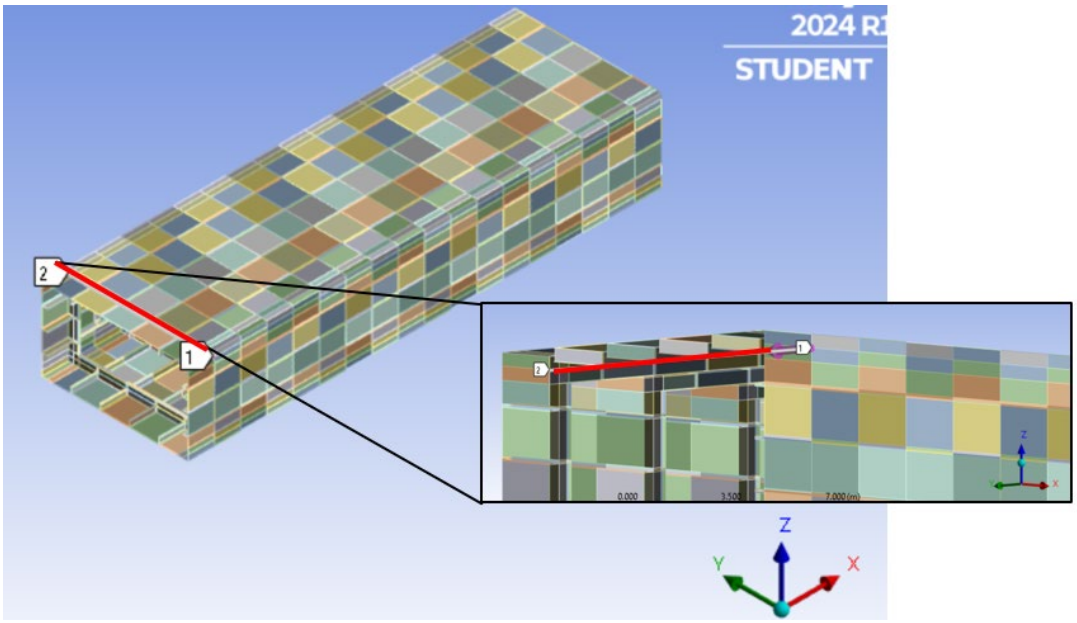

Figure 3.55 Stress path studied in the web of transverse girder (indicated by red line)

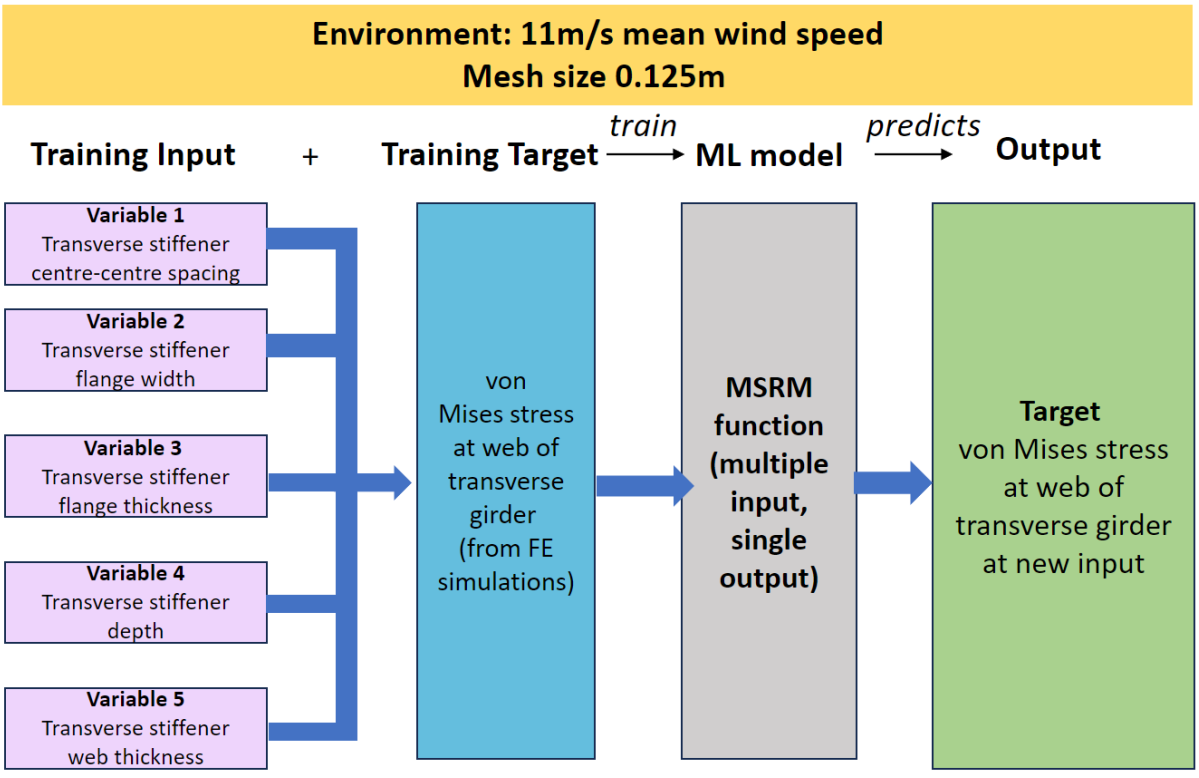

Figure 3.56 Preliminary ML model

First, check the soundness of the ML model, by using the design parameters for Design 3 as the new input. The expected output should be close to the actual value. This is indicated when the covariance is of a negligible value (negative or zero). As the covariance represents the uncertainty in the prediction, the smaller the uncertainty, the greater the accuracy of the prediction. Details of the Matlab code is appended in

Appendix E – Matlab code for ML model for von Mises stress of transverse girder.

Next, the second check of the soundness of the ML model is by removing the input training data for Design 3 and train the model using only the data from Designs 1 and 2. Then, the predicted target based on Design 3's input parameters is compared with the actual output for Design 3. Based on this, the ML model predicts the output target of Design 3 with an error of 17.5%, as presented in the Table 3.13 below.

Target output (MPa)	Actual Output (MPa)	Uncertainty (covariance)	% error
61.6522	52.482	0.5643	17.473

Table 3.13 Results of ML model predicting Design 3 target output

There are currently no specific guidelines on error tolerance for ML models in optimum design of a pontoon for an offshore wind turbine semi-submersible structure. In a study to predict the thrust load history of a wind turbine, Noppe et al. (2018) used strain measurements to train a neural network, validating the method with both simulated data and actual offshore wind turbine measurements. The technique yielded promising results, maintaining a relative error below 15%, with relatively higher accuracy in the simulated data (Masoumi, 2023). Although this 15% error threshold pertains to a different machine learning model and analysis, and a different component of the wind turbine, it can still serve as a rough guideline for error tolerance in the absence of specific literature on machine learning for optimal pontoon design.

Furthermore, the ML model will be further improved when more training data sets are added. Due to limited scope of the thesis, only the current data sets from Designs 1, 2 and 3 were used to train the ML model. Future study should consider more training input data sets. There are several factors affecting the amount of training data required, such as number of features, complexity of the model and error tolerance (Stupak, 2024). Stupak (2024) recommends, as a rule of thumb, to have the number of training data sets equivalent to ten times the number of features of the ML model. In the case of this ML model, there are five training input, so at least 50 training data sets should be included to the model.

3.5.2 MSRM function to predict the column buckling stress in web of longitudinal girder

The longitudinal girder is treated as an idealised beam-column. A reference figure from Wang et al. (2016) is as shown:

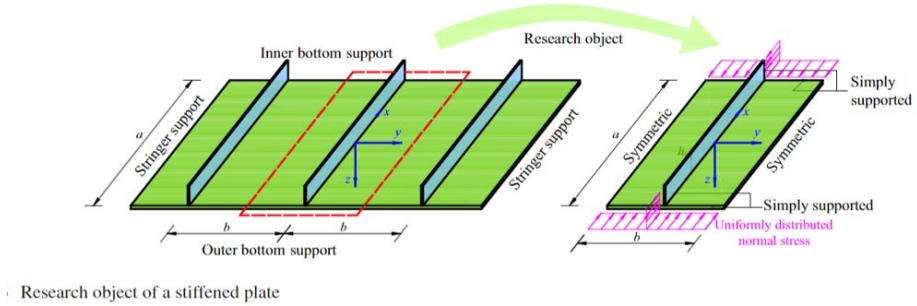

Figure 3.57 Idealised stiffened plate (Wang et al., 2016)

The longitudinal girder is idealised as beam-column with the following boundary conditions:

- Remote displacement constraint at the base, where the hinge support is located. The base of the column is free to rotate on all axes except its own, and it is restrained from displacement in all axes.
- Displacement constraint at the top of the column, where the compressive force is applied. The column has displacement constraints in all axes except in the direction where the force is applied, so that the column can move up and down under the applied load.

Details of "Remote Displacement"

Scope	
Scoping Method	Geometry Selection
Geometry	8 Edges
Coordinate System	Global Coordinate System
X Coordinate	5,7131e-016 m
Y Coordinate	-7,5 m
Z Coordinate	0,16773 m
Location	Click to Change
Definition	
Type	Remote Displacement
X Component	0, m (ramped)
Y Component	0, m (ramped)
Z Component	0, m (ramped)
Rotation X	0, ° (ramped)
Rotation Y	Free
Rotation Z	Free
Suppressed	No
Behavior	Deformable
Advanced	

Figure 3.58 Remote displacement at the pinned end of the column

Details of "Displacement"

Scope	
Scoping Method	Geometry Selection
Geometry	8 Edges
Definition	
Type	Displacement
Define By	Components
Coordinate System	Global Coordinate System
X Component	Free
Y Component	0, m (ramped)
Z Component	0, m (ramped)
Suppressed	No

Figure 3.59 Displacement constraint at the point of load application

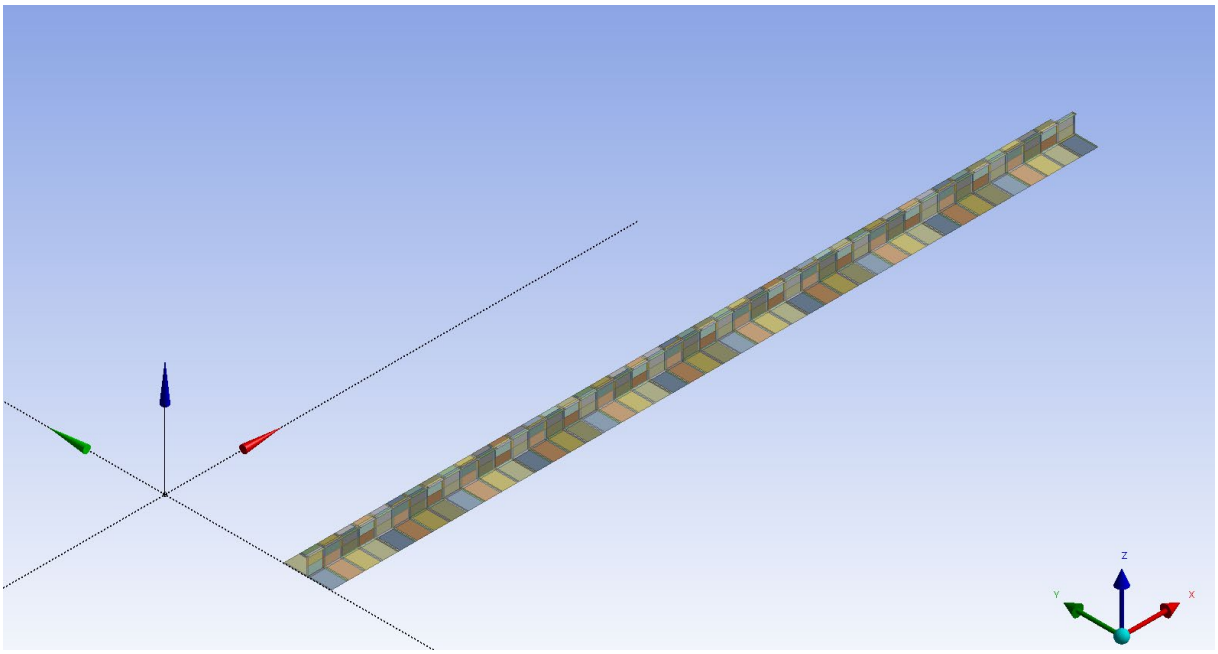

Figure 3.60 Beam column modelled in Design 1 with hull plate width 2.5m, equivalent to longitudinal girder c/c spacing

Normal stress is recorded from the Ansys simulations, via the linearised stress path on the longitudinal girder, as indicated below, in red.

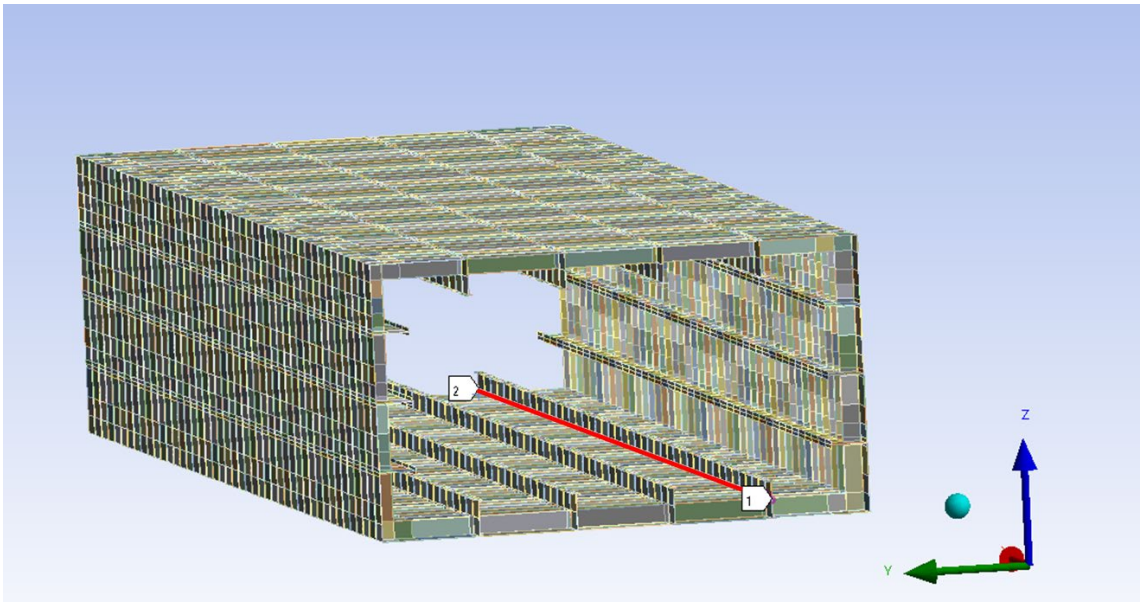

Figure 3.61 Design 1, longitudinal girder stress path

Then, an ANSYS model of only the idealised beam-column is modelled, and the compression force applied is equivalent to the normal stress multiplied by the cross section area of the beam-column.

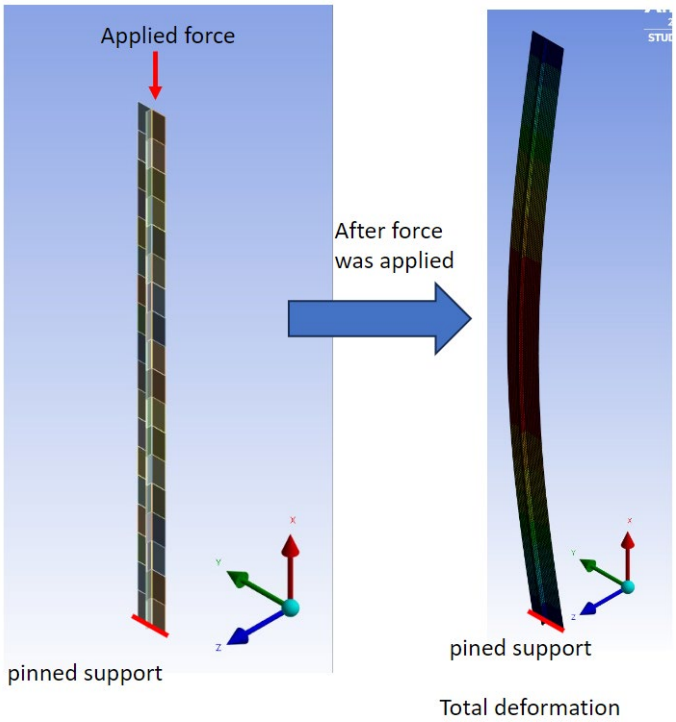

Figure 3.62 Compressive force applied on column

Buckling about the major axis is considered as a start. The first mode of buckling is analysed as it is assumed to be the most common mode of buckling for the pontoon under the loads. It is also the most conservative assumption.

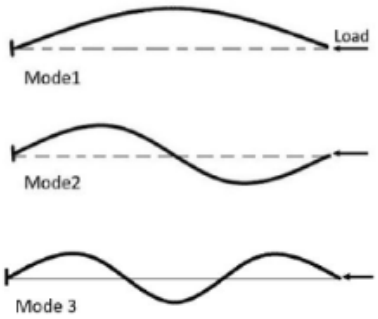

Figure 3.63 First three buckling modes of column (Salem et al., 2019)

As in the unit load method, the buckling load of the idealised beam-column is equivalent to the applied load multiplied by the load multiplier. Then, the buckling load can be compared with the design requirement from the design codes against buckling. This approach is applied for all three designs.

For design 3, as the flange width of the longitudinal stiffener (0.075m) was too small relative to the full length of the girder (40.5m), the length of the girder was modelled as 1.8m instead, which was the centre-to-centre spacing of the transverse girder.

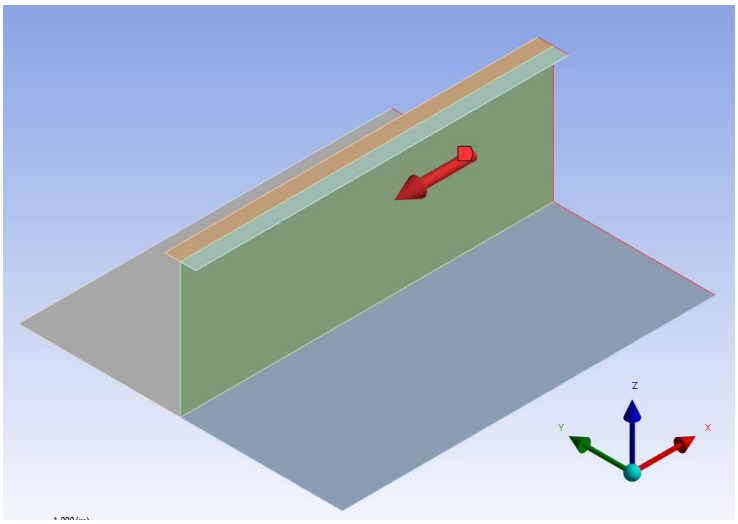

Figure 3.64 Design 3, longitudinal girder modelled as beam-column in Ansys

A summary of the results for static and buckling analyses of the longitudinal girder, for all three designs, is presented below.

From Ansys static analysis			
	Design 1	Design 2	Design 3
Normal stress in longitudinal girder (MPa)	134.01	255.59	241.09
Longitudinal girder profile size	Tbar 885x200x14x35	Tbar 425x120x12x25	Tbar 625x150x12x25
Centre-centre spacing of longitudinal girder (m)	2.5	2.5	1.5625
Cross section area (mm^2)	144 390	133100	136 250
Normal compressive force (N)	1.935×10^7	3.402×10^7	3.285×10^7
Applied force (N)	1	1	1
From Eigenvalue buckling analysis in Ansys			
	Design 1	Design 2	Design 3
Load multiplier from 1st mode of buckling	7.1796×10^6	1.1927×10^6	6.3814×10^6
Buckling load (kN) when applied force is 1N	7179.6	1192.7	6381.4

Table 3.14 Static and eigenvalue buckling analyses for the longitudinal girder

The next step would be to train the ML model. A preliminary soundness check of the ML model is conducted, by training the ML model based on input from Designs 1 and 2, and then predicting the buckling load multiplier for Design 3 based on Design 3's input. The uncertainty is zero, which indicates the ML model is extremely accurate. However, since only 2 training input data was used, and

considering the variability and interdependence of the input variables, more training data should be used to train the model.

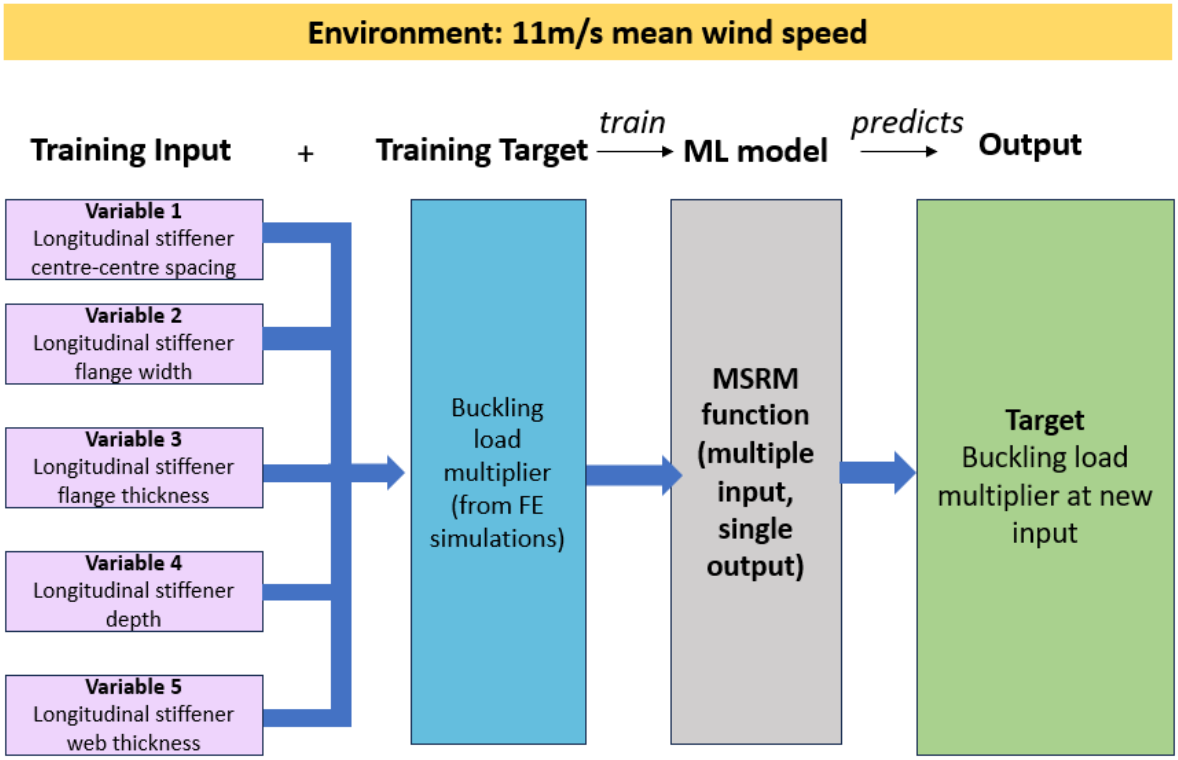

Figure 3.65 ML model to predict the buckling load of longitudinal girder

Target output (buckling load multiplier in kN)	Actual Output (buckling load multiplier in kN)	Uncertainty (covariance)	% error
6381.4	6381.4	0	0

Table 3.15 Results of ML model predicting Design 3 target output

Hence, the ML model incorporating the MSRM function seems to be valid in the design process of obtaining the optimal pontoon detailed design efficiently. However, since only three sets of training input data were used, more data should be incorporated. For instance, more variations in the longitudinal girder section sizes should be considered, and at other mean wind speeds and at other loading conditions such as at SLS (Serviceability Limit State) and ALS (Accidental Limit State).

4. Conclusion and recommendations for future work

In conclusion, this study has provided valuable insights into optimising the design of the pontoon for a 15MW offshore wind turbine, addressing key questions and contributing to a deeper understanding of using machine learning and the complex loading behaviour of the stiffened panels within the pontoon.

4.1 Conclusion

It is concluded that a pontoon design with widely spaced, relatively larger transverse girders, and relatively smaller longitudinal girders is optimum. This allocates Design 2 as the best option among the three proposed designs. The transverse girders should be relatively larger to resist the bending moment along the length of the pontoon. The length of the pontoon is the largest dimension of the pontoon, compared to its width and height. Furthermore, a hull plate thickness of 50 mm seems to fit the design loading scenario of the pontoon at rated wind speed and at ULS. This plate is able to resist bending, which is the major force on the pontoon.

Section 3.4 highlighted the challenges involved in modelling the FEM model of the ponton, with its detailed design of the girders and stiffeners. There were several assumptions to be made, such as the boundary conditions of the pontoon, the loading conditions, and how the load was to be applied onto the pontoon. The mesh convergence study also had to be conducted via a trial-and-error approach, with the conclusion that modelling an end plate to the free end of the pontoon helping to control the unnaturally high deformation of the pontoon. It was found that a mesh size of 0.125 m is optimum for the FEM model, considering the three designs that were proposed.

The ML model that fit best for the problem statement of the thesis is the Gaussian Process Regression (GPR) model, a supervised learning method modified with the MSRM function developed by Sadoughi (2017). The model performance was analysed based on the tests for von Mises stress on the transverse girder, and buckling load on the longitudinal girder of the pontoon. there was an uncertainty of around 17% for the ML model trained to predict the von Mises stress, while a startling 0% for buckling load prediction. These ML models were trained with the input from FEM analyses of the three proposed designs, at mean wind speed of 11m/s.

Finally, through studying the behaviour of buckling in the stiffened plates and proposing a design framework that transfers global loads from OPENFAST to Ansys, and utilizing existing design codes from DNV and AISC to support the pontoon layout, this thesis hopes to contribute in furthering interest in the field of incorporatng machine learning to optimise design of semi-submersible structure of

offshore wind turbines. It is evident that there is much more to be studied to enable the offshore wind turbine market to fully embrace using AI.

4.2 Recommendations for future work

Despite the strengths of this research, there are several limitations that need to be acknowledged. The following suggestions are recommended for future research:

1) Do a small-scale model 1/50th the size actual, of the semi-submersible structure to validate the FEM and machine learning model results. Experimental studies on the scaled-down version of the pontoon, under the same environmental loads and boundary conditions, would serve to validate the results obtained in the analysis. A study done by NREL on the semi-submersible for OC4 offshore wind turbine looked at three wind turbine configurations on a 1/50th scale of the model, in a wave basin subjected to load combinations of wind and wave (Robertson et al., 2014). This was done to validate the tools used to model the offshore wind turbine (Robertson et al., 2014). Similarly, such an approach should be considered for to further validate the thesis. Furthermore, the scaled-down model would also help to further study the buckling behaviour of the pontoon, as this is still a complex arena.

Figure 3-1: As-built picture of DeepCwind semisubmersible for 1/50th scale tests

Figure 4.1 Scaled-down model of semi-submersible structure by NREL (Robertson et al., 2014)

2) The analysis was conducted at the mean wind speed of 11m/s, which was taken to be representative of the rated wind speed of 10.59m/s. A more holistic approach would be to consider all the mean wind speeds within the operating range of the wind turbine. Mean wind speeds slightly past the cut-off wind speed should also be considered, to account for severe wind speeds. This would enable a more robust design of the semi-submersible.
3) The current design checks as appended in Appendix B – Detailed calculation for hull plate thickness and Appendix D – Detailed calculation for stiffener layout need to be further

validated by supporting non-linear buckling calculations and FEM software. There are also some checks in the design calculations that need further study to consider other mean wind speeds and other possible layouts of the girders and stiffeners. A cost-benefit analysis of the girder, stiffener and hull sizes should also be studied to keep the pontoon both structurally safe and cost-friendly. This would ensure the chosen pontoon design layout is optimum for all possible loading and costing scenarios of the wind turbine.

4) The current FEM model of the pontoon in this thesis should not serve as a final model. The pontoon should be modelled with the other components of the semi-submersible structure. The complexity of the FEM model would then increase, and this may affect the mesh size that would enable mesh convergence.
5) More input is needed to further validate the ML models, in order to train them to have better accuracy. A comparative analysis should be conducted to compare the optimized designs against traditional pontoon designs from existing literature in terms of structural performance, material usage, costs and environmental impact. This should be supplemented by a sensitivity analysis, to further understand the influence of different design parameters on the pontoon performance.
6) The stiffened panel design should be further validated by optimal capacity curves studied in DNV RP-C201 and The Panel Ultimate Limit State (PULS) code. The Panel Ultimate Limit State (PULS) code is used for buckling strength assessment of the stiffened plates. Six limit state functions are used to identify the critical conditions in different locations of the stiffened panel, "where a function corresponds to applied loads less than the critical condition the corresponding point" (Nguyen, 2011). The minimum of all the defined limit states determines the ultimate strength. To verify the stiffened panel design, the following procedure should be considered (Nguyen, 2011):
    a. Parametric study: For optimum layout of the stiffeners, the stiffened panel will be analysed via a parametric study of varying the stiffener dimension, stiffener thickness and stiffener spacing.
    b. Utilization ratio: The maximum utilization ratio is kept at 0.9 for optimum stiffener design, and to account for contingencies such as future increase in weight of structural members.
    c. Buckling assessment: Following which, buckling assessment of the optimal stiffened panel will be studied, with the respective optimal capacity curves studied in DNV RP-C201 and PULS. The maximum capacity of the stiffened plate is determined when the largest utilization ratio obtained for the four interaction equations is at its minimum.
    d. A comparison of assessments between DNV RP-C201 and PULS should also be considered.

7) Ansys was used to model the pontoon. SIMA should be used to cross-validate the FEM model, along with modelling the offshore wind turbine and the entire semi-submersible structure. This would complete the design of the wind turbine, and in SIMA there is possibility to run the wind and wave simulations for various time periods and design scenarios. Furthermore, under DNV, the Platework software module from SESAM can be used to run the plate check of the stiffened panels in the pontoon, to further validate current findings. The stresses can be extracted by FE analysis.

By addressing these areas, future studies can enhance the robustness of the current findings and contribute to the advancement of knowledge in utilising machine learning for design optimization of support structure for offshore wind turbines. This could yield more comprehensive results and potentially uncover new avenues for exploration.

5. References

AISC Manual of Steel Construction: Allowable Stress Design 9th Edition, ASD. (1989). American Institute of Steel Construction. https://www.aisc.org/globalassets/aisc/manual/15th-ed-ref-list/specification-for-structural-steel-buildings-allowable-stress-design-and-plastic-design.pdf

Albino, J., Gonçalves, L., & Beal, V. (2019). On the convergence of solid meshes for the prediction of part distortions due to residual stresses. *Proceedings of the Institution of Mechanical Engineers. Part C, Journal of Mechanical Engineering Science*, *233*(17), 6209–6217. https://doi.org/10.1177/0954406219861405

Allen, C., Viscelli, A., Dagher, H., Goupee, A., Gaertner, E., Abbas, N., Hall, M., & Barter, G. (2020). *Definition of the UMaine VolturnUS-S reference Platform Developed for the IEA Wind 15-Megawatt Offshore Reference Wind Turbine*. https://doi.org/10.2172/1660012

Alvaro, O. N. (2018). *TIME DOMAIN SIMULATION PARAMETERS FOR FATIGUE ASSESSMENT OF AN OFFSHORE GRAVITY BASED WIND TURBINE*. [Master Thesis, NTNU]. NTNU Open. https://ntnuopen.ntnu.no/ntnu-xmlui/handle/11250/2564489

Ansys. (2024). *Ansys Mechanical Finite Element Analysis (FEA) Software for Structural Engineering.* https://www.ansys.com/products/structures/ansys-mechanical

Bai, Y., & Jin, W. L. (2016). *Marine Structural Design (Second Edition).* https://doi.org/10.1016/B978-0-08-099997-5.00005-8.

Bai, Y., & Jin, W. L. (2016). Ultimate Strength of Plates and Stiffened Plates. In *Elsevier eBooks* (pp. 339–352). https://doi.org/10.1016/b978-0-08-099997-5.00017-4

Benmusa, A. (2020, April 28). *T-Shaped Load-Bearing Beams | BeamCut*. Beamcut. https://beamcut.com/t-shaped-load-bearing-beams/

Bleich, F., and Ramsey, L. B. (1951). *A Design Manual on the Buckling Strength of Metal Structures, Tech. Res. Bulletin No. 2-3*. The Society of Naval Architects and Marine Engineers, New York.

Bozkurt, M., Nash, D., & Uzzaman, A. (2019). *Investigation of the Stresses and Interaction Effects of Nozzle-Cylinder Intersections When Subject to Multiple External Loads*. https://doi.org/10.1115/pvp2019-93306

Brown, S. (2021, April 21). *Machine learning, explained*. MIT Sloan. https://mitsloan.mit.edu/ideas-made-to-matter/machine-learning-explained

Clean sources of generation are set to cover all of the world's additional electricity demand over the next three years - News - IEA. (2024, January 24). IEA. https://www.iea.org/news/clean-sources-of-generation-are-set-to-cover-all-of-the-world-s-additional-electricity-demand-over-the-next-three-years

Deltamarin Ltd. (2021, January 12). *Offshore engineering process | Future-proof designs | Deltamarin Ltd*. https://deltamarin.com/offshore-engineering/offshore-engineering-process/

Det Norske Veritas. (2010). DNV-OS-J103 Design of Floating Wind Turbine Structures.

Det Norske Veritas. (2010). Recommended Practice: DNV-RP-C201 Buckling Strength of Plated Structures, dated October 2010.

Det Norske Veritas. (2002). Recommended Practice: DNV-RP-C201 Buckling Strength of Plated Structures. https://www.sefindia.org/forum/files/DNV-RP-C201_2008-10_450.pdf (accessed 2 June 2024).

Det Norske Veritas. (2011). *Offshore Standard DNV-OS-C101, Design of Offshore Steel Structures, General (LRFD Method).* https://rules.dnv.com/docs/pdf/dnvpm/codes/docs/2011-04/Os-C101.pdf

Det Norske Veritas. (2002). Recommended Practice: DNV-RP-C102 Structural Design of Offshore Ships. https://home.hvl.no/ansatte/gste/ftp/MarinLab_files/Litteratur/DNV/DNV_pE13%20of%2036_scatter%20diagram.pdf (accessed 2 June 2024).

DNV GL. (2018). DNV-RP-F112 Duplex stainless steel – design against hydrogen induced stress cracking. https://pdfcoffee.com/dnvgl-rp-f112-pdf-free.html (accessed 2 June 2024).

DNV GL. User Examples for GeniE Semisub Pontoon. DNV GL, 2015. https://home.hvl.no/ansatte/tct/FTP/H2023%20Marinteknisk%20Analyse/SESAM/SESAM%20UserEamples/A2_GeniE_Semisub_pontoon.pdf

DNVGL-PS, Stipla,Theory Manual.

Ege, H. (2019). *Investigation of the Tower Design for the Offshore Wind Turbine Concept OO-Star Wind Floater*. [Master Thesis, NTNU]. NTNU Open. https://ntnuopen.ntnu.no/ntnu-xmlui/handle/11250/2622953

Eleation. (2023, June 20). *Introduction to ANSYS Mechanical for Static Analysis*. https://www.linkedin.com/pulse/introduction-ansys-mechanical-static-analysis-eleation/

Ferris, T. (2020, December 2). *3 Steps to Improve FEA Models*. Ansys Blog. https://www.ansys.com/blog/how-to-improve-fea

Fisher, J. M. (2005). Don't Stress Out. *October 2005 Modern Steel Construction SpecWise Topic 1.* Retrieved 4 June 2024, from https://www.aisc.org/globalassets/modern-steel/archives/2005/10/2005v10_specwise_stress.pdf

Floating Wind: Turning Ambition into Action. (n.d.). DNV. https://www.dnv.com/focus-areas/floating-offshore-wind/floating-wind-turning-ambition-into-action/

Floating wind. (n.d.). Equinor. https://www.equinor.com/energy/floating-wind

Floating Offshore Wind - STATE OF THE MARKET AND THE EMERGING NORWEGIAN VALUE CHAIN. (2022, June 22). Menon Economics. https://www.menon.no/publication/floating-offshore-wind/

Fujikubo, M., & Yao, T. (1999). Elastic local buckling strength of stiffened plate considering plate/stiffener interaction and welding residual stress. *Marine Structures*, *12*(9–10), 543–564. https://doi.org/10.1016/s0951-8339(99)00032-5

Gaertner, E., Rinker, J., Sethuraman, L., Zahle, F., Anderson, B., Barter, G., Abbas, N., Meng, F., Bortolotti, P., Skrzypinski, W., Scott, G., Feil, R., Bredmose, H., Dykes, K., Shields, M., Allen, C., & Viselli, A. (2020b). *IEA Wind TCP Task 37: Definition of the IEA 15-Megawatt Offshore Reference Wind Turbine*. United States. https://doi.org/10.2172/1603478

Gaspar, B., Teixeira, A., & Soares, C. (2014). Assessment of the efficiency of Kriging models for reliability analysis of complex structures. In *CRC Press eBooks* (pp. 5247–5255). https://doi.org/10.1201/b16387-762

Global Wind Energy Council. (2020). *Global Offshore Wind Report 2020*. https://gwec.net/global-offshore-wind-report-2020/

Grant, M. (2021, October 22). *Nonparametric Statistics: Overview, Types, and Examples*. Investopedia. https://www.investopedia.com/terms/n/nonparametric-statistics.asp

Hacihamud, E. (2022). *Non-linear buckling analysis of stiffened panels*. [Master Thesis, University of Stavanger]. UiS Brage. https://uis.brage.unit.no/uis-xmlui/handle/11250/3032551

Hu, Z., Liu, Y., & Wang, J. (2016b). An integrated structural strength analysis method for Spar type floating wind turbine. *China Ocean Engineering/China Ocean Engineering*, *30*(2), 217–230. https://doi.org/10.1007/s13344-016-0013-y

Hwang, J., Min, J., Ahn, Y., Kim, H., Kim, H., Roh, M., & Lee, K. (2008). Optimized methodology to build an integrated solution to offshore topside process engineering. *The Eighteenth International Offshore and Polar Engineering Conference*. https://onepetro.org/ISOPEIOPEC/proceedings-pdf/ISOPE08/All-ISOPE08/ISOPE-I-08-130/1803578/isope-i-08-130.pdf

IRENA. (2020). *Global Renewables Outlook: Energy transformation 2050 (Edition: 2020), International Renewable Energy Agency, Abu Dhabi*. https://www.irena.org/publications/2020/Apr/Global-Renewables-Outlook-2020

Ivanov, G., Hsu, I. J., & Ma, K. T. (2023). *Design Considerations on Semi-submersible Columns and Pontoons for Floating Wind*. https://doi.org/10.20944/preprints202307.0643.v1

Jang, S. B. (2007). *Lecture 7 Elastic Buckling of Stiffened Panels* [PowerPoint Slides]. OPen INteractive Structural Lab. https://ocw.snu.ac.kr/sites/default/files/NOTE/Lecture%2007%20Elastic_Buckling_of_Stiffened_Panels.pdf

Jiang, Z., Karimirad, M., & Moan, T. (2013). *Response Analysis of Parked Spar-Type Wind Turbine Considering Blade-Pitch Mechanism Fault*. *23*(02), 120–128.

Jonkman, J. (2014, November 12). *WP 1,5 MW turbine - Pitch Angle*. NREL Forum. https://forums.nrel.gov/t/wp-1-5-mw-turbine-pitch-angle/1026

Jonkman, J. M. (2007). *Dynamics Modeling and Loads Analysis of an Offshore Floating Wind Turbine*. National Renewable Energy Laboratory, Colorado, USA. https://doi.org/10.2172/921803

Jonkman, J., Butterfield, S., Musial, W., & Scott, G. (2009). *Definition of a 5-MW Reference Wind Turbine for Offshore System Development*. https://doi.org/10.2172/947422

Karkera, K. (2017, August 5). Regression Models with multiple target variables - Towards Data Science. *Medium*. https://towardsdatascience.com/regression-models-with-multiple-target-variables-8baa75aacd

Khandelwal, R. (2022, July 20). Supervised, Unsupervised, and Reinforcement Learning. *Medium*. https://arshren.medium.com/supervised-unsupervised-and-reinforcement-learning-245b59709f68

Kim, H. A., Featherston, C. A., Ussel, J., & Williams, P. A. (2007). Introducing a discrete modelling technique for buckling of panels under combined loading. *Structural and Multidisciplinary Optimization*, *36*(1), 3–13. https://doi.org/10.1007/s00158-007-0188-1

Kim, N. H. (n.d.). *Chapter 5 Finite Element Analysis of Contact Problem* [PowerPoint Slides]. University of Florida. https://mae.ufl.edu/nkim/egm6352/Chap5.pdf

Kirby, A. & Briol, F-X. (2023, July 4). *Using machine learning to design more efficient offshore wind farms*. The Alan Turing Institute. https://www.turing.ac.uk/blog/using-machine-learning-design-more-efficient-offshore-wind-farms

Laftah, R. (2007). *Buckling Behaviour of Stiffened Plate Panels Using Artificial Neural Networks*. http://dx.doi.org/10.13140/RG.2.2.10214.22086

Leimeister, M., Kolios, A., & Collu, M. (2018). Critical review of floating support structures for offshore wind farm deployment. *Journal of Physics. Conference Series*, *1104*, 012007. https://doi.org/10.1088/1742-6596/1104/1/012007

Li, K., Zheng, D., Wang, Z., Yuan, Z., & Jiang, X. (2022). Numerical investigation of the interception performance of HDPE pontoon-type port safety barrier system under boat attacking. *Ocean Engineering*, *259*, 111922. https://doi.org/10.1016/j.oceaneng.2022.111922

Li, L., Gao, Z., & Moan, T. (2013). *Joint Environmental Data at Five European Offshore Sites for Design of Combined Wind and Wave Energy Devices*. https://doi.org/10.1115/omae2013-10156

Li, W., Wang, S., Moan, T., Gao, Z., & Gao, S. (2024). Global design methodology for semi-submersible hulls of floating wind turbines. *Renewable Energy*, *225*, 120291. https://doi.org/10.1016/j.renene.2024.120291

Li, Z., Patil, M., & Yu, X. (2017). Ultimate strength of steel beam-columns under axial compression. *Proceedings of the Institution of Mechanical Engineers. Part M, Journal of Engineering for the Maritime Environment, 231*(4), 828–843. https://doi.org/10.1177/1475090216684234

Malone, T. (2021, April 21). *Machine learning, explained*. MIT Sloan. https://mitsloan.mit.edu/ideas-made-to-matter/machine-learning-explained

Marin, T. I. (2013). *Design and stress Analysis of the Column-Pontoon Connection in a Semi-Submersible Floating Wind Turbine*. Pre-project Thesis, Department of Marine Technology, NTNU.

Masoumi, M. (2023). Machine Learning Solutions for Offshore Wind Farms: A Review of Applications and Impacts. *Journal of Marine Science and Engineering*, *11*(10), 1855. https://doi.org/10.3390/jmse11101855

Matha, D., Cruz, J., Masciola, M., Bachynski, E. E., Atcheson, M., Goupee, A. J., Gueydon, S. M. H., & Robertson, A. N. (2016). Modelling of floating offshore wind technologies. In *Green energy and technology* (pp. 133–240). https://doi.org/10.1007/978-3-319-29398-1_4

Maximiano, A., Vaz, G., Torres, R., Voltá, L., & Lourenço, T. (2021). D5.4 Benchmark of PivotBuoy Compared to Other Offshore Wind Floating Systems. https://dx.doi.org/10.13140/RG.2.2.31161.65120

Moorings – Quest Floating Wind Energy. (n.d.). QFWE. https://questfwe.com/documentation-center/moorings/

Musial, W., Beiter, P., & Nunemaker, J. (2020). *Cost of floating offshore wind energy using New England Aqua Ventus Concrete semisubmersible technology*. https://doi.org/10.2172/1593700

Musial, W., Spitsen, P., Beiter, P., Duffy, P., Marquis, M., Cooperman, A., Hammond, R., & Shields, M. (2021). *Offshore Wind Market Report: 2021 Edition*. https://doi.org/10.2172/1818842

Musial, W., Spitsen, P., Duffy, P., Beiter, P., Shields, M., Hernando, D. M., Hammond, R., Marquis, M., King, J., & Sathish, S. (2023). *Offshore Wind Market Report: 2023 Edition*. https://doi.org/10.2172/2001112

National Grid. (2022). *Onshore vs offshore wind energy: what's the difference? | National Grid Group*. www.nationalgrid.com. https://www.nationalgrid.com/stories/energy-explained/onshore-vs-offshore-wind-energy

National Grid. (2022). *What is offshore wind power? | National Grid Group*. www.nationalgrid.com. https://www.nationalgrid.com/stories/energy-explained/what-offshore-wind-power

Nguyen, C. T. (2011). *Optimum layout of stiffened panels subjected to lateral pressure and inplane loads.* [Master Thesis, NTNU]. NTNU Open. https://ntnuopen.ntnu.no/ntnu-xmlui/handle/11250/238046

Noppe, N., Weijtjens, W., & Devriendt, C. (2018). Modeling of quasi-static thrust load of wind turbines based on 1 s SCADA data. *Wind Energy Science*, *3*(1), 139–147. https://doi.org/10.5194/wes-3-139-2018

Ørsted warns about rising costs of UK wind development. (2023). Financial Times. https://www.ft.com/content/4621f549-85dc-4731-b3ad-6d76969c31d4

Ostapenko, A. (1981). *Strength of Ship Hull Girders under Moment, Shear and Torque*. The Society of Naval Architects and Marine Engineers, New York. http://www.shipstructure.org/pdf/81symp12.pdf

Papi, F., & Bianchini, A. (2022). Technical challenges in floating offshore wind turbine upscaling: A critical analysis based on the NREL 5 MW and IEA 15 MW Reference Turbines. *Renewable & Sustainable Energy Reviews*, *162*, 112489. https://doi.org/10.1016/j.rser.2022.112489

Park, S., & Choung, J. (2023). Structural Design of the Substructure of a 10 MW Floating Offshore Wind Turbine System Using Dominant Load Parameters. *Journal of Marine Science and Engineering*, *11*(5), 1048. https://doi.org/10.3390/jmse11051048

Prasanna, S. (2015). *Machine Learning Made Easy*. MATLAB. https://uk.mathworks.com/videos/machine-learning-with-matlab-100694.html

Ren, C., & Xing, Y. (2023). AK-MDAmax: Maximum fatigue damage assessment of wind turbine towers considering multi-location with an active learning approach. *Renewable Energy*, *215*, 118977. https://doi.org/10.1016/j.renene.2023.118977

Ren, C., & Xing, Y. (2023b). Applying a machine learning method for cumulative fatigue damage estimation of the IEA 15MW wind turbine with monopile support structures. *IOP Conference Series. Materials Science and Engineering*, *1294*(1), 012014. https://doi.org/10.1088/1757-899x/1294/1/012014

Robertson, A., Jonkman, J., Masciola, M., Song, H., Goupee, A., Coulling, A., & Luan, C. (2014). *Definition of the Semisubmersible Floating System for Phase II of OC4*. https://doi.org/10.2172/1155123

Roehm, P. M. (2017). *Minimizing Run Time of Finite Element Analyses: Applications in Conformable CNG Tank Modeling*. [Master Thesis, Michigan Technological University]. https://doi.org/10.37099/mtu.dc.etdr/380

Rutledge, D. R., & Ostapenko, A. (1968). *Ultimate strength of longitudinally stiffened plate panels (large and small b/t, general material properties), September 1968*. http://preserve.lehigh.edu/cgi/viewcontent.cgi?article=2670&context=engr-civil-environmental-fritz-lab-reports

Sadoughi. (2017). *GitHub - mksadoughi/Multi-output-Gaussian-Process*. GitHub. https://github.com/mksadoughi/Multi-output-Gaussian-Process

Sakib, M. S., & Griffith, D. T. (2022). Parked and operating load analysis in the aerodynamic design of multi-megawatt-scale floating vertical-axis wind turbines. *Wind Energy Science*, *7*(2), 677–696. https://doi.org/10.5194/wes-7-677-2022

Salem, M. B., Hussein, H., Aiche, G., Haddab, Y., Lutz, P., Rubbert, L., & Renaud, P. (2019). Characterization of bistable mechanisms for microrobotics and mesorobotics. *Journal of Micro-bio Robotics*, *15*(1), 65–77. https://doi.org/10.1007/s12213-019-00113-3

Sandua-Fernández, I., Vittori, F., Eguinoa, I., & Cheng, P. W. (2022). Impact of hydrodynamic drag coefficient uncertainty on 15 MW floating offshore wind turbine power and speed control. *Journal of Physics. Conference Series*, *2362*(1), 012037. https://doi.org/10.1088/1742-6596/2362/1/012037

SesamX. (2020, April 7). *The shell finite element explained*. Affordable structural analysis software | FEA | SesamX. https://www.sesamx.io/blog/shell_finite_element/

Shirzadeh, R., Weijtjens, W., Guillaume, P., & Devriendt, C. (2014). The dynamics of an offshore wind turbine in parked conditions: a comparison between simulations and measurements. *Wind Energy*, *18*(10), 1685–1702. https://doi.org/10.1002/we.1781

Stevens, N. (2019, June 22). Practical Tips for Dealing with Stress Singularities | Nick J Stevens. *Medium*. https://medium.com/@nickjstevens/practical-tips-for-dealing-with-stress-singularities-nick-j-stevens-1fe6a57d55a9

Stupak, T. (2024, January 12). *How Much Data Is Required To Train ML Models in 2024?* Akkio. https://www.akkio.com/post/how-much-data-is-required-to-train-ml#:~:text=The%20amount%20of%20training%20data,or%20more%20examples%20than%20features.

T-beam. (2023, November 25). Wikipedia. https://en.wikipedia.org/wiki/T-beam

Tvare, O. (2014). *Fatigue Analysis of Column-Pontoon Connection in a Semi-submersible Floating Wind Turbine.* [Master Thesis, NTNU]. NTNU Open. https://ntnuopen.ntnu.no/ntnu-xmlui/handle/11250/2433678

Vedvik, N. P. (2021). *Elements.* https://folk.ntnu.no/nilspv/TMM4175/elements.html#:~:text=Shear%20locking%20occurs%20in%20first,too%20stiff%20in%20bending%20modes.

Vittori, F. E. (2015). *Design and Analysis of Semi-submersible Floating Wind Turbines with focus on Structural Response Reduction*. [Master Thesis, NTNU]. NTNU Open. https://ntnuopen.ntnu.no/ntnu-xmlui/handle/11250/2350699

Wang, J., Guo, J., Yao, X. L., & Zhang, A. M. (2016b). Dynamic buckling of stiffened plates subjected to explosion impact loads. *Shock Waves*, *27*(1), 37–52. https://doi.org/10.1007/s00193-016-0638-z

Wang, S., Xing, Y., Balakrishna, R., Shi, W., & Xu, X. (2023). Design, local structural stress, and global dynamic response analysis of a steel semi-submersible hull for a 10-MW floating wind turbine. *Engineering Structures/Engineering Structures (Online)*, *291*, 116474. https://doi.org/10.1016/j.engstruct.2023.116474

Wayman, E., Sclavounos, P., Butterfield, S., Jonkman, J., & Musial, W. (2006). Coupled Dynamic Modeling of Floating Wind Turbine Systems. *Offshore Technology Conference*. https://doi.org/10.4043/18287-ms

WindEurope. (2022, May 4). *Financing and investment trends 2021*. WindEurope. https://windeurope.org/intelligence-platform/product/financing-and-investment-trends-2021/

What Is Machine Learning (ML)? | IBM. (n.d.). https://www.ibm.com/topics/machine-learning

What Is Machine Learning? (n.d.). MATLAB & Simulink. https://uk.mathworks.com/discovery/machine-learning.html

Yadav, A., Bareth, R., Kochar, M., Pazoki, M., & Sehiemy, R. a. E. (2023). Gaussian process regression-based load forecasting model. *IET Generation, Transmission & Distribution*, *18*(5), 899–910. https://doi.org/10.1049/gtd2.12926

Yang, H. S., Alkhabbaz, A., Edirisinghe, D. S., Tongphong, W., & Lee, Y. H. (2022). FOWT Stability Study According to Number of Columns Considering Amount of Materials Used. *Energies*, *15*(5), 1653. https://doi.org/10.3390/en15051653

Yao, T., & Fujikubo, M. (2016). Fundamental Theory and Methods of Analysis to Simulate Buckling/Plastic Collapse Behavior. In *Elsevier eBooks* (pp. 35–74). https://doi.org/10.1016/b978-0-12-803849-9.00003-4

Yilmaz, O. C. (2014). *The Optimization of Offshore Wind Turbine Towers Using Passive Tuned Mass Dampers*. https://doi.org/10.7275/5394885

Young, W. C., & Budynas, R. G. (2002). Roark's formulas for stress and strain by Warren C. Young and Richard G. Budynas. Mcgraw-Hill. https://jackson.engr.tamu.edu/wp-content/uploads/sites/229/2023/03/Roarks-formulas-for-stress-and-strain.pdf

Yu, Z., Amdahl, J., & Sha, Y. (2018). Large inelastic deformation resistance of stiffened panels subjected to lateral loading. *Marine Structures*, *59*, 342–367. https://doi.org/10.1016/j.marstruc.2018.01.005

Appendix A – OPENFAST Input file

IEA-15-240-RWT-UMaineSemi.fst

```
------- OpenFAST INPUT FILE -------------------------------------------
IEA 15 MW offshore reference model on UMaine VolturnUS-S semi-submersible floating platform
---------------------- SIMULATION CONTROL --------------------------------------
False                   Echo        - Echo input data to <RootName>.ech (flag)
"FATAL"                 AbortLevel  - Error level when simulation should abort (string) {"WARNING", "SEVERE", "FATAL"}
4000.0                  TMax        - Total run time (s)
0.025                   DT          - Integration time step (s)
2                       InterpOrder - Interpolation order for input/output time history (-) {1=linear, 2=quadratic}
0                       NumCrctn    - Number of correction iterations (-) {0=explicit calculation, i.e., no corrections}
99999.0                 DT_UJac     - Time between calls to get Jacobians (s)
1000000.0               UJacSclFact - Scaling factor used in Jacobians (-)
---------------------- FEATURE SWITCHES AND FLAGS ------------------------------
      1   CompElast       - Compute structural dynamics (switch) {1=ElastoDyn; 2=ElastoDyn + BeamDyn for blades}
      1   CompInflow      - Compute inflow wind velocities (switch) {0=still air; 1=InflowWind; 2=external from OpenFOAM}
      2   CompAero        - Compute aerodynamic loads (switch) {0=None; 1=AeroDyn v14; 2=AeroDyn v15}
      1   CompServo       - Compute control and electrical-drive dynamics (switch) {0=None; 1=ServoDyn}
      1   CompHydro       - Compute hydrodynamic loads (switch) {0=None; 1=HydroDyn}
      0   CompSub         - Compute sub-structural dynamics (switch) {0=None; 1=SubDyn; 2=External Platform MCKF}
      3   CompMooring     - Compute mooring system (switch) {0=None; 1=MAP++; 2=FEAMooring; 3=MoorDyn; 4=OrcaFlex}
      0   CompIce         - Compute ice loads (switch) {0=None; 1=IceFloe; 2=IceDyn}
      0   MHK             - MHK turbine type (switch) {0=Not an MHK turbine; 1=Fixed MHK turbine; 2=Floating MHK turbine}
---------------------- ENVIRONMENTAL CONDITIONS --------------------------------
9.81                    Gravity     - Gravitational acceleration (m/s^2)
1.225                   AirDens     - Air density (kg/m^3)
1025                    WtrDens     - Water density (kg/m^3)
1.464e-05               KinVisc     - Kinematic viscosity of working fluid (m^2/s)
335                     SpdSound    - Speed of sound in working fluid (m/s)
103500                  Patm        - Atmospheric pressure (Pa) [used only for an MHK turbine cavitation check]
1700                    Pvap        - Vapour pressure of working fluid (Pa) [used only for an MHK turbine cavitation check]
200                      WtrDpth     - Water depth (m)
0                       MSL2SWL     - Offset between still-water level and mean sea level (m) [positive upward]
---------------------- INPUT FILES ---------------------------------------------
"IEA-15-240-RWT-UMaineSemi_ElastoDynU6.dat"    EDFile          - Name of file containing ElastoDyn input parameters (quoted
string)
""                      BDBldFile(1) - Name of file containing BeamDyn input parameters for blade 1 (quoted string)
""                      BDBldFile(2) - Name of file containing BeamDyn input parameters for blade 2 (quoted string)
""                      BDBldFile(3) - Name of file containing BeamDyn input parameters for blade 3 (quoted string)
"../IEA-15-240-RWT/IEA-15-240-RWT InflowFile.dat"    InflowFile      - Name of file containing inflow wind input parameters
(quoted string)
"../IEA-15-240-RWT/IEA-15-240-RWT_AeroDyn15.dat"  AeroFile     - Name of file containing aerodynamic input parameters (quoted
string)
"IEA-15-240-RWT-UMaineSemi ServoDyn.dat"    ServoFile       - Name of file containing control and electrical-drive input
parameters (quoted string)
"IEA-15-240-RWT-UMaineSemi_HydroDyn.dat"      HydroFile       - Name of file containing hydrodynamic input parameters (quoted
string)
"none"                  SubFile         - Name of file containing sub-structural input parameters (quoted string)
"IEA-15-240-RWT-UMaineSemi_MoorDyn.dat"      MooringFile     - Name of file containing mooring system input parameters (quoted
string)
"none"                  IceFile         - Name of file containing ice input parameters (quoted string)
---------------------- OUTPUT --------------------------------------------------
False                   SumPrint    - Print summary data to "<RootName>.sum" (flag)



10.0                    SttsTime    - Amount of time between screen status messages (s)
99999.0                 ChkptTime   - Amount of time between creating checkpoint files for potential restart (s)
default                 DT_Out      - Time step for tabular output (s) (or "default")
0.000000                TStart      - Time to begin tabular output (s)
1                       OutFileFmt  - Format for tabular (time-marching) output file (switch) {1: text file [<RootName>.out],
2: binary file [<RootName>.outb], 3: both}
True                    TabDelim    - Use tab delimiters in text tabular output file? (flag) {uses spaces if false}
"ES10.3E2"              OutFmt      - Format used for text tabular output, excluding the time channel.  Resulting field should
be 10 characters. (quoted string)
---------------------- LINEARIZATION -------------------------------------------
False                   Linearize   - Linearization analysis (flag)
False                   CalcSteady  - Calculate a steady-state periodic operating point before linearization? [unused if
Linearize=False] (flag)
3                       TrimCase    - Controller parameter to be trimmed {1:yaw; 2:torque; 3:pitch} [used only if
CalcSteady=True] (-)
0.001                   TrimTol     - Tolerance for the rotational speed convergence [used only if CalcSteady=True] (-)
0.01                    TrimGain    - Proportional gain for the rotational speed error (>0) [used only if CalcSteady=True]
(rad/(rad/s) for yaw or pitch; Nm/(rad/s) for torque)
0                       Twr_Kdmp    - Damping factor for the tower [used only if CalcSteady=True] (N/(m/s))
0                       Bld_Kdmp    - Damping factor for the blades [used only if CalcSteady=True] (N/(m/s))
2                       NLinTimes   - Number of times to linearize (-) [>=1] [unused if Linearize=False]
30.000000, 60.000000    LinTimes    - List of times at which to linearize (s) [1 to NLinTimes] [used only when Linearize=True
and CalcSteady=False]
1                       LinInputs   - Inputs included in linearization (switch) {0=none; 1=standard; 2=all module inputs
(debug)} [unused if Linearize=False]
1                       LinOutputs  - Outputs included in linearization (switch) {0=none; 1=from OutList(s); 2=all module
outputs (debug)} [unused if Linearize=False]
False                   LinOutJac   - Include full Jacobians in linearization output (for debug) (flag) [unused if
Linearize=False; used only if LinInputs=LinOutputs=2]
False                   LinOutMod   - Write module-level linearization output files in addition to output for full system?
(flag) [unused if Linearize=False]
---------------------- VISUALIZATION -------------------------------------------
0                       WrVTK       - VTK visualization data output: (switch) {0=none; 1=initialization data only; 2=animation}
2                       VTK_type    - Type of VTK visualization data: (switch) {1=surfaces; 2=basic meshes (lines/points);
3=all meshes (debug)} [unused if WrVTK=0]
False                   VTK_fields  - Write mesh fields to VTK data files? (flag) {true/false} [unused if WrVTK=0]
15.0                    VTK_fps     - Frame rate for VTK output (frames per second){will use closest integer multiple of DT}
[used only if WrVTK=2]

```

Appendix B – Detailed calculation for hull plate thickness

To check if the provided hull plate thickness is sufficient to resist bending:

Because bending moment drives the design of hull, following calculations are to derive the hull thickness:

yellow cells indicate input	red cell indicates need to check

at rated wind speed 10.59m/s
using the data for turbulent wind at 11m/s,

resolved global forces and moments at the horizontal pontoon;

Fx	5640	kN
Fy	-777	kN
Fz	-24300	kN
Mx	116000	kNm
My	672000	kNm
Mz	24900	kNm

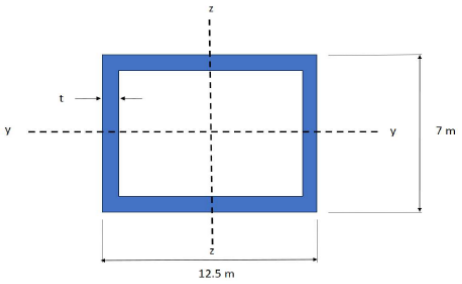

check: to find minimum thickness of hull under bending moment

As per DNV-OS-C101, Section 5, F201 and DNV-ST-0119, Clause 7.1.6.3:

F 200 Minimum thickness

201 The thickness of plates should not to be less than:

$$t = \frac{14.3 t_0}{\sqrt{f_{yd}}} \quad \text{(mm)}$$

f_{yd} = design yield strength f_y/γ_M
f_y is the minimum yield stress (N/mm²) as given in Sec.4 Table D1
t_0 = 7 mm for primary structural elements
= 5 mm for secondary structural elements
γ_M = material factor for steel
= 1.15.

t	=	14.3*t0/√fyd	
where:			
t0	=	7 mm	(for primary structures)
fy	=	235 MPa	(Normal strength steel)
ym, material factor for steel	=	1.15	(Ref. Section 5, B101)

B. Flat Plated Structures and Stiffened Panels

B 100 General

101 The material factor γ_M for plated structures is 1.15.

fyd	=	204.3478 MPa	
hence,			
t	=	8 mm	

minimum thickness wrt bending My (major axis BM)

t	=	50 mm	(obtained iteratively)
My	=	672000 kNm	(the moment to resist)
distance from extreme fibre of cross section to neutral axis, y	=	3.5 m	
MOI about y-y axis, Iy	=	1/12 * (12.5 * 7^3) - 1/12 * (12.5 - 2t) * (7 - 2t)^3	
	=	17.83237 m^4	
Moment capacity about y-y axis	=	fyd * Iy / y	
	=	1041144 kNm	

F3. ALLOWABLE STRESS: BENDING OF BOX MEMBERS, RECTANGULAR TUBES AND CIRCULAR TUBES

1. Members With Compact Sections

For members bent about their strong or weak axes, members with compact sections as defined in Sect. B5 and flanges continuously connected to the webs, the allowable stress is

$$F_b = 0.66\, F_y \qquad \text{(F3-1)}$$

bending moment utilization ratio	=	0.645444	(max is 0.66 as per AISC 9th Ed, Eqn F3-1 for compact section & 0.6 for Eqn F3-3, non-compact)
Is the provided hull thickness OK?	=	ok	(assume the box hull section is compact)

minimum thickness wrt bending Mz (minor axis BM)

thickness of hull cross section, t	=	0.05 m	(same as input in cell C42)
Mz	=	24900 kNm	(the moment to resist)
distance from extreme fibre of cross section to neutral axis, z	=	6.25 m	
MOI about z-z axis, Iz	=	1/12 * (7* 12.5^3) - 1/12 * (7 - 2t) * (12.5 - 2t)^3	
	=	43.01412 m^4	
Moment capacity about z-z axis	=	fyd * Iz / z	
	=	1406375 kNm	
bending moment utilization ratio	=	0.017705	(max is 0.66 as per AISC 9th Ed, Eqn F3-1 for compact section & 0.6 for Eqn F3-3, non-compact)
Is the provided hull thickness OK?	=	ok	(assume the box hull section is compact)

check shear stress

width of hull cross section	=	12.5 m	
height of hull cross section	=	7 m	
thickness of hull cross section	=	0.05 m	(same as input in cell C28)

shear area	= depth x web thickness, assuming only webs take shear)			
	=	0.35	m^2	(as per AISC 9th Ed, Eqn F4-1)
shear force	=	24300	kN	(=Fz)
shear stress, τ	=	69.42857	MPa	
design shear stress, τd	=	τ * γm		
	=	79.84286	MPa	

F4. ALLOWABLE SHEAR STRESS

For $h/t_w \leq 380/\sqrt{F_y}$, on the overall depth times the web thickness, the allowable shear stress is

$$F_v = 0.40\ F_y \qquad \text{(F4-1)}$$

allowable shear stress Fv	=	0.4 Fy		(as per AISC 9th Ed, Eqn F4-1)
	=	94	MPa	
Is the provided hull thickness OK?	=	ok		

Is overall check ok with selected hull thickness?		OK

Appendix C – Section profile properties of girders

The section properties of the girders were referenced from the section profile database in the SESAM GeniE software.

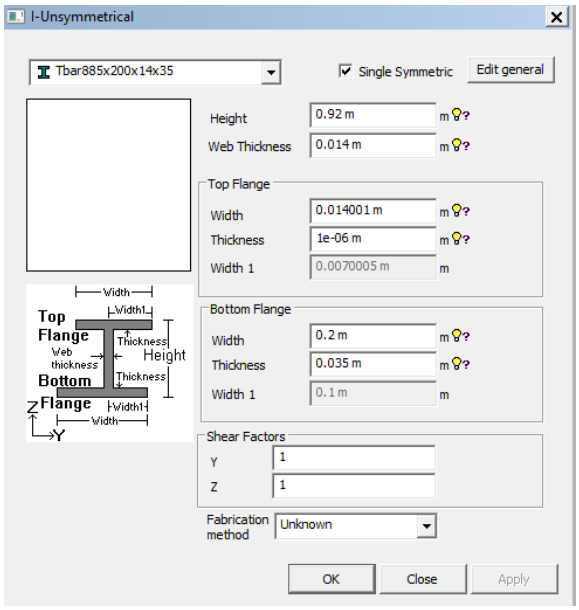

Figure A- 1 Section profile of Tbar885x200x14x35 (SESAM GeniE)

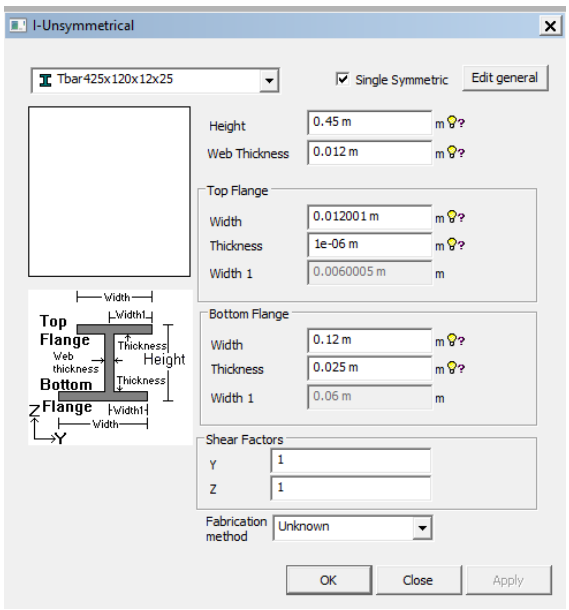

Figure A- 2 Section profile of Tbar425x120x12x25 (SESAM GeniE)

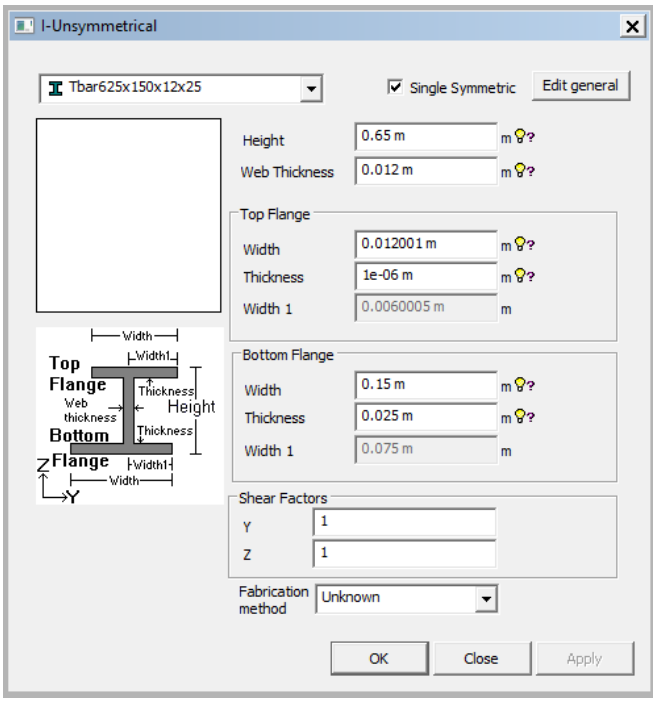

Figure A- 3 Section profile of Tbar625x150x12x25 (SESAM GeniE)

To clarify, there are no bottom flanges in the T-bar sections. It only comprises of a top flange and a web.

Appendix D – Detailed calculation for stiffener layout

DNV-RP-C201

Example of a stiffened plate panel

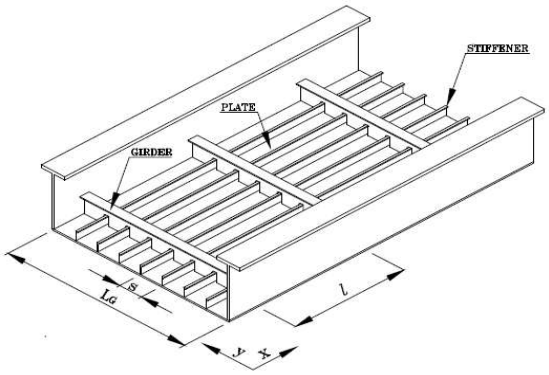

Figure 3-1 Stiffened plate panel

Because bending moment drives the design of hull, following calculations are to derive the hull thickness:

yellow cells indicate input	red cell indicates need to check

at rated wind speed 10.59m/s

using the data for turbulent wind at 11m/s,

resolved global forces and moments at the horizontal pontoon;

Fx	5640	kN
Fy	-777	kN
Fz	-24300	kN
Mx	116000	kNm
My	672000	kNm
Mz	24900	kNm

dimensions of pontoon cross section

length of hull	=	40.5	m
width of hull	=	12.5	m
surface area of hull face	=	506.25	m2
hull plate thickness	=	50	mm

dimensions of idealised stiffened panel as per DNVGL-PS, Stipla,Theory Manual

face considered = top/bottom

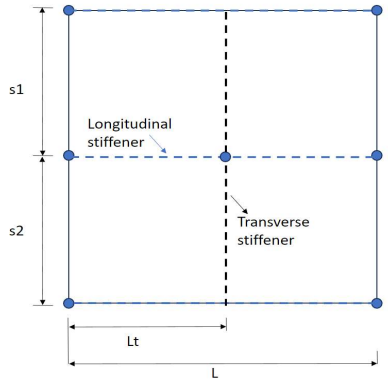

longitudinal stiffener c/c spacing, s1 (=s2)	=	2.5	m
transverse stiffener c/c spacing, Lt	=	0.9	m
surface area of idealised stiffened panel	=	s1 * Lt	
	=	9	m2

loads applied to idealised stiffened panel

Fx	100.2667	kN
Fy	-13.81333	kN
Fz	-432	kN
Mx	2062.222	kNm
My	11946.67	kNm
Mz	442.6667	kNm

Check hull plate thickness OK under pressure load

From Roark's Formulas for Stress & Strain (Young & Budynas, 2002)

TABLE 11.4 Formulas for flat plates with straight boundaries and constant thickness

NOTATION: The notation for Table 11.2 applies with the following modifications: a and b refer to plate dimensions, and when used as subscripts for stress, they refer to the stresses in directions parallel to the sides a and b, respectively. σ is a bending stress which is positive when tensile on the bottom and compressive on the top if loadings are considered vertically downward. R is the reaction force per unit length normal to the plate surface exerted by the boundary support on the edge of the plate. r'_o is the equivalent radius of contact for a load concentrated on a very small area and is given by $r'_o = \sqrt{1.6r_o^2 + t^2} - 0.675t$ if $r_o < 0.5t$ and $r'_o = r_o$ if $r_o \geq 0.5t$

Case no., shape, and supports	Case no., loading	Formulas and tabulated specific values
1. Rectangular plate; all edges simply supported 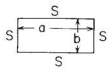	1a. Uniform over entire plate	(At center) $\sigma_{max} = \sigma_b = \frac{\beta q b^2}{t^2}$ and $y_{max} = \frac{-\alpha q b^4}{Et^3}$ (At center of long sides) $R_{max} = \gamma q b$

a/b	1.0	1.2	1.4	1.6	1.8	2.0	3.0	4.0	5.0	∞
β	0.2874	0.3762	0.4530	0.5172	0.5688	0.6102	0.7134	0.7410	0.7476	0.7500
α	0.0444	0.0616	0.0770	0.0906	0.1017	0.1110	0.1335	0.1400	0.1417	0.1421
γ	0.420	0.455	0.478	0.491	0.499	0.503	0.505	0.502	0.501	0.500

(Ref. 21 for $\nu = 0.3$)

longer side length, a	=	c/c spacing between longitudinal stiffeners
	=	2.5 m
shorter side length, b	=	c/c spacing between transverse stiffeners
	=	0.9 m

a/b	1	1.2	1.4	1.6	1.8	2
β	0.2874	0.3762	0.453	0.5172	0.5688	0.6102
a/b	3	4	5	infinity		
β	0.7134	0.741	0.7476	0.75		

aspect ratio, a/b	=	ok
β	=	0.75
pressure load, q	=	Fz / surface area
	=	-48 kN/m2

stress at center of plate, σmax	=	β*q*b^2/t^2	
	=	-11.664 MPa	(negative value indicates stress acting downwards)
allowable stress of plate	=	235 MPa	
material factor, γ_M	=	1.15	(ref. DNV-RP-C201, section 2)
design yield stress	=	204.35 MPa	
stress check OK?		OK if σmax < design yield stress	
		NOT ok if otherwise (need to adjust hull thickness	
	=	ok	and/or stiffener layout)
utilisation ratio	=	0.057	

Check shear resistance of stiffened panel as per DNV-RP-C201, Section 7.6

7.6 Resistance of stiffened panels to shear stresses

The resistance towards shear stresses τ_{Rd} is found as the minimum of τ_{Rdy}, τ_{Rdl} and τ_{Rds} according to the following:

$$\tau_{Rdy} = \frac{f_y}{\sqrt{3} \cdot \gamma_M} \qquad (7.45)$$

$$\tau_{Rdl} = \frac{\tau_{crl}}{\gamma_M} \qquad (7.46)$$

$$\tau_{Rds} = \frac{\tau_{crs}}{\gamma_M} \qquad (7.47)$$

where τ_{crl} is obtained from eq. (7.6) and τ_{crs} is obtained from:

$$\tau_{crs} = \frac{36 \cdot E}{s \cdot t \cdot l^2} \cdot \sqrt[4]{I_p \cdot I_s^3} \qquad (7.48)$$

with:

$$I_p = \frac{t^3 \cdot s}{10.9} \qquad (7.49)$$

and I_s= moment of inertia of stiffener with full plate width.

cross section of the longitudinal stiffener and full plate width

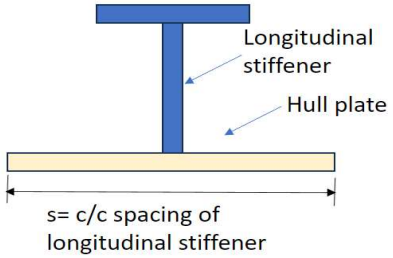

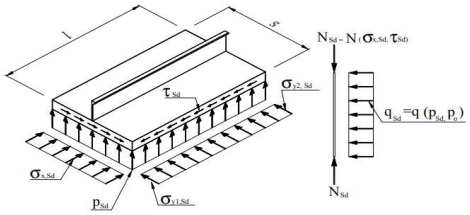

using ANSYS to compute the MOI,
https://courses.ansys.com/index.php/courses/tips-and-tricks-for-structural-simulation-in-ansys-mechanical/le

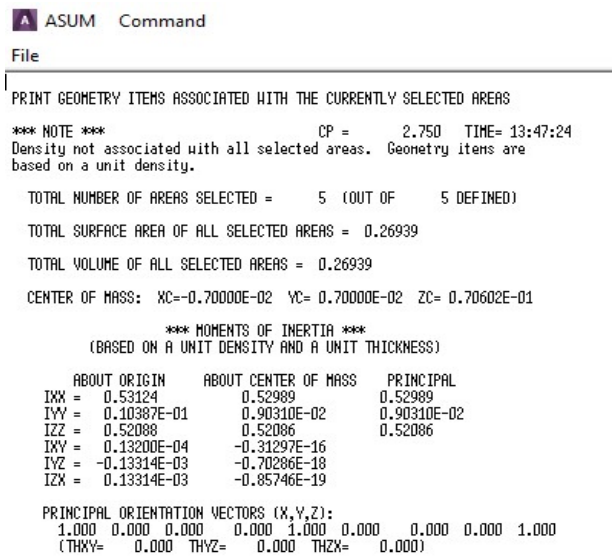

MOI of stiffener with full plate width, Is (about major Z axis)	=	5.21E-01	m^4
	=	5.21E+11	mm^4
polar MOI, Ip	=	t^3 * s /10.9	
where			
t	=	hull plate thickness	
	=	50	mm
s, stiffener spacing	=	c/c spacing of longitudinal stiffeners	
	=	2.5	m
Hence,			
polar MOI, Ip	=	2.86697E-05	m^4
	=	2.87E+07	mm^4
l, stiffener length (=c/c spacing of transverse stiffener)	=	0.9	m
Young's modulus, E	=	211000	MPa
36 E	=	7596000	MPa
s*t*l^2	=	1.0125E+11	mm^4
(Ip*Is^3)^1/4	=	4.49E+10	mm^4
τ_crs	=	3.37E+06	MPa
τ_Rds	=	τ_crs / γ_M	
	=	2.93E+06	MPa
_crl	=	critical shear stress for the plate panel between 2 stiffeners	

$$\tau_{crl} = k_l \cdot 0.904 \cdot E \cdot \left(\frac{t}{s}\right)^2 \quad \textbf{(7.6)}$$

where:

$$k_l = 5.34 + 4\left(\frac{s}{l}\right)^2, \text{for } l \geq s \quad \textbf{(7.7)}$$

$$= 5.34\left(\frac{s}{l}\right)^2 + 4, \text{for } l < s$$

k_l	=	45.2037037		*l<s*

As per DNV–RP-C201, Section 3.6: This Recommended Practice is best suited to rectangular plates and stiffened panels with stiffener length being larger than the stiffener spacing (l > s).

_crl	=	3.45E+03	MPa	
τ_Rdl	=	τ_crl / γ_M		
	=	3.00E+03	MPa	
τ_Rdy	=	117.98	MPa	(eqn 7.45)
_Rd, resistance to shear stress	=	min(τ_Rds, τ_Rdl, τ_Rdy)		
	=	117.98	MPa	
shear area	=	assume only web of stiffener and hull plate contribute to shear resistance		
stiffener web depth	=	885	mm	(longitudinal stiffener, design 1)
stiffener web thickness	=	14	mm	
hull plate thickness	=	50	mm	
assume load spreading effect of 1:5,				
hull plate length considered	=	2 (5* hull plate thickness) + stiffener web thickness		
	=	514	mm	(ref AISC 9th Ed, Eqn K1-9)
shear area	=	38090	mm^2	
shear force to resist	=	Fz		
	=	-432	kN	
shear stress to resist	=	-11.34155946	MPa	
shear stress utilisation ratio	=	shear stress to resist /τ_Rd		
	=	0.10		
stress check OK? (shear resistance of stiffened panel)		OK if shear stress < τ_Rd NOT ok if otherwise (need to adjust hull thickness		
	=	**ok**		and/or stiffener layout)

Stiffener axial capacity as per DNV-RP-C201, Section 7.2

7.2 Forces in the idealised stiffened plate

Stiffened plates subjected to combined forces, see Figure 7-1 should be designed to resist an equivalent axial force according to eq. (7.1) and an equivalent lateral load according to eq. (7.8).

The equivalent axial force should be taken as:

$$N_{Sd} = \sigma_{x,Sd}(A_s + st) + \tau_{tf} st \qquad (7.1)$$

where

A_s = cross sectional area of stiffener

s = distance between stiffeners

t = plate thickness

$\sigma_{x,Sd}$ = axial stress in plate and stiffener with compressive stresses as positive

$$\tau_{tf} = \tau_{Sd} - \tau_{crg} \quad \text{for } \tau_{Sd} > \frac{\tau_{crl}}{\gamma_M} \qquad (7.2)$$

and tension field action is allowed

$$\tau_{tf} = 0 \quad \text{otherwise} \qquad (7.3)$$

axial force to resist, Nsd = Fx + My / half depth of stiffener (depth =920mm)
= 26071.28 kN

As, cross sectional area of stiffener = longitudinal stiffener T bar 885x200x14x35
= 19390 mm2

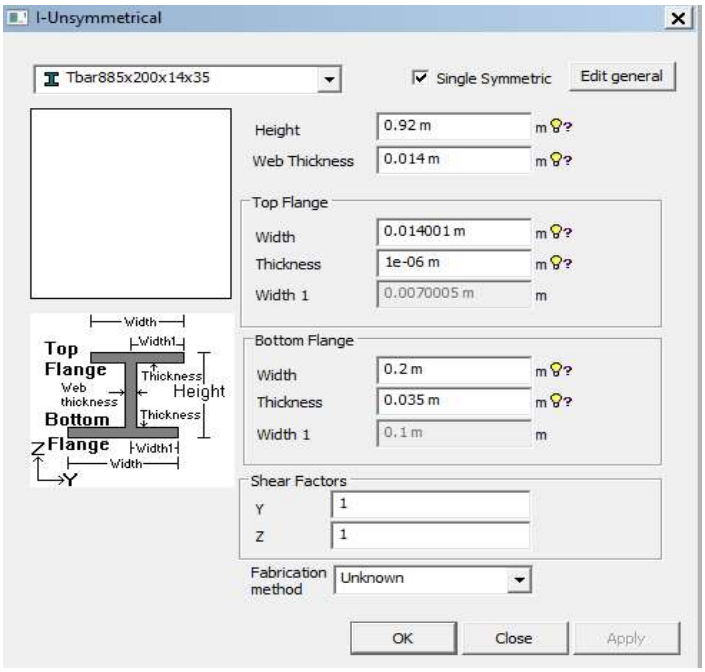

(From Sesam section database)

s*t, cross sectional area of hull plate considered	=	0.125 m2
τ_tf	=	0 (assume no tension field action)
σsd, axial stress in plate and stiffener	=	Nsd / (As + s*t)
	=	180.56 MPa

From DNV-RP-C102, Section 6.2:
https://home.hvl.no/ansatte/gste/ftp/MarinLab_files/Litteratur/DNV/DNV_pE13%20of%2036_scatter%20diagram.pdf

6.2. General principles

The ULS capacity checks include both checks of yield and buckling resistance. The yield check reads :

$$\sigma_{ed} \leq \frac{1}{\gamma_m} f_y$$

where:

σ_{ed} = Design Von Mises equivalent stress (including load factors)

γ_m = Material factor = 1.15

f_y = Characteristic yield strength of the material

allowable axial stress	=	204.35 MPa

2 Safety format

This Recommended Practice is written in the load and resistance factor design format (LRFD format) to suit the DNV Offshore Standard DNV-OS-C101. This standard make use of material (resistance) and loadfactors as safety factors.

This Recommended Practice may be used in combination with a working stress design format (WSD) by the following method. For the formulas used in this standard use a material factor $\gamma_M = 1.15$. The checks should be made using a modified allowable usage factor taken as UF·1.15, where UF is the allowable usage factor according to the WSD standard.

allowable utilisation ratio	=	1/1.15
	=	0.87
utilisation ratio	=	0.88

Stiffener axial capacity check OK?

ok if UF < 1
not ok if otherwise
ok

Check axial stress of stiffener and stiffened plate

From ANSYS, the MOI properties of the stiffener and plate:

ASUM Command

File

```
PRINT GEOMETRY ITEMS ASSOCIATED WITH THE CURRENTLY SELECTED AREAS

*** NOTE ***                            CP =       2.750   TIME= 13:47:24
Density not associated with all selected areas.  Geometry items are
based on a unit density.

  TOTAL NUMBER OF AREAS SELECTED =      5  (OUT OF      5 DEFINED)

  TOTAL SURFACE AREA OF ALL SELECTED AREAS =  0.26939

  TOTAL VOLUME OF ALL SELECTED AREAS =  0.26939

  CENTER OF MASS:  XC=-0.70000E-02  YC= 0.70000E-02  ZC= 0.70602E-01

                 *** MOMENTS OF INERTIA ***
          (BASED ON A UNIT DENSITY AND A UNIT THICKNESS)

      ABOUT ORIGIN     ABOUT CENTER OF MASS    PRINCIPAL
   IXX =   0.53124          0.52989          0.52989
   IYY =   0.10387E-01      0.90310E-02      0.90310E-02
   IZZ =   0.52088          0.52086          0.52086
   IXY =   0.13200E-04     -0.31297E-16
   IYZ =  -0.13314E-03     -0.70286E-18
   IZX =   0.13314E-03     -0.85746E-19

   PRINCIPAL ORIENTATION VECTORS (X,Y,Z):
     1.000  0.000  0.000    0.000  1.000  0.000    0.000  0.000  1.000
     (THXY=    0.000  THYZ=    0.000  THZX=    0.000)
```

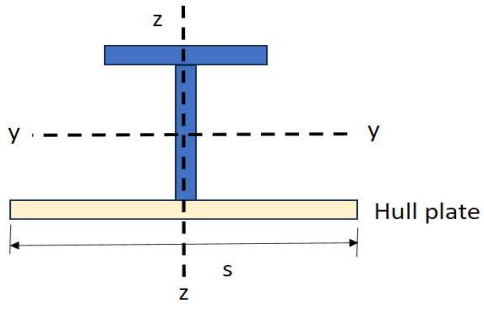

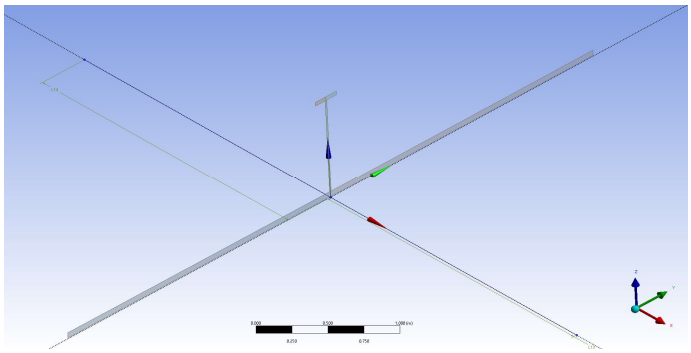

cross sectional area of stiffener and plate, A	=	As + s*t	
	=	144390	mm2
axial force	=	Fx	
	=	100.27	kN
Fx/A	=	0.694415587	MPa
Iy, MOI about y axis (minor axis)	=	9.03E-03	m4
	=	9.03E+09	mm4

distance from base to neutral axis	=	7.06E-02	m
y = total depth - dist from base to neutral axis	=	849.40	mm
My, Minor axis bending moment	=	11946.67	kNm
Minor axis bending stress	=	My * y /Iy	
	=	1123.63	MPa
Iz, MOI about z axis (major axis)	=	5.21E-01	m4
	=	5.21E+11	mm4
z, distance from base to neutral axis	=	1.25	m
(half the width)	=	1250	mm
Mz, Major axis bending moment	=	442.67	kNm
Major axis bending stress	=	Mz * z /Iz	
	=	1.06	MPa
Total axial stress	=	Fx /A + minor axis bending stress + major axis bending stress	
	=	1125.38	MPa
allowable axial stress	=	0.66 Fy	(from AISC)
	=	155.1	MPa
utilisation factor	=	total axial stress / allowable axial stress	
	=	7.26	
From DNV-RP-C201, Section 2: **axial stress check of stiffener and plate OK?**	=	OK if UF < 1/1.15, NOT OK if otherwise	
	=	**not ok**	

Check column buckling of stiffeners, as per AISC

Treat the stiffener and plate as a column,

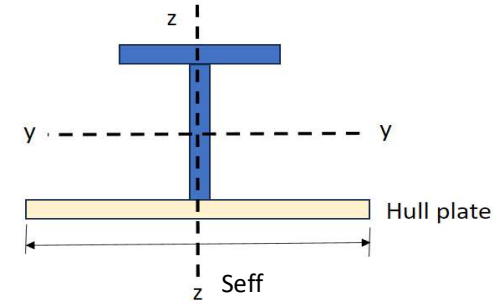

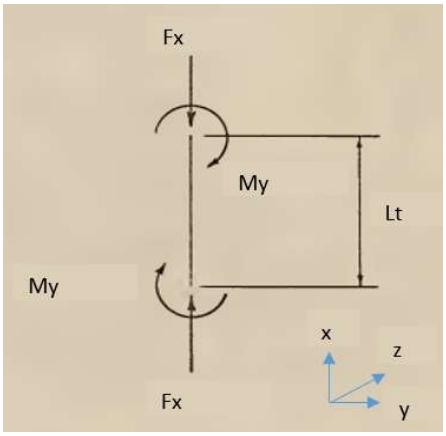

ASUM Command

File

```
PRINT GEOMETRY ITEMS ASSOCIATED WITH THE CURRENTLY SELECTED AREAS

*** NOTE ***                            CP =       2.750   TIME= 13:47:24
Density not associated with all selected areas.  Geometry items are
based on a unit density.

  TOTAL NUMBER OF AREAS SELECTED =      5  (OUT OF      5 DEFINED)

  TOTAL SURFACE AREA OF ALL SELECTED AREAS =  0.26939

  TOTAL VOLUME OF ALL SELECTED AREAS =  0.26939

  CENTER OF MASS:  XC=-0.70000E-02  YC= 0.70000E-02  ZC= 0.70602E-01

                 *** MOMENTS OF INERTIA ***
         (BASED ON A UNIT DENSITY AND A UNIT THICKNESS)

      ABOUT ORIGIN     ABOUT CENTER OF MASS    PRINCIPAL
  IXX =   0.53124          0.52989           0.52989
  IYY =   0.10387E-01      0.90310E-02       0.90310E-02
  IZZ =   0.52088          0.52086           0.52086
  IXY =   0.13200E-04     -0.31297E-16
  IYZ =  -0.13314E-03     -0.70286E-18
  IZX =   0.13314E-03     -0.85746E-19

  PRINCIPAL ORIENTATION VECTORS (X,Y,Z):
    1.000  0.000  0.000    0.000  1.000  0.000    0.000  0.000  1.000
    (THXY=    0.000  THYZ=    0.000  THZX=    0.000)
```

s, c/c spacing between longitudinal stiffeners	=	2.5	m
Lt, c/c spacing between transverse stiffeners	=	0.9	m
Fx, axial compression force on ¨column¨	=	100.27	kN
My, moment on ¨column¨	=	11946.67	kNm
Mz, moment on ¨column¨	=	442.67	kNm

wrt Example on pg 50 of (Chen, 1967) https://core.ac.uk/download/pdf/33362643.pdf

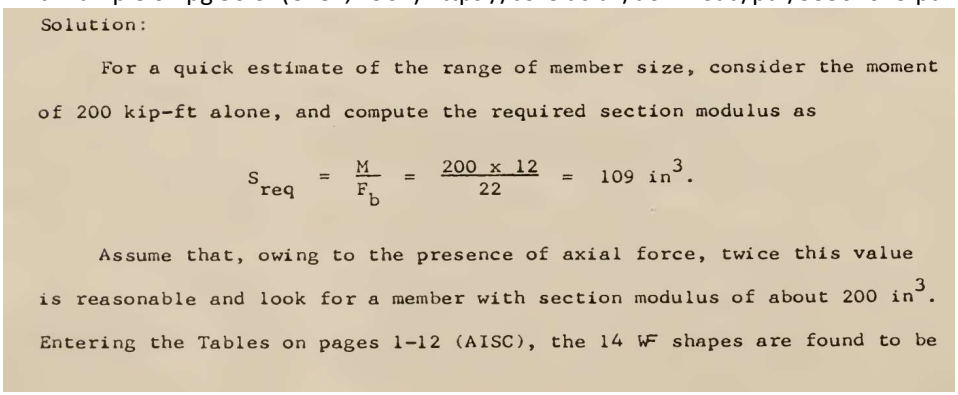

Solution:

For a quick estimate of the range of member size, consider the moment of 200 kip-ft alone, and compute the required section modulus as

$$S_{req} = \frac{M}{F_b} = \frac{200 \times 12}{22} = 109 \text{ in}^3.$$

Assume that, owing to the presence of axial force, twice this value is reasonable and look for a member with section modulus of about 200 in^3.

Entering the Tables on pages 1-12 (AISC), the 14 WF shapes are found to be

Iy, MOI about y axis	=	9.03E+09	mm4	
y, distance from base to neutral axis	=	849.398	mm	
A, cross section area	=	269390	mm2	
Iz, MOI about z axis	=	5.21E+11	mm4	
z, distance from base to neutral axis	=	1250	mm	
section modulus about y-y axis, Sy	=	Iy /y		
	=	1.06E+07	mm3	
section modulus about z-z axis, Sz	=	Iz /z		
	=	4.17E+08	mm3	

for a quick estimate of the required section modulus, consider moment alone,

Sreqm, required section modulus, y axis	=	My/Fb		
Fb, allowable bending stress	=	204.35	MPa	(as per DNV-RP-C102,
Sreqm, y axis	=	5.85E+07	mm3	Section 6.2, Fb = Fy /γM)

Sreqm, required section modulus, z axis	=	Mz/Fb		
Fb, allowable bending stress	=	204.35	MPa	(as per DNV-RP-C102,
Sreqm, z axis	=	2.17E+06	mm3	Section 6.2, Fb = Fy /γM)

Due to additional presence of axial force, assume that twice the value of Sreqm is reasonable:

Sreq, y axis	=	2 * Sreqm,y	
required section modulus considering both moment and axial force	=	1.17E+08	mm3

Sreq, z axis	=	2 * Sreqm,z	
required section modulus considering both moment and axial force	=	4.33E+06	mm3

is provided section modulus sufficient? (y axis)	=	OK if Sreq < Sy, NOT ok if otherwise
	=	**not ok**
is provided section modulus sufficient? (z axis)	=	OK if Sreq < Sz, NOT ok if otherwise
	=	**ok**
ry, radius of gyration about y axis	=	√(Iy/A)
	=	183.10 mm
rz, radius of gyration about z axis	=	√(Iz/A)
	=	1390.50 mm

Table C-C2.1

Buckled shape of column is shown by dashed line	(a)	(b)	(c)	(d)	(e)	(f)
Theoretical K value	0.5	0.7	1.0	1.0	2.0	2.0
Recommended design value when ideal conditions are approximated	0.65	0.80	1.2	1.0	2.10	2.0
End condition code	Rotation fixed and translation fixed Rotation free and translation fixed Rotation fixed and translation free Rotation free and translation free					

Ky, effective length factor about y axis	=	0.8	(assume pin-fixed and sidesway buckling prevented) bigger K is more conservative
Kz, effective length factor about z axis	=	0.8	(assume pin-fixed and sidesway buckling prevented)
ℓy, length about y axis (= c/c spacing between longitudinal stiffeners)	=	2.5	m
ℓz, length about z axis (= c/c spacing between transverse stiffeners)	=	0.9	m
Ky * ℓy, effective length about y axis	=	2	m
Kz * ℓz, effective length about z axis	=	0.72	m

Ky * ℓy / ry, effective slenderness ratio about y axis	=	10.92
Kz * ℓz / rz, effective slenderness ratio about z axis	=	0.52

E2. ALLOWABLE STRESS

On the gross section of axially loaded compression members whose cross sections meet the provisions of Table B5.1, when Kl/r, the largest effective slenderness ratio of any unbraced segment is less than C_c, the allowable stress is:

$$F_a = \frac{\left[1 - \frac{(Kl/r)^2}{2C_c^2}\right] F_y}{\frac{5}{3} + \frac{3(Kl/r)}{8C_c} - \frac{(Kl/r)^3}{8C_c^3}} \qquad \text{(E2-1)}$$

where

$$C_c = \sqrt{\frac{2\pi^2 E}{F_y}}$$

On the gross section of axially loaded compression members, when Kl/r exceeds C_c, the allowable stress is:

$$F_a = \frac{12\pi^2 E}{23(Kl/r)^2} \qquad \text{(E2-2)}$$

Fy, yield stress	=	235	MPa
	=	33	ksi
E, Young's Modulus	=	211000	MPa

5-120 NUMERICAL VALUES From AISC 9th Edition

TABLE 4
VALUES OF C_c

For Use with Equations (E2-1) and (E2-2) and in Table 3

F_y (ksi)	C_c	F_y (ksi)	C_c
33	131.7	46	111.6
35	127.9	50	107.0
36	126.1	55	102.0
39	121.2	60	97.7
40	119.6	65	93.8
42	116.7	90	79.8
45	112.8	100	75.7

Cc, effective slenderness limit	=	131.7	
is the column stocky or slender?		slender if Kl/r > Cc, stocky if otherwise	
about y axis	=	**stocky**	*use equation E2-1*
about z axis	=	**stocky**	*use equation E2-1*
Kl/r/Cc, y axis	=	0.0829	
Kl/r/Cc, z axis	=	0.0039	
Fay, allowable stress about y axis (if axial force alone existed)	=	137.95	MPa

Faz, allowable stress about z axis
(if axial force alone existed) = 140.87 MPa

Cm, Reduction factor = 1 (conservatively assume same moment at top and bottom of column)

check Column for combined compression and bending as per AISC 9th Ed, Section H1:

H1. AXIAL COMPRESSION AND BENDING

Members subjected to both axial compression and bending stresses shall be proportioned to satisfy the following requirements:

$$\frac{f_a}{F_a} + \frac{C_{mx} f_{bx}}{\left(1 - \frac{f_a}{F'_{ex}}\right) F_{bx}} + \frac{C_{my} f_{by}}{\left(1 - \frac{f_a}{F'_{ey}}\right) F_{by}} \le 1.0 \qquad \text{(H1-1)}$$

$$\frac{f_a}{0.60F_y} + \frac{f_{bx}}{F_{bx}} + \frac{f_{by}}{F_{by}} \le 1.0 \qquad \text{(H1-2)}$$

When $f_a/F_a \le 0.15$, Equation (H1-3) is permitted in lieu of Equations (H1-1) and (H1-2):

$$\frac{f_a}{F_a} + \frac{f_{bx}}{F_{bx}} + \frac{f_{by}}{F_{by}} \le 1.0 \qquad \text{(H1-3)}$$

In Equations (H1-1), (H1-2) and (H1-3), the subscripts x and y, combined with subscripts b, m and e, indicate the axis of bending about which a particular stress or design property applies, and

F_a = axial compressive stress that would be permitted if axial force alone existed, ksi

F_b = compressive bending stress that would be permitted if bending moment alone existed, ksi

$$F'_e = \frac{12\,\pi^2 E}{23(Kl_b/r_b)^2}$$

= Euler stress divided by a factor of safety, ksi (In the expression for F'_e, l_b is the actual unbraced length *in the plane of bending* and r_b is the corresponding radius of gyration. K is the effective length factor *in the plane of bending*.) As in the case of F_a, F_b and $0.60F_y$, F'_e may be increased ⅓ in accordance with Sect. A5.2.

f_a = computed axial stress, ksi

fa, computed axial stress = Fx / A
= 0.372 MPa

fa/Fay = 0.0027 *(since fa/Fa < 0.15, use equation H1-3)*
fa/Faz = 0.0026 *(since fa/Fa < 0.15, use equation H1-3)*

fby, bending stress about y axis = My*y/Iy
= 1123.63 MPa
fbz, bending stress about z axis = Mz*z/Iz
= 1.06 MPa
Same allowable bending stress as per DNV-RP-C201, section 2, Fb = Fy /γM ,
fby/Fb = 5.50
fbz/Fb = 0.01

check the column for combined bending and compression as per equation H1-3:
overall utilization ratio = Max (fa/Fay, fa/Faz) + fby/Fb + fbz/Fb
= 5.51

OK?	OK if utilization ratio < 1, NOT ok if otherwise
	not ok

Check stiffener spacing as per DNV-RP-C201, Section 7.3

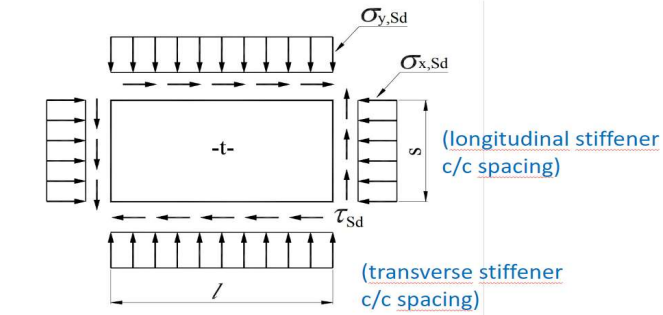

Figure 6-4 Biaxially loaded plate with shear

(plan view of hull plate)

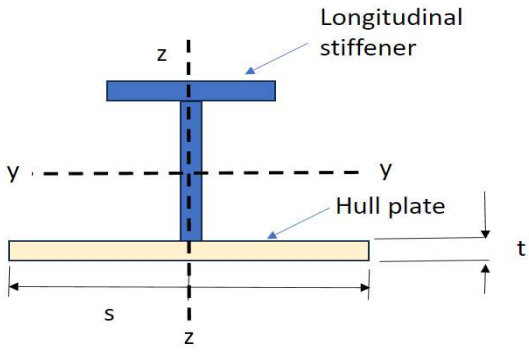

t, hull plate thickness	=	50	mm
s, longitudinal stiffener spacing	=	2.5	m
l, transverse stiffener spacing	=	0.9	m

to check transverse stiffener spacing:

As, shear area	=	l * t	
	=	45	m2
Fs, shear force considered	=	Fx + My / half depth of longitudinal stiffener (depth = 0.92m)	
	=	26071.28	kN
τSd, design shear stress	=	Fs / As	
	=	0.58	MPa
τRd, design shear resistance	=	fy / (√3 * ɣM)	(Ref DNV-RP-C201, eqn 7.18)
	=	117.98	MPa

The plate between stiffeners shall be checked for:

$$\tau_{Sd} \le \tau_{Rd} = \frac{f_y}{\sqrt{3} \cdot \gamma_M} \qquad \textbf{(7.18)}$$

transverse stiffener spacing OK? OK if τSd < τRd, NOT ok if otherwise (as per Eqn 7.18)

ok

usage factor 0.0049

to check longitudinal stiffener spacing:

At, transverse area	=	t * s	
	=	125000	mm2
y, distance from base of section to NA	=	849.398	mm
Iy, MOI of section about y-y axis	=	9.03E+09	mm4
My	=	1.19E+04	kNm
σb1, bending stress from My	=	My * y / Iy	
	=	1123.63	MPa

transverse force in x direction	=	Fx	
	=	100.27	kN
σx,Sd, transverse stress	=	Fx / At + σb1	
	=	1124.43	MPa

to find σx,R, buckling resistance of plate under transverse compression force

Psd, design lateral pressure	=	Fz / (s*l)	
	=	0.192	MPa

The reduction factor due to lateral load k_p may, in lieu of more accurate results, be calculated as:

$$k_p = 1.0 \quad \text{for} \quad p_{Sd} \le 2 \cdot \left(\frac{t}{s}\right)^2 \cdot f_y \qquad \textbf{(6.10)}$$

otherwise

$$k_p = 1.0 - h_\alpha \cdot \left(\frac{p_{Sd}}{f_y} - 2 \cdot \left(\frac{t}{s}\right)^2\right) \quad , \quad \text{but } k_p \ge 0$$

where

$$h_\alpha = 0.05 \cdot \frac{s}{t} - 0.75 \quad \text{but } h_\alpha \ge 0 \qquad \textbf{(6.11)}$$

2(t/s)^2 * fy	=	0.188	MPa
is Psd ≤ 2(t/s)^2 * fy?		**no, need to calculate kp**	

ha	=	1.75	(eqn 6.11)
kp, reduction factor due to lateral load	=	0.99997	(can also assume kp =1 for faster calculation)

$$\kappa = 1.0 \quad \text{for} \quad \lambda_c \le 0.2 \qquad \textbf{(6.7)}$$

$$\kappa = \frac{1}{2 \cdot \bar{\lambda}_c^2} \cdot \left(1 + \mu + \bar{\lambda}_c^2 - \sqrt{\left(1 + \mu + \bar{\lambda}_c^2\right)^2 - 4 \cdot \bar{\lambda}_c^2}\right)$$

$$\text{for } 0.2 < \bar{\lambda}_c < 2.0$$

$$\kappa = \frac{1}{2 \cdot \bar{\lambda}_c^2} + 0.07 \quad \text{for} \quad \bar{\lambda}_c \ge 2.0$$

and $\bar{\lambda}_c$ is:

$$\bar{\lambda}_c = 1.1 \cdot \frac{s}{t} \cdot \sqrt{\frac{f_y}{E}} \qquad \textbf{(6.8)}$$

and μ is:

$$\mu = 0.21 \cdot \left(\bar{\lambda}_c - 0.2\right) \qquad \textbf{(6.9)}$$

λc	=	1.84	(eqn 6.8)
μ	=	0.34	(eqn 6.9)
κ	=	0.26	(eqn 6.7)

to find σx,R, buckling resistance of plate under transverse compression force
replace ℓ with s in eqn 6.6:

$$\sigma_{y,R} = \left[\frac{1.3 \cdot t}{l} \cdot \sqrt{\frac{E}{f_y}} + \kappa \cdot \left(1 - \frac{1.3 \cdot t}{l} \cdot \sqrt{\frac{E}{f_y}}\right)\right] \cdot f_y \cdot k_p \qquad \textbf{(6.6)}$$

σx,R = 196.62 MPa

The design buckling resistance of a plate under transverse compression force may be found from:

$$\sigma_{y,Rd} = \frac{\sigma_{y,R}}{\gamma_M} \qquad \textbf{(6.5)}$$

σx,Rd, design buckling resistance of plate under transverse compression force = σx,R / ɣM (Eqn 6.5)
= 170.97 MPa

$$k_{sp} = \sqrt{1.0 - 3 \cdot \left(\frac{\tau_{Sd}}{f_y}\right)^2} \qquad \textbf{(7.20)}$$

Ksp = 1.00

$$\sigma_{y,Sd} \le k_{sp} \cdot \sigma_{y,Rd} \qquad \textbf{(7.19)}$$

longitudinal stiffener spacing OK? OK if σx,Sd < Ksp * σx, Rd, NOT ok if otherwise, (as per Eqn 7.19)
not ok

utilisation ratio = 6.58

summary of results		
description of check	**result**	**usage factor**
Check hull plate thickness OK under pressure load	**ok**	0.057
Check shear resistance of stiffened panel as per DNV-RP-C201, Section 7.6	**ok**	0.10
Stiffener axial capacity as per DNV-RP-C201, Section 7.2	**ok**	0.88
Check axial stress of stiffener and stiffened plate	**not ok**	7.26
check Column for combined compression and bending as per AISC 9th Ed, Section H1:	**not ok**	5.51
to check transverse stiffener spacing:	**ok**	0.0049
to check longitudinal stiffener spacing:	**not ok**	6.58

Appendix E – Matlab code for ML model for von Mises stress of transverse girder

```
clc
clear all
% This code has sourced from Mohammadkazem Sadoughi, who developed the code
% at Iowa State University (4/05/2017). The matlab file MRSM.m contains the
% code for building the multi-variate Gaussian process. The inputs are the
% training data and based on that the hyperparametrs is tuned and the
% regression coefficient, trend function and covariance matrix will be
% defined.
% url: https://github.com/mksadoughi/Multi-output-Gaussian-Process

%% The original code has been modified for the purpose of this thesis

% for this matlab code to work, it requires all other supporting codes in
% the folder to be present
% Also, optimization toolbox must be installed to matlab

% Define a simple input matrix X with 3 samples and five features
% each sample represent each of the 3 designs
% the five features are the input parameters
% i.e.
% Xdesign no. = [centre-to-centre spacing between transverse stiffeners (m),
% transverse stiffener flange width (mm),
% transverse stiffener flange thickness (mm),
% transverse stiffener full depth (mm),
% transverse stiffener web thickness (mm)]

% source of data: designs 1, 2 and 3 at mesh size 0.125m, at mean wind
% speed of 11m/s
% design 1
X1 = [0.9, 120, 25, 450, 12]

% design 2
X2 = [2.25, 200, 35, 920, 14]

% % design 3
X3 = [0.9, 200, 35, 920, 14]

% input matrix X with 3 samples each containing the 5 input variables
X = [X1; X2; X3]
% X = [X1; X2]

% corresponding output matrix with 3 samples and 1 target
% the 3 samples represent the 3 designs
% the 1 target represents the output, which is the membrane + bending
% stress, in MPa, from ANSYS FEM simulation
% i.e. Y = [design 1's stress value; design 2's; design 3's]
Y = [35.746; 66.322; 52.482]
% Y = [35.746; 66.322]
%%
% Build a MRSM model over the data, where MGP is the trained model
MGP = MRSM (X, Y);

%%
% Predict the response at a new input point "X_" using the trained model.
```

```
% i.e. a new set of input for
% centre-to-centre spacing between transverse stiffeners (m),
% transverse stiffener flange width (mm),
% transverse stiffener flange thickness (mm),
% transverse stiffener full depth (mm),
% transverse stiffener web thickness (mm)
X_ = [0.9, 200, 35, 920, 14] % input design 3's input variables

% Y_ is the mean value of prediction of output
% S_ is the covariance matrix summarizing the uncertainty of prediction
% the smaller the value of S_, the lower the uncertainty, hence
% more accurate the prediction
[Y_, S_] = predict_resp(MGP, X_)
```

Appendix F – Matlab code for ML model for buckling load multiplier of longitudinal girder

```
clc
clear all
% This code has sourced from Mohammadkazem Sadoughi, who developed the code
% at Iowa State University (4/05/2017). The matlab file MRSM.m contains the
% code for building the multi-variate Gaussian process. The inputs are the
% training data and based on that the hyperparametrs is tuned and the
% regression coefficient, trend function and covariance matrix will be
% defined.
% url: https://github.com/mksadoughi/Multi-output-Gaussian-Process

%% The original code has been modified for the purpose of this thesis

% for this matlab code to work, it requires all other supporting codes in
% the folder to be present
% Also, optimization toolbox must be installed to matlab

% Define a simple input matrix X with 3 samples and five features
% each sample represent each of the 3 designs
% the five features are the input parameters
% i.e.
% Xdesign no. = [centre-to-centre spacing between longitudinal stiffeners (m),
% longitudinal stiffener flange width (mm),
% longitudinal stiffener flange thickness (mm),
% longitudinal stiffener full depth (mm),
% longitudinal stiffener web thickness (mm)]

% source of data: designs 1, 2 and 3, at mean wind
% speed of 11m/s
% design 1
X1 = [2.5, 200, 35, 920, 14]

% design 2
X2 = [2.5, 120, 25, 450, 12]

% % design 3
X3 = [1.5625, 150, 25, 650, 12]

% input matrix X with 3 samples each containing the 5 input variables
X = [X1; X2; X3]
% X = [X1; X2]

% corresponding output matrix with 3 samples and 1 target the 3 samples
% represent the 3 designs the 1 target represents the output, which is the
% buckling load multiplier, from ANSYS FEM simulation
% i.e. Y = [design 1's load multiplier; design 2's; design 3's]
Y = [7.1796e+006; 1.1927e+006; 6.3814e+006]

%%
% Build a MRSM model over the data, where MGP is the trained model
MGP = MRSM (X, Y);

%%
% Predict the response at a new input point "X_" using the trained model.
% i.e. a new set of input for
```

```
% centre-to-centre spacing between transverse stiffeners (m),
% transverse stiffener flange width (mm),
% transverse stiffener flange thickness (mm),
% transverse stiffener full depth (mm),
% transverse stiffener web thickness (mm)
X_ = [1.5625, 150, 25, 650, 12] % input design 3's input variables

% Y_ is the mean value of prediction of output
% S_ is the covariance matrix summarizing the uncertainty of prediction
% the smaller the value of S_, the lower the uncertainty, hence
% more accurate the prediction
[Y_, S_] = predict_resp(MGP, X_)
```

Appendix G – Supporting Matlab codes for ML models

The following list of Matlab codes are developed by Mohammadkazem Sadoughi (2017). They need to accompany the ML model code in order for the ML model to run.

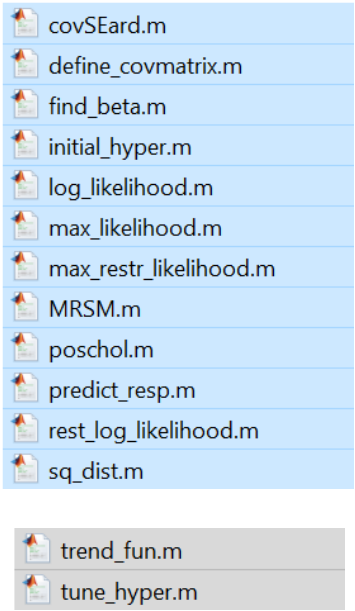

Figure G-1 List of supporting Matlab codes for ML model to run

Appendix G.1 Matlab code for covSEard.m Sadoughi (2017)

```
function K= covSEard(hyp, x, z)
n=size(x,1);
m=size(z,1);
for i=1:n
    for j=1:m
        K(i,j)=exp(-sum( hyp.*((x(i,:)-z(j,:)).^2) ));
    end
end
% K= A+A'-diag(diag(A));
End
```

Appendix G.2 Matlab code for define_covmatrix.m Sadoughi (2017)

```
function z_mn=define_covmatrix(model,X1,X2)
% This function uses Non-separable Linear Model of Coregionalization (NLMC) to
build the covariance among each set of points.

for i=1:model.m
    L(:,:,i) = model.cov_model(model.hyper.teta(i,:), X1, X2);
end
z_mn=[];
for i=1:size(X1,1)
    supplement=[];
```

```
    for j=1:size(X2,1)

model.cov{i,j}=model.hyper.A*diag(reshape(L(i,j,:),model.m,1))*model.hyper.A';
        supplement=[supplement, model.cov{i,j}];
    end
    z_mn=[z_mn;supplement];
end

if isequal(X1,X2)==1
    z_mn= triu(z_mn)+triu(z_mn)'-diag(diag(z_mn));
    [V,D]=eig(z_mn);
    d=diag(D);
    d(d<=.001)=0.001;
    z_mn= V*diag(d)*V';
end

end
```

Appendix G.3 Matlab code for find_beta.m Sadoughi (2017)

```
function beta=find_beta(model)

zchol=poschol(model.z_mn);

alpha1 = (zchol\(zchol'\model.ymn));
alpha2=(zchol\(zchol'\model.fn));
alpha3=model.fn'*alpha2;
alpha3chol=chol(alpha3);
alpha4=(alpha3chol\(alpha3chol'\model.fn'));
beta=alpha4*alpha1;


end
```

Appendix G.4 Matlab code for initial_hyper.m Sadoughi (2017)

```
function model=initial_hyper(model)

% This function gives the initial values to all hyperparameters used in this
algorithm.

model.hyper.teta=ones(model.m,model.d);
model.hyper.A=[1 0.05 0.03
0.01;0.05,1,0.02,0.01;0.03,0.02,1,0.04;0.01,0.01,0.04,1];

model.zigma0=diag(ones(model.m,1));
[V, D]=eig(model.zigma0);
model.hyper.A=V*(D^0.5)*V';

end
```

Appendix G.5 Matlab code for log_likelihood.m Sadoughi (2017)

```
function [lml] = log_likelihood(hyper_param, model,i)

% This function estimates the restricted likelihood.

y=model.Y(:,i);
fn=reshape(model.fn,model.m,model.n,model.p);
f=reshape(fn(i,:,:), model.n,model.p);

K = model.cov_model(hyper_param, model.X, model.X);
Kchol = chol(K);

alpha1=y-f*model.beta;
alpha2 = (Kchol\(Kchol'\alpha1));
sigma2=alpha1'*alpha2/model.n;

lml=0.5*model.n*(sigma2)+0.5*log(det(K));

end
```

Appendix G.6 Matlab code for max_likelihood.m Sadoughi (2017)

```
function model= max_likelihood(model)

% This function is used when we only want to tune the decay parameters in each
single response separately.

for i=1:model.m
    problem.f = @(x) log_likelihood(x,model,i);
    A = [];
    b = [];
    Aeq = [];
    beq = [];
    lb= 0.01*ones(1,model.d);
    ub= 100*ones(1,model.d);
    x0 = model.hyper.teta(i,:);
    options = optimset('Display', 'off') ;
    nonlcon=[];
    model.hyper.teta(i,:) =
fmincon(problem.f,x0,A,b,Aeq,beq,lb,ub,nonlcon,options);
end

end
```

Appendix G.7 Matlab code for max_restr_likelihood.m Sadoughi (2017)

```
function model= max_restr_likelihood(model)

% This function is used when we want to tune all hyperparameters simultaneously.
% To find the global optimum point we use Globalsearch function in Matlab.
```

```
MLE = @(x) rest_log_likelihood(x,model);      % define the likelihood function

% Set the consitraints used in optimization
A = [];
b = [];
Aeq = [];
beq = [];

%  Inital sets for parametrs of  z0
n1=model.m*(model.m-1)/2;
lb1= zeros(1,n1);
ub1= model.s*ones(1,n1);
x01 = 0.1*ones(1,n1);

% Initial sets for parameters of  teta
n2=model.m*model.d;
lb2= 0.01*ones(1,n2);
ub2= 10*ones(1,n2);
x02 =0.2*ones(1,n2);

% Combining all parameters:
n=n1+n2;
lb=[lb1,lb2];
ub=[ub1,ub2] ;
x0 =[x01,x02];

%% Optimization
% There are two options for optimization: 1- using direct fmincon function
% based on a single inital point x0. This is a faster method but can only
% find the local minima. 2- Using global search which can find the global
% minima. This method is more accurate but takes more time.

if strcmp(model.optim,'fmincon')     % Option 1:
    options = optimset('Display', 'off') ;
    nonlcon=[];
    x= fmincon(MLE,x0,A,b,Aeq,beq,lb,ub, nonlcon, options);
else   % Option 2:
    opts = optimoptions(@fmincon,'Algorithm','interior-point');
    problem =
createOptimProblem('fmincon','objective',MLE,'x0',x0,'lb',lb,'ub',ub,'options',opt
s);
    gs = GlobalSearch('NumTrialPoints',300);
    [x,f] = run(gs,problem);
end

%% Update hyperparametrs
% Update the matrix A
k=1;
for i=1: model.m
    for j=i+1:model.m
        z0(i,j)=x(k);
        k=k+1;
    end
end
if model.m==1;
    z0=[];
end

z0=[z0;zeros(1,model.m)];
```

```
z0=z0+z0'+diag(ones(model.m,1));
[V, D]=eig(z0);
model.hyper.A=V*(D^0.5)*V';

% Update the hyperparameters teta
teta=x(n1+1:end);
teta=reshape(teta,model.m,model.d);
model.hyper.teta=teta;

end
```

Appendix G.8 Matlab code for MRSM.m Sadoughi (2017)

```
function model=MRSM(input,output,option)

% This code has been written by Mohammadkazem Sadoughi at Iowa State
% University (4/05/2017). This file is the main code for building the multi-
variate
% Gaussian process. The inputs are the training data and based on that the
% hyperparametrs is tuned and the regression coefficient, trend function and
% covariance matrix will be defined.

if exist( 'option', 'var' )

    if isempty(option.s)              % Upper bound for matrix A elements. Setting
this parameter to a very small value means we do not consider any correlation amng
the responses
        model.s=0.6;
    else
        model.s=option.s;
    end

    if isempty(option.degree)         % Degree of polynomial functions: can be
zero, one, two or....
        model.degree=2;
    else
        model.degree=option.degree;
    end

    if isempty(option.optim)           %  Optimization method
        model.optim='fmincon';
    else
        model.optim=option.optim;
    end
else
        model.s=0.6;
        model.degree=0;
        model.optim='fmincon';
end

model.X=input;
model.Y=output;                  % Matrix of (model.n by model.m )

model.d=size(input,2);           % Dimesntion of input variables
model.n=size(input,1);           % Number of training points
model.m=size(output,2);          % Number of responses
```

```
model.ymn=reshape(output',model.m*model.n,1);              % Reshape the output to
a vector of (model.m * model.n by 1)

model.cov_model = @(hyp, x, z, i)covSEard(hyp, x, z);      % Define the covariance
model (hbere we used the SEARD)

[model.fn, model.p]=trend_fun(model,model.X);              % Define the shape of
trend function and Fn

model=initial_hyper(model);                                % Initialize
hyperparametrs

model=tune_hyper(model);                                   % Tune hyperparametrs
end
```

Appendix G.9 Matlab code for poschol.m Sadoughi (2017)

```
function Mchol=poschol(M)
M=abs(M);
M= triu(M)+triu(M)'-diag(diag(M));
[V,D]=eig(M);
d=diag(D);
d(d<=10e-10)=10e-10;
Mchol= V*diag(d)*V';
Mchol=chol(Mchol);
end
```

Appendix G.10 Matlab code for predict_resp.m Sadoughi (2017)

```
function [y, s, model]=predict_resp(model,x)

model.x_pred=x;
model.n0=size(x,1);
model.z_0n0n=define_covmatrix(model,model.x_pred,model.X);
z0=model.hyper.A*model.hyper.A';
n=size(model.x_pred,1);
model.z0=repmat(z0,n,1);

%% Prediction at new points
alpha1=model.ymn-model.fn*model.beta;
zchol=poschol(model.z_mn);
alpha2 = (zchol\(zchol'\alpha1));
model.f0=trend_fun(model,model.x_pred);
y=model.f0*model.beta+model.z_0n0n*alpha2;
y=reshape(y,model.m,model.n0)';

%% uncertainity in preictoin at new points
alpha3=(zchol\(zchol'\model.fn));
u=model.f0-model.z_0n0n*alpha3;
alpha4=model.fn'*alpha3;
alpha4chol=poschol(alpha4);
alpha5=(alpha4chol\(alpha4chol'\u'));
alpha6=(zchol\(zchol'\model.z_0n0n'));

for i=1:n
```

```
    for j=1:model.m
        for jj=1:model.m
            alpha7(model.m*(i-1)+1+(j-1),jj)=model.z_0n0n(model.m*(i-1)+1+(j-
1),:)*alpha6(:,model.m*(i-1)+jj);
            alpha8(model.m*(i-1)+1+(j-1),jj)=u(model.m*(i-1)+1+(j-
1),:)*alpha5(:,model.m*(i-1)+jj);
        end
    end
end
s=model.z0-alpha7+alpha8;

end
```

Appendix G.11 Matlab code for rest_log_likelihood.m Sadoughi (2017)

```
function [lml] = rest_log_likelihood(x, model)

% This function calculates the restricted likelihod at each set of hyperparametrs

n1=model.m*(model.m-1)/2;
n2=model.m*model.d;

k=1;

for i=1: model.m
    for j=i+1:model.m
    z0(i,j)=x(k);
    k=k+1;
    end
end

if model.m==1;
    z0=[];
end

z0=[z0;zeros(1,model.m)];
z0=z0+z0'+diag(ones(model.m,1));

[V, D]=eig(z0);
model.hyper.A=V*(D^0.5)*V';
teta=x(n1+1:end);
teta=reshape(teta,model.m,model.d);
y=model.ymn;
f=model.fn;

model.hyper.teta=teta;
model.z_mn=define_covmatrix(model,model.X,model.X); % update the value of model.
zmn
model.beta=find_beta(model); % update beta values

%% Determine the restricted likelihood function
zmnchol = poschol(model.z_mn);
alpha1=y-f*model.beta;
alpha2 = (zmnchol\(zmnchol'\alpha1));
sigma2=alpha1'*alpha2;
alpha3=(zmnchol\(zmnchol'\f));
alpha4=f'*alpha3;
```

```
% RMLE
lml=0.5*(sigma2)+0.5*log(det(model.z_mn))+0.5*log(det(alpha4));
% MLE
% lml=0.5*(sigma2)+0.5*log(det(model.z_mn));
end
```

Appendix G.12 Matlab code for sq_dist.m

Sadoughi (2017)

```
% sq_dist - a function to compute a matrix of all pairwise squared distances
% between two sets of vectors, stored in the columns of the two matrices, a
% (of size D by n) and b (of size D by m). If only a single argument is given
% or the second matrix is empty, the missing matrix is taken to be identical
% to the first.
%
% Usage: C = sq_dist(a, b)
%    or: C = sq_dist(a)  or equiv.: C = sq_dist(a, [])
%
% Where a is of size Dxn, b is of size Dxm (or empty), C is of size nxm.
%
% Copyright (c) by Carl Edward Rasmussen and Hannes Nickisch, 2010-12-13.

function C = sq_dist(a, b)

if nargin<1  || nargin>3 || nargout>1, error('Wrong number of arguments.'); end
bsx = exist('bsxfun','builtin');      % since Matlab R2007a 7.4.0 and Octave 3.0
if ~bsx, bsx = exist('bsxfun'); end      % bsxfun is not yes "builtin" in Octave
[D, n] = size(a);

% Computation of a^2 - 2*a*b + b^2 is less stable than (a-b)^2 because numerical
% precision can be lost when both a and b have very large absolute value and the
% same sign. For that reason, we subtract the mean from the data beforehand to
% stabilise the computations. This is OK because the squared error is
% independent of the mean.
if nargin==1                                                % subtract mean
  mu = mean(a,2);
  if bsx
    a = bsxfun(@minus,a,mu);
  else
    a = a - repmat(mu,1,size(a,2));
  end
  b = a; m = n;
else
  [d, m] = size(b);
  if d ~= D, error('Error: column lengths must agree.'); end
  mu = (m/(n+m))*mean(b,2) + (n/(n+m))*mean(a,2);
  if bsx
    a = bsxfun(@minus,a,mu); b = bsxfun(@minus,b,mu);
  else
    a = a - repmat(mu,1,n);  b = b - repmat(mu,1,m);
  end
end

if bsx                                                % compute squared distances
  C = bsxfun(@plus,sum(a.*a,1)',bsxfun(@minus,sum(b.*b,1),2*a'*b));
else
  C = repmat(sum(a.*a,1)',1,m) + repmat(sum(b.*b,1),n,1) - 2*a'*b;
end
```

```
C = max(C,0);          % numerical noise can cause C to negative i.e. C > -1e-14
```

Appendix G.13 Matlab code for trend_fun.m

Sadoughi (2017)

```
function [f p]=trend_fun(model,X)

% This file has been written by Mohammadkazem Sadoughi, at Iowa State
% University (4/05/2017). This file defines different type of trend function
% based on the degree of polynomials

n=size(X,1);
model.ss=1;
f=[];


switch model.degree

    case 0  % f(x)= 1
        p=1;
        for i=1:n;
            for j=1:model.m
                supplement=[1];
                f=[f;supplement];
            end
        end

    case 1  % f(x)= 1,  x
        p=1+model.d;
        for i=1:n;
            for j=1:model.m
                supplement=[1,X(i,:)];
                f=[f;supplement];
            end
        end

    case 2  % f(x)= 1 , x , x2
        p=1+model.d*(model.d+3)/2;
        for i=1:n;
            for j=1:model.m
                supplement=[1,X(i,:)];
                for k=1:model.d
                    for l=k:model.d
                        supplement=[supplement,X(i,k)*X(i,l)];
                    end
                end
                f=[f;supplement];
            end

        end

    case 7   % f(x)= 1 , x , y , xy, x2, y2, x2y
    case 8   % f(x)= 1 , x , y , xy, x2, y2, x2y, xy2
    case 9   % f(x)= 1 , x , y , xy, x2, y2, x2y, xy2, x3
    case 10  % f(x)= 1 , x , y , xy, x2, y2, x2y, xy2, x3, y3

    otherwise
    disp('other value for p')
end
```

```
end
```

Appendix G.14 Matlab code for tune_hyper.m Sadoughi (2017)

```
function model=tune_hyper(model)

% This file has been written by Mohammadkazem Sadoughi, at Iowa State
% University (4/05/2017). This file tunes the hyperparameters used in
% covariance metrix of multivariate Gaussian process

model = max_restr_likelihood(model);                    % Using MLE technique to
tune the matrix A and hyperparametrs teta.

model.z_mn=define_covmatrix(model,model.X,model.X);     % Define the covariance
matrix between training points

model.beta=find_beta(model);                            % Define the trend function
coefficients
end
```

Appendix H OPENFAST Inflow input file

```
------- InflowWind v3.01.* INPUT FILE ------------------------------------------------------------------------
IEA 15 MW Offshore Reference Turbine
---------------------------------------------------------------------------------------------------------------
False                   Echo        - Echo input data to <RootName>.ech (flag)
3                       WindType    - switch for wind file type (1=steady; 2=uniform; 3=binary TurbSim FF; 4=binary Bladed-style FF; 5=HAWC format; 6=User defined; 7=native Bladed FF)
0.0                     PropagationDir - Direction of wind propagation (meteoroligical rotation from aligned with X (positive rotates towards -Y) -- degrees)
0.0                     VFlowAng    - Upflow angle (degrees) (not used for native Bladed format WindType=7)
1                       NWindVel    - Number of points to output the wind velocity    (0 to 9)
0.0                     WindVxiList - List of coordinates in the inertial X direction (m)
0.0                     WindVyiList - List of coordinates in the inertial Y direction (m)
150.0                   WindVziList - List of coordinates in the inertial Z direction (m)
================== Parameters for Steady Wind Conditions [used only for WindType = 1] =========================
24.0                    HWindSpeed  - Horizontal windspeed                            (m/s)
150.0                   RefHt       - Reference height for horizontal wind speed      (m)
0.12                    PLexp       - Power law exponent                              (-)
================== Parameters for Uniform wind file   [used only for WindType = 2] ============================
"none"                  Filename_Uni - Filename of time series data for uniform wind field.      (-)
150.0                   RefHt_Uni   - Reference height for horizontal wind speed              (m)
240.0                   RefLength   - Reference length for linear horizontal and vertical sheer (-)
================== Parameters for Binary TurbSim Full-Field files   [used only for WindType = 3] ==============
"15MWS2318573U6.bts"                FileName_BTS - Name of the Full field wind file to use (.bts)
================== Parameters for Binary Bladed-style Full-Field files   [used only for WindType = 4] =========
"none"                  FilenameRoot - Rootname of the full-field wind file to use (.wnd, .sum)
False                   TowerFile   - Have tower file (.twr) (flag)
================== Parameters for HAWC-format binary files  [Only used with WindType = 5] =====================
"none"                  FileName_u  - name of the file containing the u-component fluctuating wind (.bin)
"none"                  FileName_v  - name of the file containing the v-component fluctuating wind (.bin)
"none"                  FileName_w  - name of the file containing the w-component fluctuating wind (.bin)
64                      nx          - number of grids in the x direction (in the 3 files above) (-)
32                      ny          - number of grids in the y direction (in the 3 files above) (-)
32                      nz          - number of grids in the z direction (in the 3 files above) (-)
16.0                    dx          - distance (in meters) between points in the x direction    (m)
3.0                     dy          - distance (in meters) between points in the y direction    (m)
3.0                     dz          - distance (in meters) between points in the z direction    (m)
150.0                   RefHt_Hawc  - reference height; the height (in meters) of the vertical center of the grid (m)
-------------   Scaling parameters for turbulence   ---------------------------------------------------------
2                       ScaleMethod - Turbulence scaling method   [0 = none, 1 = direct scaling, 2 = calculate scaling factor based on a desired standard deviation]
1.0                     SFx         - Turbulence scaling factor for the x direction (-)   [ScaleMethod=1]
1.0                     SFy         - Turbulence scaling factor for the y direction (-)   [ScaleMethod=1]
1.0                     SFz         - Turbulence scaling factor for the z direction (-)   [ScaleMethod=1]
1.2                     SigmaFx     - Turbulence standard deviation to calculate scaling from in x direction (m/s)    [ScaleMethod=2]
0.8                     SigmaFy     - Turbulence standard deviation to calculate scaling from in y direction (m/s)    [ScaleMethod=2]
0.2                     SigmaFz     - Turbulence standard deviation to calculate scaling from in z direction (m/s)    [ScaleMethod=2]
-------------   Mean wind profile parameters (added to HAWC-format files)   ----------------------------------
12.0                    URef        - Mean u-component wind speed at the reference height (m/s)
2                       WindProfile - Wind profile type (0=constant;1=logarithmic,2=power law)
0.2                     PLExp_Hawc  - Power law exponent (-) (used for PL wind profile type only)
0.03                    Z0          - Surface roughness length (m) (used for LG wind profile type only)
0                       XOffset     - Initial offset in +x direction (shift of wind box) (-)
===================== OUTPUT ==================================================
False                   SumPrint    - Print summary data to <RootName>.IfW.sum (flag)
OutList      - The next line(s) contains a list of output parameters.  See OutListParameters.xlsx for a listing of available output channels, (-)
WindlVelX
END of input file (the word "END" must appear in the first 3 columns of this last OutList line)
---------------------------------------------------------------------------------------
```